

博士論文

Identification of TEX264 as a novel receptor for ER autophagy

(小胞体選択的オートファジーの新規レセプターTEX264の同定)

千野遥

**Identification of TEX264 as a novel receptor for ER
autophagy**

Affiliation: Department of Respiratory Medicine, Graduate School of Medicine,
The University of Tokyo, Tokyo 113-0033, Japan

Supervisor: Takahide Nagase

Haruka Chino

Contents

	Pages
Abbreviation.....	4
Abstract.....	6
Introduction.....	8
Material and Methods.....	14
Results.....	27
Discussion.....	75
References.....	81
Acknowledgement.....	94

ABBREVIATION LIST

AIM : Atg8 interacting motif

AMBRA1 : Autophagy And Beclin 1 Regulator 1

ATG : autophagy-related gene

CCPG1 : cell-cycle progression gene 1

DMEM : Dulbecco's Modified Eagle Medium

ER : Endoplasmic reticulum

FAM134B : Family With Sequence Similarity 134 Member B

FBS : Fetal bovine serum

GABARAP : Gamma-aminobutyric acid receptor-associated protein

GFP : green fluorescence protein

GIM : GABARAP interacting motif

HSP90 : heat shock protein 90

IDR : intrinsically disordered region

LC3 : Microtubule-associated proteins 1A/1B light chain 3

LIR : LC3 interacting region

MEF : mouse embryonic fibrosis

MS : mass spectrometry

PBS : Phosphate buffered salts

PI3K : Phosphoinositide 3-kinase

RFP : red fluorescence protein

RTN3 : Reticulon 3

RTN4 : Reticulon 4

SEC62 : preprotein translocation factor

TEX264 : testis-expressed protein 264

ULK1 : Unc51 like linase 1

VPS34 : Phosphatidylinositol 3-Kinase Catalytic Subunit Type 3

WT : wild-type

ABSTRACT

Autophagy has been considered to exert non-selective bulk degradation of intracellular components. Now it is clear that certain proteins and organelles are selectively degraded by autophagy. Identification and characterization of substrates and receptors for selective autophagy will accelerate our understanding of mechanisms and significance of selective autophagy. Typical substrates and receptors of selective autophagy have LC3-interacting regions (LIRs) that bind to autophagosomal LC3/GABARAP family proteins. Here, I performed a differential interactome screen using a wild-type LC3B and a LIR recognition-deficient mutant, and identified TEX264 as a novel receptor for autophagic degradation of the endoplasmic reticulum (ER-phagy). TEX264 is an ER protein with a single transmembrane domain and a LIR motif. TEX264 interacts with LC3/GABARAP family proteins more efficiently and is expressed more ubiquitously than previously known ER-phagy receptors. TEX264 is recruited to autophagosomes through binding with LC3s/GABARAPs and degraded by autophagy in cultured cells and mouse tissues. ER-phagy is profoundly blocked by deletion of TEX264 alone and almost completely by additional deletion of already reported ER-phagy receptors FAM134B and CCPG1. A long intrinsically disordered region of TEX264 is required for its ER-phagy receptor function to bridge the gap between the ER and autophagosomal

membranes independently of its amino acid sequence. These results suggest that

TEX264 is a major ER-phagy receptor.

.

Keywords:

Selective autophagy, ER-phagy, intrinsically disordered region, organellar contact site

INTRODUCTION

In all living organisms, intracellular components are renovated. During renovation, not only synthesis but also degradation plays the important roles in maintaining cellular homeostasis. Eukaryotic cells have two major degradation pathways involving the lysosome and proteasome [1]. The proteasome recognizes ubiquitinated short-lived protein and degrades them into peptides. Lysosomal degradation can be classified into endocytosis and autophagy dependent on delivery pathways. Macroautophagy (referred to as autophagy hereinafter) degrades cytoplasmic components whereas endocytosis degrades plasma membrane proteins and extracellular materials. During autophagy, a portion of the cytoplasm including organelles is enclosed by a membrane sac called the isolation membrane (also known as the phagophore) to form an autophagosome [1-3]. The autophagosome subsequently fuses with lysosomes to become the autolysosome, in which engulfed materials are degraded by lysosomal enzymes (Figure 1). This process is mediated by >40 autophagy-related (*ATG*) genes [4]. They function as six distinct steps. During stress condition, ULK1 complex (consisting of ULK1, ATG13, FIP200 and ATG101) is phosphorylated at initiation step of autophagy. Activated ULK1 complex are recruited to autophagosome formation site with ATG9 and phosphorylated PI3K complex (consisting class III PI3K, VPS34, Beclin1, ATG15, AMBRA1 and

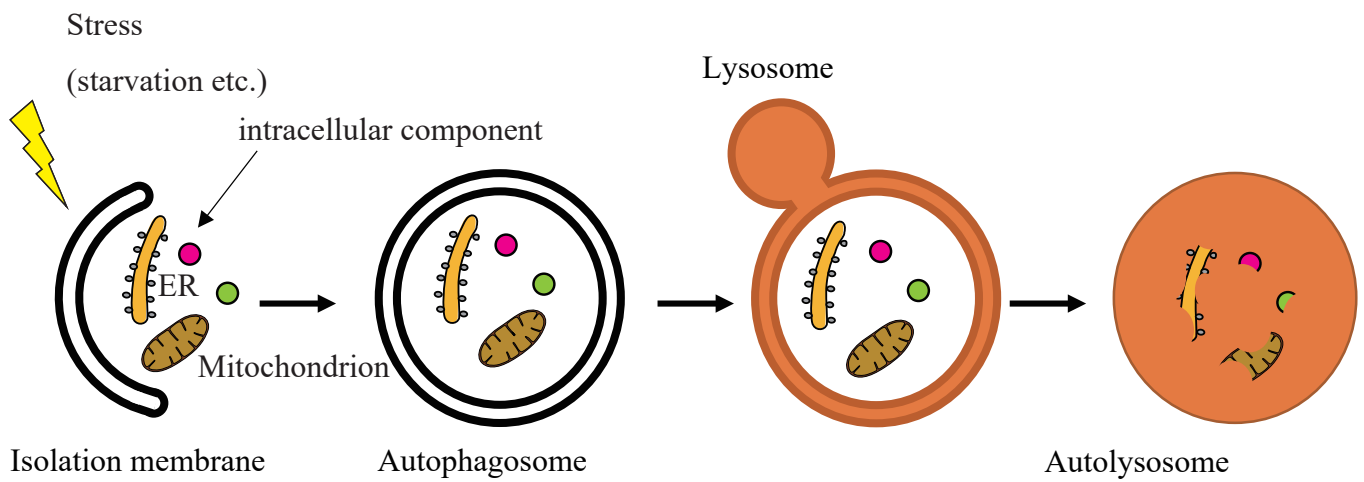


Figure 1. Scheme of autophagy

Upon starvation, a membranous sac called the isolation membrane elongates and sequesteres cytosolic components to form a double-membrane vesicle (the autophagosome). Then lysosomes fuse with autophagosomes to become autolysosomes and degrade internal materials.

p115), which activates PI3P. Afterwards, ATG2-WIPI complex and two ubiquitin-like conjugation system (ATG12-ATG5-ATG16L1 complex and LC3/GABARAP-phosphatidylethanolamine) are recruited to elongation of autophagosome [5,6].

Previously, autophagy was thought to be a non-selective bulk degradation pathway; however, it is now clear that some proteins and damaged organelles are selectively recognized and degraded by autophagy [1,7] (Figure 2). Examples of selective targets are soluble proteins such as p62 (also known as SQSTM1), damaged organelles including mitochondria and lysosomes, protein aggregates, intracellular pathogens, and the endoplasmic reticulum (ER) [8-13]. These various types of selective autophagy are important for homeostasis under physiological conditions and are also related to human diseases [6,14,15]. Identification and characterization of substrates and receptors for selective autophagy will accelerate our understanding of mechanisms and significance of selective autophagy.

In general, these selective substrates are directly or indirectly recognized by Atg8 or its homologs present on the autophagic membranes [7,16]. In yeasts, selective substrates, such as Ape1, are recognized by autophagy receptors (e.g. Atg19 and Atg34) containing the Atg8-interacting motif (AIM) and are delivered to the vacuole via autophagy or the cytoplasm-to-vacuole targeting pathway that resembles autophagy

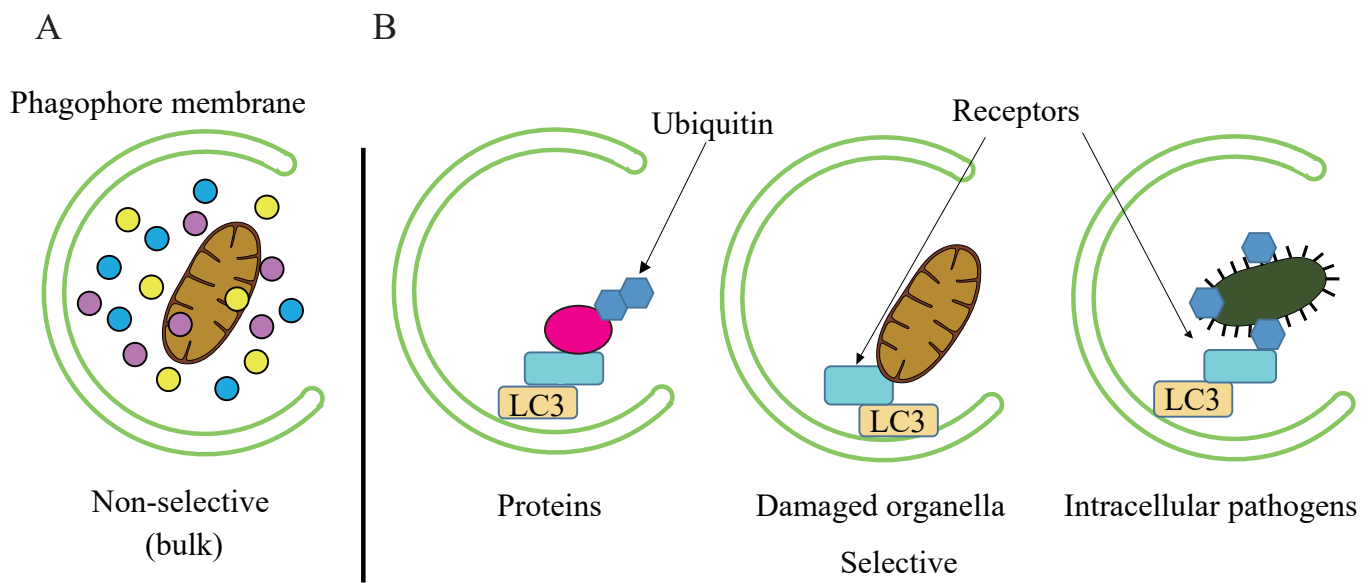


Figure 2. selective autophagy and non-selective autophagy

(A) Autophagy degrades intracellular components mostly in a nonselective manner.

(B) Some specific proteins (often ubiquitinated), damaged organelle such as depolarized mitochondria, and invading bacteria can be selectively degraded by autophagy. A defect in autophagy leads to formation of protein aggregates, ROS production, and chronic infection.

[17]. In mammals, the Atg8 homologs are classified into two subfamilies: the microtubule-associated protein light chain 3 (LC3) and gamma-aminobutyric acid receptor-associated protein (GABARAP) [18] families. Selective substrates that have LC3-interacting regions (LIRs) or GABARAP-interacting motifs (GIMs) can be directly recognized by autophagic membranes [19-21]. Alternatively, autophagy adaptors or receptors that have LIR/GIMs mediate recognition of selective substrates, often in an ubiquitination-dependent manner [7,16]. The canonical AIM/LIR/GIMs consist of a consensus motif [W/F/Y]xx[L/I/V] surrounded by at least one proximal acidic residue [22]. ATG8 homologs recognize the first and fourth hydrophobic residues in AIM/LIR/GIMs using hydrophobic pockets that are conserved among Atg8 homologs [17].

Autophagic degradation of ER fragments, which is termed ER-phagy, is a selective type of autophagy. Yeasts have two ER-phagy receptors, namely, Atg39 and Atg40, which are AIM-containing ER membrane proteins that play key roles in sequestering ER fragments into autophagosomes [23]

In mammals, four ER-phagy receptors have been identified so far: FAM134B [24], RTN3 [25], CCPG1 [26], and SEC62 [27]. Their functions may be different spatiotemporally [9,11,28,29]. FAM134B and RTN3 are important for starvation-

induced degradation of ER sheets and tubules, respectively [24,25]. SEC62 mediates the clearance of excess ER membranes and proteins during the recovery phase of ER stress [27]. CCPG1 is induced during ER stress and activates autophagic degradation of peripheral ER [26]. Phenotypes of mice lacking *Fam134b* and *Ccpg1*, as well as human patients with mutations in *FAM134B*, suggest that FAM134B and CCPG1 are required for homeostasis in peripheral sensory neurons and the pancreas, respectively [24,26,30]. However, other tissues are almost normal or unaffected in the absence of these ER-phagy receptors, and known ER-phagy receptors are required only partially, implying that there might be an unidentified functionally redundant molecule involved.

In this study, to identify the novel selective autophagy substrates or receptors/adaptors, I performed differential interactome analysis using a wild-type (WT) LC3B and a LIR recognition-defective LC3B mutant. One of the identified selective substrates was TEX264. Further analysis revealed that TEX264 is a ubiquitously expressed ER-phagy receptor that contributes most to ER-phagy in mammals. These results suggest that TEX264 is a major ER-phagy receptor.

Materials and Methods

Cell culture

HeLa cells, HEK293T cells, and mouse embryonic fibroblasts (MEFs) were cultured in Dulbecco's modified Eagle's medium (DMEM) (D6546; Sigma-Aldrich) supplemented with 10% fetal bovine serum (FBS) (S1820-500; Biowest) and 2 mM L-glutamine (25030-081; Gibco) in a 5% CO₂ incubator. For the starvation treatment, cells were washed twice with phosphate-buffered saline (PBS) and incubated in amino acid-free DMEM (048-33575; Wako Pure Chemical Industries) without serum. Fip200-WT MEF cells [31] and *FIP200*-KO HeLa cells [32] have been described previously. For the bafilomycin A₁ treatment, cells were cultured with 100 nM bafilomycin A₁ (B1793; Sigma-Aldrich) for 2 h. HeLa cells stably expressing pCW57.1-CMV-ssRFP-GFP-KDEL were cultured with 0.5 µg/mL doxycycline (D3447; Sigma-Aldrich) for 24 h. Thereafter, cells were washed with PBS twice and incubated in DMEM or amino acid-free DMEM without serum for 9 h.

Plasmids

cDNAs encoding human *TEX264* (NP_001230654), *FAM134B* (NP_001030022),

NP_061873.2), *CCPG1* (NP_004739.3), *SEC62* (NP_003253.1), *RTN3* (NP_00125218.1), *SEC61B* [33], cytochrome *b₅* [34], *FIP200* [35], *LC3A* (NP_115903.1), *LC3B* (NP_073729), *LC3C* (NP_001004343), *GABARAP* (NP_009209), *GABARAPL1* (NP_113600), and *GABARAPL2* (NP_009216) were inserted into pMRX-IP [36], pMRX-IN [37], or pMRXIB [37] (these plasmids were generated from pMXs [38]). DNAs encoding enhanced GFP, codon-optimized mRuby3 (modified from pKanCMV-mClover3-mRuby3; 74252; Addgene), and 3×FLAG were also used for tagging. Truncated constructs were prepared by PCR-mediated site-directed mutagenesis. To generate pCW57.1-CMV-ssRFP-GFP-KDEL, the minimal CMV promoter and DNA sequences encoding the signal sequence of BIP and RFP-GFP-KDEL were subcloned into pCW57.1 backbone vector [33]. Single guide RNAs (sgRNAs) targeting *TEX264* (5'-GCTGCCTTGAGGTGCAGTGT-3', 5'-GGAAATCCACAAGTAGCCAT-3'), *FAM134B* (5'-GTCTGACACAGACGTCTCAG-3'), *CCPG1* (5'-TTCTAACTTAGGTGGCTCAA-3'), and *FIP200* (5'-TATGTATTTCTGGTTAACAC-3') were cloned into pSpCas9(BB)-2A-GFP (a gift from Dr. F. Zhang, Broad Institute of Massachusetts Institute of Technology; Addgene #48138).

Antibodies and reagents

For immunoblotting, mouse monoclonal anti-HSP90 (610419; BD Biosciences) and anti-protein disulfide isomerase (PDI) (SPA891; Stressgen) antibodies, rabbit polyclonal anti-LC3 (which recognizes both LC3A and LC3B; [39]), anti-p62 (PM045; MBL), anti-GFP (A6455; Thermo Fisher Scientific), anti-FLAG (F7425; Sigma-Aldrich), anti-FAM134B (21537-1-AP; Proteintech), anti-CCPG1 (13861-1-AP; Proteintech), anti-RTN3 (12055-2-AP; Proteintech), anti-SEC62 (NBP1-84045; Novus), anti-LC3A (4599s; Cell signaling), anti-LC3B (4108s; Cell signaling), anti-LC3C (14736s; Cell signaling), anti-GABARAP (13733s; Cell signaling), anti-GABARAPL1 (ab86497; Abcam), anti-GABARAPL2 (ab126607; Abcam), anti-GRP78 (ab21685; Abcam), anti-PARP (9542s; Cell signaling) anti-RFP (a gift from Dr. T. Endo, Kyoto Sangyo University) antibodies, rat monoclonal anti-HA (11 867 423 001; Roche) antibody, and goat polyclonal anti-cathepsin D (sc-6486; Santa Cruz Biotechnology, Inc.) antibodies were used as primary antibodies. Anti-mouse (111-035-003), anti-goat (305-035-003) and anti-rabbit (111-035-144) horseradish peroxidase (HRP)-conjugated IgGs (Jackson ImmunoResearch Laboratories, Inc.) were used as secondary antibodies.

For immunostaining, mouse monoclonal anti-LC3 (which recognizes mainly LC3A; CTB-LC3-2-IC; Cosmo Bio), rabbit polyclonal anti-FIP200/RB1CC1 (17250-1-AP;

Proteintech), anti-WIP1 (SAB4200400; Sigma-Aldrich), and anti-SEC61 β (15087-1-AP; Proteintech) antibodies and rat monoclonal anti-LAMP1 (ab24245; Abcam) were used as primary antibodies. Alexa Fluor 568-conjugated anti-mouse IgG (A-11004; Thermo Fisher Scientific) and anti-rabbit IgG (A-11011; Thermo Fisher Scientific) antibodies, and Alexa Fluor 660-conjugated anti-rabbit IgG (A-21074; Molecular Probes) antibodies were used as secondary antibodies. Rabbit polyclonal anti-TEX264 (NBP1-89866; Novus), anti-RTN4 (Novus; NB100-56681) and anti-LAMP-1 (ab24170; Abcam) antibodies were used for immunoblotting and immunofluorescence. For transient transfection, Lipofectamine 2000 (11668019; Thermo Fisher Scientific), Fugene HD (VPE2311; Promega), and ViaFect (E4981; Promega) were used according to the manufacturers' instructions.

RNAi

Stealth RNAi oligonucleotides were purchased from Thermo Fisher Scientific. The following sequences were used: human *TEX264* siRNA (antisense, 5'-UGUCAUAGUAGACAGCGAUGGAGCG-3', and sense, 5'-CGCUCCAUCGCUGUCUACUAUGACA-3'); human *FAM134B* siRNA (antisense, 5'- UGCUGAUUGCGUCUCUUUGCUUGGU-3', and sense, 5'-

ACCAAGCAAAGAGACGCAAUCAGCA-3'); human *CCPG1* siRNA (antisense, 5'-UCCAAUAUAGAUACUGUCUUCGGG-3', and sense 5'-CCCGAAGACAGUAUCUAUAUUGGAA-3',); human *RTN3* siRNA (antisense, 5'-AAGAGACGAAUAAUGAGUUUCAGGG-3', and sense, 5'-CCCUGAAACUCAUUAUUCGUCUCUU-3'); and human *SEC62* siRNA (antisense 5'- UAAACACCUACUCUCAUUUCUGCUG-3', and sense 5'-CAGCAGAAAUGAGAGUAGGUGUUUA-3'). The siRNA oligonucleotides for human *FIP200* (antisense, 5'- UUUCUUGGCAACUUCAUACAUUUCC-3'; and sense 5'- GGAAAUGUAUGAAGUUGCCAAGAAA-3'); and luciferase (antisense, 5'-AAUUAAGUCCGCUUCUAAGGUUUC-3'; and sense, 5'-CGCGGUCGGUAAAGUUGUCCAUUU-3') have been previously reported [40]. The stealth RNAi oligonucleotides were transfected into cells using Lipofectamine RNAiMAX (13778150; Thermo Fisher Scientific) according to the manufacturer's instructions. Cells were harvested 3 days after transfection.

Preparation of lentivirus and retrovirus

To prepare the lentivirus, HEK293T cells were transiently transfected with a lentiviral vector together with pCMV-VSV-G (a gift from Dr. R. A. Weinberg, Whitehead

Institute for Biomedical Research) and psPAX2 (a gift from Dr. D. Trono, Ecole Polytechnique Federale de Lausanne) using Lipofectamine 2000 (11668019; Thermo Fisher Scientific) or Fugene HD (VPE2311; Promega). After cells were cultured for 2–3 days, the supernatant was collected and passed through a 0.45- μ m syringe filter unit (SLHV033RB; EMD Millipore). To prepare the retrovirus, HEK293T cells were transiently transfected with a retroviral vector together with pCG-VSV-G and pCG-gag-pol (gifts from Dr. T. Yasui, Osaka University) using Lipofectamine 2000 or Fugene HD, and viral particles were collected from the supernatant as described above.

Generation of stable cell lines

Cells were cultured with retrovirus or lentivirus and 8 μ g/mL polybrene (H9268; Sigma-Aldrich), and stable transformants were selected with puromycin (P8833; Sigma-Aldrich), blasticidin (022-18713; Wako Pure Chemical Industries), or geneticin (10131; Thermo Fisher Scientific).

Establishment of TEX264-KO, FAM134B-KO and CCPG1-KO cells

HeLa cells stably expressing the ER-phagy probe were transfected with pX458 encoding sgRNAs targeting *TEX264*, *FAM134B*, and *CCPG1* using ViaFect (E4981; Promega) or Fugene HD (VPE2311; Promega). Two days after transfection, GFP-positive cells were isolated using a cell sorter (MoFlo Astrios EQ; Beckman Coulter), and single clones were obtained. Clones with mutations in both alleles were identified by immunoblotting and confirmed by sequencing of genomic DNA.

Immunoprecipitation and immunoblotting

Cell lysates were prepared in a lysis buffer (50 mM Tris-HCl, pH 7.5, 150 mM NaCl, 1 mM EDTA, 1% Triton X-100, 1 mM Na₃VO₄, PhosSTOP (4906837001; Roche) and complete EDTA-free protease inhibitor (05056489001; Roche)). After centrifugation at 17,700 × g for 10 min, the supernatants were subjected to immunoprecipitation using anti-FLAG M2 affinity gel (A2220; Sigma-Aldrich). Precipitated immunocomplexes were washed three times in washing buffer (50 mM Tris-HCl, pH 7.5, 150 mM NaCl, 1 mM EDTA, and 1% Triton X-100) and boiled in sample buffer (46.7 mM Tris- HCl, pH 6.8, 5% glycerol, 1.67% sodium dodecyl sulfate, 1.55% dithiothreitol, and 0.02% bromophenol blue). Samples were subsequently separated by sodium dodecyl sulfate polyacrylamide gel electrophoresis and transferred to Immobilon-P polyvinylidene difluoride membranes (IPVH00010; EMD Millipore). Immunoblotting analysis was

performed with the indicated antibodies. Super-Signal West Pico Chemiluminescent Substrate (1856135; Thermo Fisher Scientific) or Immobilon Western Chemiluminescent HRP Substrate (P90715; EMD Millipore) was used to visualize the signals, which were detected on a Fusion System Solo 7S (M&S Instruments Inc.). Contrast and brightness adjustment and quantification were performed using Fiji software (ImageJ; National Institutes of Health [41]) and Photoshop CS6 (Adobe).

Immunocytochemistry

Cells grown on coverslips were washed with PBS and fixed with 4% paraformaldehyde in PBS for 10 min at room temperature or fixed in 100% methanol for 15 min at -30°C . Fixed cells were permeabilized with 50 $\mu\text{g}/\text{mL}$ digitonin (D141; Sigma-Aldrich) in PBS for 5 min, blocked with 3% bovine serum albumin in PBS for 15 min, and then incubated with primary antibodies for 1 h. After washing three times with PBS, cells were incubated with Alexa Fluor 488/568/660-conjugated goat anti-mouse or anti-rabbit IgG secondary antibodies for 1 h. Fluorescence microscopy was performed on a confocal laser microscope (FV1000 IX81; Olympus) with a 100 \times oil-immersion objective lens (1.40 NA; Olympus) and captured with FluoView software (Olympus). The number of punctate structures and the colocalization rate were determined using

Fiji software (ImageJ).

Cell fractionation

Cells from four 10-cm dishes were harvested and washed twice with ice-cold PBS. The cell pellets were collected after centrifugation at $700 \times g$ for 5 min and resuspended in 2 mL ice-cold homogenization buffer (250 mM sucrose, 20 mM HEPES-KOH, pH 7.4, 1 mM EDTA, and complete EDTA-free protease inhibitor). Cells were then disrupted through a narrow-gauge syringe. The homogenized cells were centrifuged twice at $3,000 \times g$ for 10 min to remove cell debris and undisrupted cells. To enrich membrane fraction, the supernatant was centrifuged at $100,000 \times g$ for 60 min. The pellet was suspended with homogenization buffer. For the protease protection assay, each fraction was incubated with and without 100- $\mu\text{g}/\text{mL}$ proteinase K (P6556; Sigma-Aldrich) for 30 min on ice before proceeding to the next step. Proteins in each fraction were isolated by trichloroacetic acid precipitation. The final pellet was suspended in sample buffer and boiled.

Electron microscopy

Cells were cultured on cell-tight C-2 cell disks (MS-0113K; Sumitomo Bakelite) and

fixed in 2.5% glutaraldehyde (G015; TAAB Laboratories Equipment) in 0.1 M phosphate buffer (pH 7.4) for 2 h on ice. The cells were washed with 0.1 M phosphate buffer (pH 7.4) three times, postfixed in 1% osmium tetroxide in 0.1 M phosphate buffer (pH 7.4) for 2 h, dehydrated, and embedded in Epon 812 according to a standard procedure. Ultrathin sections were cut and stained with uranyl acetate and lead citrate and observed using an H-7100 transmission electron microscope (Hitachi).

Mass spectrometry (MS) sample preparation

For differential analysis of WT LC3B and the LC3B^{K51A} mutant-interacting proteins, HEK293 cells transfected with each protein expression plasmid were lysed with lysis buffer (20 mM HEPES-NaOH, pH 7.5, containing 1% digitonin, 150 mM NaCl, 50 mM NaF, 1 mM Na₃VO₄, 5 µg/mL leupeptin, 5 µg/mL aprotinin, 3 µg/mL pepstatin A, and 1 mM phenylmethylsulfonylfluoride) and centrifuged at 20,000 × *g* for 10 min to remove insoluble materials. The supernatants were subjected to immunoprecipitation using anti-FLAG M2 magnetic beads (M8823; Sigma-Aldrich). Precipitated immunocomplexes were washed three times in washing buffer (10 mM Hepes-NaOH, pH 7.5, 150 mM NaCl, and 0.1% Triton X-100) and eluted with FLAG peptides. The samples obtained were subjected to trichloroacetic acid precipitation. The resulting pellets were dissolved in 0.1 M ammonium bicarbonate (pH 8.8) containing 7 M guanidine hydrochloride,

reduced using 5 mM TCEP (tris-(2-carboxyethyl)phosphine; 77720; Thermo Fisher Scientific), and subsequently alkylated using 10 mM iodoacetamide. After alkylation, samples were digested with lysyl-endopeptidase (129-02541; Wako Pure Chemical Industries) for 3 h at 37 °C and then further digested with trypsin (4352157; Sigma-Aldrich) for 14 h at 37 °C.

Liquid chromatography-tandem MS analysis

Digested peptide samples were analyzed using a nanoscale liquid chromatography-tandem MS (MS/MS) system as previously described [42]. The peptide mixture was applied to a Mightysil-PR-18 (Kanto Chemical) frit-less column (45 × 0.150 mm ID) and separated using a 0–40% gradient of acetonitrile containing 0.1% formic acid for 80 min at a flow rate of 100 nL/min. Eluted peptides were sprayed directly into a Triple TOF 5600+ mass spectrometer (Sciex). MS and MS/MS spectra were obtained using the information-dependent mode. Up to 25 precursor ions above an intensity threshold of 50 counts/s were selected for MS/MS analyses from each survey scan. All MS/MS spectra were searched against protein sequences of NCBI nonredundant human protein data set (NCBI RefSeq Release 71, containing 179,460 entries) using the Protein Pilot software package (Sciex). Protein quantification was performed using the iBAQ method

(Schwanhausser et al., 2011) without conversion to absolute amounts using universal proteomics standards (iBQ). The iBQ value was calculated by dividing the sum of the ion intensities of all the identified peptides of each protein by the number of theoretically measurable peptides.

Doxycycline treatment

HeLa cells stably expressing ER-phagy probe were cultured with 0.5 µg/mL doxycycline (D3447; Sigma-Aldrich) for 24 h. Thereafter, cells were washed with PBS twice and incubated in DMEM (D6546; Sigma-Aldrich) supplemented with 10% FBS (S1820-500; Biowest), 2 mM L-glutamine (25030-081; Gibco) or amino acid-free DMEM (048-33575; Wako Pure Chemical Industries) without serum followed by confocal microscopy or biochemical analysis.

Mice

All animal experiments were approved by the Institutional Animal Care and Use Committee of the University of Tokyo. *Atg5^{-/-};NSE-Atg5* mice [43] and *Fip200^{lox/lox};Nestin-Cre* mice [44] have been previously described. To obtain postnuclear supernatants, tissue homogenates were centrifuged at 500 × g for 10 min,

and the supernatants were boiled in sample buffer.

Intrinsically disordered region (IDR) prediction

Amino acid sequences of each protein were obtained from the NCBI protein database.

The disordered regions were predicted using the PSIPRED protein sequence analysis workbench (<http://bioinf.cs.ucl.ac.uk/psipred/>).

Quantification and statistical analysis

Two groups of data were evaluated by unpaired two-tailed Student's *t* test, and multiple comparison tests were performed by one-way analysis of variance (ANOVA) followed by the Sidak's multiple comparison test. The distribution of the data was assumed to be normal, but this was not formally tested.

Results

Differential interactome screening identified TEX264 as a novel LC3B-interacting protein

To identify novel substrates and receptors of selective autophagy, I searched for proteins that interacted with LC3B in a LIR-dependent manner. Because lysine 51 of human LC3B is critical for recognition of the LIR [22], it was expected that selective substrates interact with WT LC3B but not the LC3B^{K51A} mutant. In collaboration with Drs. Natsume and Hatta, immunoprecipitates were obtained using WT LC3B and the LC3B^{K51A} mutant as baits from HEK293T cells and subjected to MS (Figure 3A) [42]. I identified 87 proteins that specifically interacted with WT LC3B but not with LC3B^{K51A} (Table 1). As a positive control, p62 (also known as SQSTM1) was detected as one of the top candidates (Figure 3B). Among these proteins detected by differential interactome screening, we focused on TEX264 because it showed a high binding score and has never been studied in the context of autophagy.

TEX264 was originally identified as a testis-expressing membrane protein and is reported to be highly expressed in colorectal cancer [45-47]. However, the function of TEX264 remains unknown. Immunoprecipitation analysis confirmed that TEX264

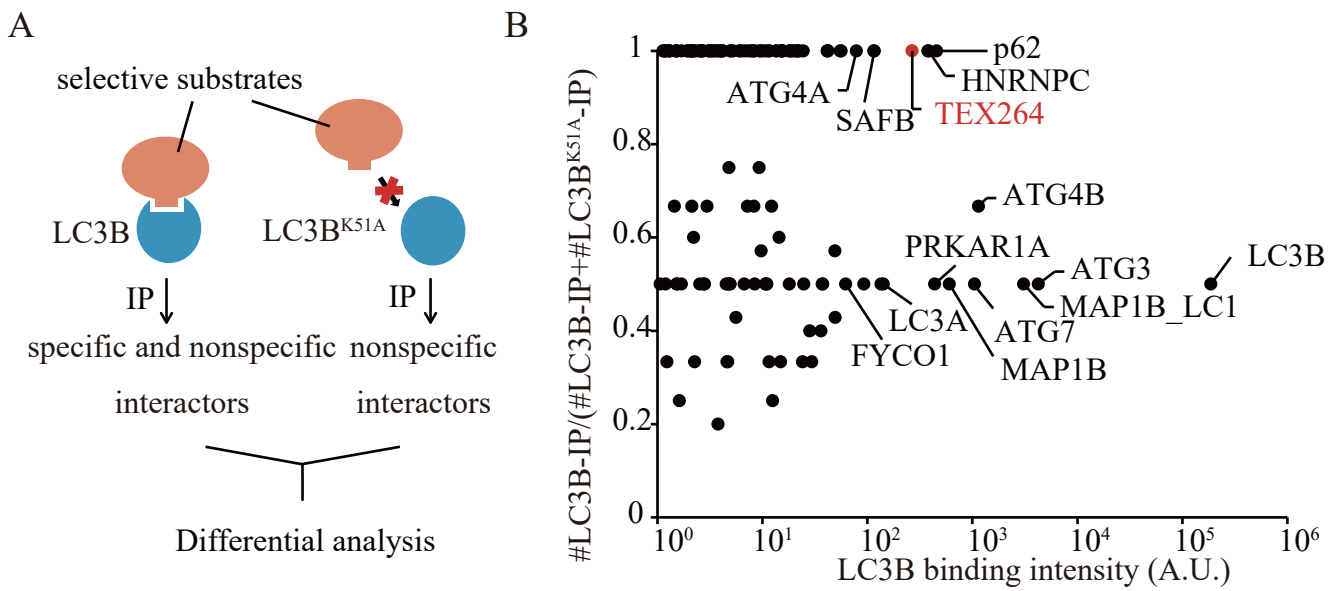


Figure 3. Differential interactome screening identified TEX264 as a novel LC3B-interacting protein

(A) Strategy used to identify selective LC3-interacting proteins.

(B) Results of the differential interactome screening. Four independent immunoprecipitates and MS analyses were conducted with LC3B or LC3B^{K51A} as baits. The X axis represents LC3B binding intensity quantified by iBAQ method. Depending on the bait it interacted with, the total number of times an interacting protein was determined as #LC3B-IP or #LC3B^{K51A}-IP. The #LC3B-IP/(#LC3B-IP + #LC3B^{K51A}-IP) ratio is shown on the Y axis.

Table 1. The results of the screen for LC3B-binding proteins by immunoprecipitation (IP) and mass spectrometry (n=4)

Protein	Description	# of detection in IP		the average of iBQ values	
		LC3B	LC3BK51A	LC3B	LC3BK51A
ABCE1	ATP-binding cassette sub-family E member 1	1	1	6.706127368	3.799612632
ABHD10	mycophenolic acid acyl-glucuronide esterase, mitochondrial; isoform	1	0	6.024635556	n.d.
ABLIM1	actin-binding LIM protein 1; isoform unknown	0	0	n.d.	n.d.
ABP125 SEC31A	NOT mergeable descriptions	0	4	n.d.	2.63228137
ACO2	aconitate hydratase, mitochondrial	0	0	n.d.	n.d.
ACTN1 ACTN2	; alpha-actinin-1 (isoform unknown) or alpha-actinin-2 (isoform unkn	0	0	n.d.	n.d.
ACTN1 ACTN2 ACTN3 ACTN4	; alpha-actinin-1 (isoform unknown) or alpha-actinin-2 (isoform unkn	1	1	1.061082176	2.621896322
ACTN1 ACTN2 ACTN4	; alpha-actinin-1 (isoform unknown) or alpha-actinin-2 (isoform unkn	0	1	n.d.	1.457541657
ACTN1 ACTN3 ACTN4	; alpha-actinin-1 (isoform unknown) or alpha-actinin-3 (isoform unkn	0	0	n.d.	n.d.
AHSG	alpha-2-HS-glycoprotein	0	0	n.d.	n.d.
AKAP11	A-kinase anchor protein 11; isoform unknown	4	0	15.39410701	n.d.
ALDH7A1	alpha-aminoacidic semialdehyde dehydrogenase; isoform unknown	0	1	n.d.	3.921801471
ALYREF	THO complex subunit 4; isoform unknown	2	0	55.07351744	n.d.
ANKFY1	rabankyrin-5; isoform unknown	3	4	5.58711203	6.516301128
ANP32A	acidic leucine-rich nuclear phosphoprotein 32 family member A; isofo	0	0	n.d.	n.d.
ANXA5	annexin A5	0	0	n.d.	n.d.
AP1B1 AP2B1	; AP-1 complex subunit beta-1 (isoform unknown) or AP-2 complex	0	0	n.d.	n.d.
AP2M1	AP-2 complex subunit mu; isoform unknown	0	1	n.d.	2.276173256
AP3M1 AP3M2	AP-3 complex subunit; mu-1 (isoform unknown) or mu-2	1	0	8.238856203	n.d.
ARHGEF18	rho guanine nucleotide exchange factor 18; isoform unknown	0	0	n.d.	n.d.
ARMCX5-GPRASP2	G-protein coupled receptor-associated sorting protein 2	1	0	1.500416327	n.d.
ATAD3A ATAD3C	ATPase family AAA domain-containing protein; 3A (isoform unknown)	0	0	n.d.	n.d.
ATG12	ubiquitin-like protein ATG12; isoform unknown	1	0	20.134696	n.d.
ATG16L1	autophagy-related protein 16-1; isoform unknown	4	0	7.233362731	n.d.
ATG2A	autophagy-related protein 2 homolog A; isoform unknown	1	0	2.124317297	n.d.
ATG3	ubiquitin-like-conjugating enzyme ATG3; isoform unknown	4	4	4237.627281	1328.681566
ATG4A	cysteine protease ATG4A; isoform unknown	4	0	78.55149318	n.d.
ATG4B	cysteine protease ATG4B; isoform unknown	4	2	1143.29078	54.65454412
ATG5	autophagy protein 5	4	0	7.729194737	n.d.
ATG7	ubiquitin-like modifier-activating enzyme ATG7; isoform unknown	2	4	1048.171839	529.6997898
ATP2A1 ATP2A2 ATP2A3	sarcoplasmic/endoplasmic reticulum calcium ATPase; 1 (isoform ur	0	0	n.d.	n.d.
ATP2A2	sarcoplasmic/endoplasmic reticulum calcium ATPase 2; isoform un	0	1	n.d.	4.186889167
ATP51	ATP synthase subunit e, mitochondrial	1	1	92.2215	77.80005556
ATP5L	ATP synthase subunit g, mitochondrial	4	4	134.5669578	96.95037031
ATP6AP2	renin receptor	1	0	4.187418421	n.d.
ATP6V1A ATP6V1A2	; ATPase, H ⁺ transporting, lysosomal 70kD, V1 subunit A, isoform 2	0	0	n.d.	n.d.
ATP6V1E1 ATP6V1E2	V-type proton ATPase subunit E; 1 (isoform unknown) or 2 (isoform	0	0	n.d.	n.d.
ATP6V1F	V-type proton ATPase subunit F; isoform AP17 or 7 precursor or hE	1	3	12.48008636	13.75677576
BABAM1	BRIS and BRCA1-A complex member 1; isoform unknown	1	0	3.991866667	n.d.
BAG6	large proline-rich protein BAG6; isoform unknown	0	1	n.d.	3.12196087
BCAP31	B-cell receptor-associated protein 31; isoform unknown	0	3	n.d.	11.22825455
BICD1 BICD2	protein bicaudal D homolog; 1 (isoform unknown) or 2 (isoform unkn	0	0	n.d.	n.d.
BLK CDK20 FGFR1 FGFR2 FGFR3	NOT mergeable descriptions	0	0	n.d.	n.d.
BRCC3	lys-63-specific deubiquitinase BRCC36; isoform unknown	0	0	n.d.	n.d.
BSDC1	BSD domain-containing protein 1; isoform unknown	0	0	n.d.	n.d.
BSG	basigin; isoform unknown	0	0	n.d.	n.d.
BTF3	transcription factor BTF3; isoform unknown	0	0	n.d.	n.d.
BUB3	mitotic checkpoint protein BUB3; isoform unknown	0	0	n.d.	n.d.
C19orf43	uncharacterized protein C19orf43	0	0	n.d.	n.d.
CALD1 LOC55873	NOT mergeable descriptions	0	1	n.d.	1.010196961
CAMK2A CAMK2B CAMK2D	calcium/calmodulin-dependent protein kinase type II subunit; alpha	0	0	n.d.	n.d.
CAPZA1 CAPZA2	F-actin-capping protein subunit; alpha-1 or alpha-2	0	2	n.d.	32.88794265
CAPZA2	F-actin-capping protein subunit alpha-2	0	0	n.d.	n.d.
CBR1	carbonyl reductase [NADPH] 1; isoform unknown	0	0	n.d.	n.d.
CBX3 HECH	NOT mergeable descriptions	0	1	n.d.	11.5067
CDC27	cell division cycle protein 27 homolog; isoform unknown	1	0	3.048882353	n.d.
CDC27 RPS2 RPS2P31 RPS2P40	NOT mergeable descriptions	3	2	14.40355911	17.22033704
CDK1 CDK12 CDK13 CDK14 CDK15	; cyclin-dependent kinase 12 (isoform unknown) or cyclin-dependent	2	0	11.63942203	n.d.
CDK5RAP3	CDK5 regulatory subunit-associated protein 3; isoform unknown	1	4	3.776024638	282.654371
CLASP1 CLASP2	CLIP-associating protein; 1 (isoform unknown) or 2 (isoform unknow	0	1	n.d.	1.128555753
CLEC2D NPM1	NOT mergeable descriptions	0	1	n.d.	3.862985343
CLPB	caseinolytic peptidase B protein homolog; isoform unknown	0	1	n.d.	1.638372656
COPS3	COP9 signalosome complex subunit 3; isoform unknown	0	2	n.d.	20.22126518
COPS6	COP9 signalosome complex subunit 6	3	1	9.330477778	11.90574242
COPS8	COP9 signalosome complex subunit 8; isoform unknown	0	0	41.9995	n.d.
COX2	cytochrome c oxidase II [Homo sapiens ssp. Denisova]	1	1	n.d.	19.16342
COX6C	cytochrome c oxidase subunit 6C	0	0	n.d.	n.d.
CSF1R MAPK4 MAPK6 ROS1	NOT mergeable descriptions	2	1	8.28510478	10.84099081
CSNK1A1	casein kinase I isoform alpha; isoform unknown	1	0	9.593538235	n.d.
CSNK2B	casein kinase II subunit beta; isoform unknown	0	0	n.d.	n.d.
CSTF2 CSTF2T	cleavage stimulation factor subunit 2; or tau variant	0	2	n.d.	3.6401312
CTCF HMGB1 HMGB1P40 HMGB	NOT mergeable descriptions	0	0	n.d.	n.d.
CTR9	RNA polymerase-associated protein CTR9 homolog	1	0	1.2767625	n.d.
CTSA	lysosomal protective protein; isoform unknown	0	0	n.d.	n.d.
CYFIP1	cytoplasmic FMR1-interacting protein 1; isoform unknown	0	0	n.d.	n.d.
CYFIP1 CYFIP2	cytoplasmic FMR1-interacting protein; 1 (isoform unknown) or 2	0	0	n.d.	n.d.
DAXX	death domain-associated protein 6; isoform unknown	1	0	2.702658889	n.d.
DCTN4	dynactin subunit 4; isoform unknown	0	2	n.d.	9.01359375
DDRGK1	DDRGK domain-containing protein 1	0	4	n.d.	353.4548768
DDX39A DDX39B	; ATP-dependent RNA helicase DDX39A (isoform unknown) or splice	1	0	10.12259144	n.d.
DHDDS	dehydrodolichyl diphosphate syntase complex subunit DHDDS; isofo	1	0	2.215307273	n.d.
DHX40	probable ATP-dependent RNA helicase DHX40; isoform unknown	0	0	n.d.	n.d.
DIAPH1	protein diaphanous homolog 1; isoform unknown	0	3	n.d.	1.798305035
DIAPH3	protein diaphanous homolog 3; isoform unknown	0	0	n.d.	n.d.
DNAJA2	dnad homolog subfamily A member 2	0	0	n.d.	n.d.
DNAJC14 LOC100131859 SARNP	NOT mergeable descriptions	0	0	n.d.	n.d.
DNAJC14 SARNP	NOT mergeable descriptions	0	1	n.d.	2.518367229
EEF1A1	elongation factor 1-alpha 1	0	0	n.d.	n.d.
EIF2AK3	eukaryotic translation initiation factor 2-alpha kinase 3	0	1	n.d.	1.508394483
EIF2B EIF2B4	translation initiation factor; eIF-2B subunit delta (isoform unknown) c	0	0	n.d.	n.d.
EIF2B3	translation initiation factor eIF-2B subunit gamma; isoform unknown	1	0	3.394747222	n.d.

EIF4A3	eukaryotic initiation factor 4A-III	0	1	n.d.	5.233531429
ELP2	elongator complex protein 2; isoform unknown	0	1	n.d.	2.315169388
EMC1	ER membrane protein complex subunit 1	2	2	1.189878226	1.410652016
EMC8	ER membrane protein complex subunit 8; isoform 1	1	1	37.1842	36.53890833
EPS15L1	epidermal growth factor receptor substrate 15-like 1; isoform unknown	0	1	n.d.	2.20071875
ERBB2IP	protein LAP2; isoform unknown	0	0	n.d.	n.d.
ERC2	ERC protein 2; isoform unknown	0	1	n.d.	1.329307576
ERCC6L	DNA excision repair protein ERCC-6-like	0	1	n.d.	1.716542222
ERP44	endoplasmic reticulum resident protein 44	0	1	n.d.	8.192276923
EXOC3	exocyst complex component 3; isoform unknown	0	1	n.d.	2.770462609
EXOC7	exocyst complex component 7; isoform unknown	0	0	n.d.	n.d.
FAM126A	hyccin; isoform unknown	0	0	n.d.	n.d.
FAR1	fatty acyl-CoA reductase 1	2	1	2.12127125	4.15157375
FARSB	phenylalanine--tRNA ligase beta subunit; isoform unknown	0	1	n.d.	2.620011236
FBXO20 LMO7	only protein family	1	1	4.911797849	3.485895762
FBXO21	F-box only protein 21; isoform unknown	0	0	n.d.	n.d.
FHL1	four and a half LIM domains protein 1; isoform unknown	0	0	n.d.	n.d.
FKBP15	FK506-binding protein 15; isoform unknown	0	0	n.d.	n.d.
FKBP8	peptidyl-prolyl cis-trans isomerase FKBP8; isoform unknown	1	0	3.705791379	n.d.
FLJ90311 MTMR14	myotubularin-related protein 14#isoform 1 family	4	3	49.00639793	42.09856844
FLNA FLNB	; filamin-A (isoform unknown) or filamin-B (isoform unknown)	3	1	4.806316531	1.350681355
FYCO1	FYVE and coiled-coil domain-containing protein 1; isoform unknown	4	4	62.15581656	3.110996688
GABARAPL2	gamma-aminobutyric acid receptor-associated protein-like 2	0	1	n.d.	18.191584
GAPVD1	GTPase-activating protein and VPS9 domain-containing protein 1; isoform unknown	0	1	n.d.	1.603805389
GATAD2A	transcriptional repressor p66-alpha; isoform unknown	1	1	1.523167619	2.248185714
GBAS	protein NipSnap homolog 2; isoform unknown	3	0	56.31691733	n.d.
GBF1	Golgi-specific brefeldin A-resistance guanine nucleotide exchange factor 1	2	2	1.530810329	0.955067136
GCG	glucagon	0	1	n.d.	62.57207843
GFAP VIM	NOT mergeable descriptions	0	0	n.d.	n.d.
GKLP SCYL1	NOT mergeable descriptions	4	0	8.433262979	n.d.
GLB1	beta-galactosidase; isoform unknown	0	0	n.d.	n.d.
GNAI1 GNAI2 GNAI3 GNAL GNAO1	; guanine nucleotide-binding protein G(i) subunit alpha-1 (isoform unknown)	0	2	n.d.	6.064870855
GPHN	gephyrin; isoform unknown	1	0	3.933644898	n.d.
HAT1	histone acetyltransferase type B catalytic subunit; isoform unknown	0	0	n.d.	n.d.
HAUS4	HAUS augmin-like complex subunit 4; isoform unknown	0	0	n.d.	n.d.
HAUS6	HAUS augmin-like complex subunit 6; isoform unknown	0	1	n.d.	1.015556944
HEATR3	HEAT repeat-containing protein 3; isoform unknown	1	0	1.161607143	n.d.
HIST1H1A HIST1H1B HIST1H1C HIST1H1D HIST1H1E HIST1H1F HIST1H1G HIST1H1H HIST1H1I HIST1H1J HIST1H1K HIST1H1L HIST1H1M HIST1H1N HIST1H1O HIST1H1P HIST1H1Q HIST1H1R HIST1H1S HIST1H1T HIST1H1U HIST1H1V HIST1H1W HIST1H1X HIST1H1Y HIST1H1Z	histone: H1.1 or H1.5 or H1.2 or H1.3 or H1.4 or H1t	2	1	7.181436581	8.392321318
HIST1H4C HIST1H4E HIST1H4I HIST1H4J HIST1H4K HIST1H4L HIST1H4M HIST1H4N HIST1H4O HIST1H4P HIST1H4Q HIST1H4R HIST1H4S HIST1H4T HIST1H4U HIST1H4V HIST1H4W HIST1H4X HIST1H4Y HIST1H4Z	histone H4	0	0	n.d.	n.d.
HNI	hematological and neurological expressed 1 protein; isoform unknown	0	0	n.d.	n.d.
HNRNPA1 HNRNPA1L2 HNRNPA3	heterogeneous nuclear ribonucleoprotein; A1-like 2 or A1 (isoform unknown)	0	1	n.d.	17.35457211
HNRNPC HNRNPCL1 HNRNPCL2	heterogeneous nuclear ribonucleoprotein C-like 1 or ribonucleoprotein C-like 2	3	0	377.8780579	n.d.
HNRNPCL1 HNRNPCL2	heterogeneous nuclear ribonucleoprotein C-like 1 or ribonucleoprotein C-like 2	2	0	384.0713585	n.d.
HNRNPR	heterogeneous nuclear ribonucleoprotein R; isoform unknown	1	0	1.944320536	n.d.
HNRNPUL1	heterogeneous nuclear ribonucleoprotein U-like protein 1; isoform unknown	2	1	12.28001034	7.972155172
HSP90AA1 HSP90AB1 HSP90AB3	heat shock protein; HSP 90-alpha (isoform unknown) or HSP 90-beta	2	0	18.51908497	n.d.
HSP90AB1 HSP90AB6P	heat shock protein; HSP 90-beta (isoform unknown) or 90kDa alpha	0	0	n.d.	n.d.
HSP90AB4P	heat shock protein 90kDa alpha (cytosolic), class B member 4,	0	1	n.d.	24.6790338
HSPA1L	heat shock 70 kDa protein 1-like; isoform unknown	1	0	3.628136364	n.d.
HSPA2 HSPA8 HSPA8P8	heat shock-related 70 kDa protein 2 or shock cognate 71 kDa protein	0	1	n.d.	5.5997999
HSPA8 HSPA8P20	heat shock; 70kDa protein 8 pseudogene 20 or cognate 71 kDa protein	0	1	n.d.	12.77101787
HUGT2 UGGT2##UDP-glucose	glycoprotein glucosyltransferase 2 family	0	1	n.d.	54.13967828
IMPDH1	inosine-5'-monophosphate dehydrogenase 1; isoform unknown	0	1	n.d.	3.147955405
IMPDH1 IMPDH2	inosine-5'-monophosphate dehydrogenase; 1 (isoform unknown) or 2	0	0	n.d.	n.d.
IPO7 IPO8	; importin-7 or importin-8 (isoform unknown)	0	0	n.d.	n.d.
IRGQ	immunity-related GTPase family Q protein; isoform unknown	2	0	17.88694388	n.d.
KATNA1	katanin p60 ATPase-containing subunit A1; isoform unknown	0	0	n.d.	n.d.
KHDRBS1 KHDRBS2	KH domain-containing, RNA-binding, signal; transduction-associated	0	0	n.d.	n.d.
KIF4A	chromosome-associated kinesin KIF4A	0	0	n.d.	n.d.
KLC1	kinesin light chain 1; isoform unknown	2	2	1.689965891	1.066465891
KMT2A SEPT6	NOT mergeable descriptions	0	1	n.d.	0.912118801
KPNA3	importin subunit alpha-4	1	2	4.676561905	5.809394048
KPNA3 KPNA4	importin subunit; alpha-4 or alpha-3	1	0	9.377129524	n.d.
KPNA5 KPNA6	importin subunit; alpha-6 (isoform unknown) or alpha-7 (isoform unknown)	1	0	2.151574464	n.d.
KRT1 KRT2	keratin, type II cytoskeletal; 1 or 2 epidermal	0	0	n.d.	n.d.
KRT1 KRT2 KRT5 KRT6A KRT6B KRT6C KRT6D KRT6E KRT6F KRT6G KRT6H KRT6I KRT6J KRT6K KRT6L KRT6M KRT6N KRT6O KRT6P KRT6Q KRT6R KRT6S KRT6T KRT6U KRT6V KRT6W KRT6X KRT6Y KRT6Z	keratin, type II cytoskeletal 1 or keratin, type II cytoskeletal 2 epidermal	0	0	n.d.	n.d.
KRT1 KRT2 KRT7	keratin, type II cytoskeletal; 1 or 2 epidermal or 1b	0	2	n.d.	1.603344718
KRT10	keratin, type I cytoskeletal 10; isoform unknown	1	1	2.531169444	5.310897222
KRT2	keratin, type II cytoskeletal 2 epidermal	1	0	4.073948352	n.d.
KRT9	keratin, type I cytoskeletal 9	0	2	n.d.	82.72447761
LBR	lamin-B receptor; isoform unknown	0	0	n.d.	n.d.
LETM1	LETM1 and EF-hand domain-containing protein 1, mitochondrial; isoform unknown	1	2	1.228255906	1.535880709
LINC00176	long intergenic non-protein coding RNA 176	0	0	n.d.	n.d.
LMO7	LIM domain only protein 7; isoform unknown	1	4	0.622093976	0.841398569
LOC100128744 RPL18	NOT mergeable descriptions	1	0	5.273425227	n.d.
LOC100996643 LOC101928195 LOC101928196 LOC101928197 LOC101928198 LOC101928199 LOC101928200 LOC101928201 LOC101928202 LOC101928203 LOC101928204 LOC101928205 LOC101928206 LOC101928207 LOC101928208 LOC101928209 LOC101928210 LOC101928211 LOC101928212 LOC101928213 LOC101928214 LOC101928215 LOC101928216 LOC101928217 LOC101928218 LOC101928219 LOC101928220 LOC101928221 LOC101928222 LOC101928223 LOC101928224 LOC101928225 LOC101928226 LOC101928227 LOC101928228 LOC101928229 LOC101928230 LOC101928231 LOC101928232 LOC101928233 LOC101928234 LOC101928235 LOC101928236 LOC101928237 LOC101928238 LOC101928239 LOC101928240 LOC101928241 LOC101928242 LOC101928243 LOC101928244 LOC101928245 LOC101928246 LOC101928247 LOC101928248 LOC101928249 LOC101928250 LOC101928251 LOC101928252 LOC101928253 LOC101928254 LOC101928255 LOC101928256 LOC101928257 LOC101928258 LOC101928259 LOC101928260 LOC101928261 LOC101928262 LOC101928263 LOC101928264 LOC101928265 LOC101928266 LOC101928267 LOC101928268 LOC101928269 LOC101928270 LOC101928271 LOC101928272 LOC101928273 LOC101928274 LOC101928275 LOC101928276 LOC101928277 LOC101928278 LOC101928279 LOC101928280 LOC101928281 LOC101928282 LOC101928283 LOC101928284 LOC101928285 LOC101928286 LOC101928287 LOC101928288 LOC101928289 LOC101928290 LOC101928291 LOC101928292 LOC101928293 LOC101928294 LOC101928295 LOC101928296 LOC101928297 LOC101928298 LOC101928299 LOC101928300 LOC101928301 LOC101928302 LOC101928303 LOC101928304 LOC101928305 LOC101928306 LOC101928307 LOC101928308 LOC101928309 LOC101928310 LOC101928311 LOC101928312 LOC101928313 LOC101928314 LOC101928315 LOC101928316 LOC101928317 LOC101928318 LOC101928319 LOC101928320 LOC101928321 LOC101928322 LOC101928323 LOC101928324 LOC101928325 LOC101928326 LOC101928327 LOC101928328 LOC101928329 LOC101928330 LOC101928331 LOC101928332 LOC101928333 LOC101928334 LOC101928335 LOC101928336 LOC101928337 LOC101928338 LOC101928339 LOC101928340 LOC101928341 LOC101928342 LOC101928343 LOC101928344 LOC101928345 LOC101928346 LOC101928347 LOC101928348 LOC101928349 LOC101928350 LOC101928351 LOC101928352 LOC101928353 LOC101928354 LOC101928355 LOC101928356 LOC101928357 LOC101928358 LOC101928359 LOC101928360 LOC101928361 LOC101928362 LOC101928363 LOC101928364 LOC101928365 LOC101928366 LOC101928367 LOC101928368 LOC101928369 LOC101928370 LOC101928371 LOC101928372 LOC101928373 LOC101928374 LOC101928375 LOC101928376 LOC101928377 LOC101928378 LOC101928379 LOC101928380 LOC101928381 LOC101928382 LOC101928383 LOC101928384 LOC101928385 LOC101928386 LOC101928387 LOC101928388 LOC101928389 LOC101928390 LOC101928391 LOC101928392 LOC101928393 LOC101928394 LOC101928395 LOC101928396 LOC101928397 LOC101928398 LOC101928399 LOC101928400 LOC101928401 LOC101928402 LOC101928403 LOC101928404 LOC101928405 LOC101928406 LOC101928407 LOC101928408 LOC101928409 LOC101928410 LOC101928411 LOC101928412 LOC101928413 LOC101928414 LOC101928415 LOC101928416 LOC101928417 LOC101928418 LOC101928419 LOC101928420 LOC101928421 LOC101928422 LOC101928423 LOC101928424 LOC101928425 LOC101928426 LOC101928427 LOC101928428 LOC101928429 LOC101928430 LOC101928431 LOC101928432 LOC101928433 LOC101928434 LOC101928435 LOC101928436 LOC101928437 LOC101928438 LOC101928439 LOC101928440 LOC101928441 LOC101928442 LOC101928443 LOC101928444 LOC101928445 LOC101928446 LOC101928447 LOC101928448 LOC101928449 LOC101928450 LOC101928451 LOC101928452 LOC101928453 LOC101928454 LOC101928455 LOC101928456 LOC101928457 LOC101928458 LOC101928459 LOC101928460 LOC101928461 LOC101928462 LOC101928463 LOC101928464 LOC101928465 LOC101928466 LOC101928467 LOC101928468 LOC101928469 LOC101928470 LOC101928471 LOC101928472 LOC101928473 LOC101928474 LOC101928475 LOC101928476 LOC101928477 LOC101928478 LOC101928479 LOC101928480 LOC101928481 LOC101928482 LOC101928483 LOC101928484 LOC101928485 LOC101928486 LOC101928487 LOC101928488 LOC101928489 LOC101928490 LOC101928491 LOC101928492 LOC101928493 LOC101928494 LOC101928495 LOC101928496 LOC101928497 LOC101928498 LOC101928499 LOC101928500 LOC101928501 LOC101928502 LOC101928503 LOC101928504 LOC101928505 LOC101928506 LOC101928507 LOC101928508 LOC101928509 LOC101928510 LOC101928511 LOC101928512 LOC101928513 LOC101928514 LOC101928515 LOC101928516 LOC101928517 LOC101928518 LOC101928519 LOC101928520 LOC101928521 LOC101928522 LOC101928523 LOC101928524 LOC101928525 LOC101928526 LOC101928527 LOC101928528 LOC101928529 LOC101928530 LOC101928531 LOC101928532 LOC101928533 LOC101928534 LOC101928535 LOC101928536 LOC101928537 LOC101928538 LOC101928539 LOC101928540 LOC101928541 LOC101928542 LOC101928543 LOC101928544 LOC101928545 LOC101928546 LOC101928547 LOC101928548 LOC101928549 LOC101928550 LOC101928551 LOC101928552 LOC101928553 LOC101928554 LOC101928555 LOC101928556 LOC101928557 LOC101928558 LOC101928559 LOC101928560 LOC101928561 LOC101928562 LOC101928563 LOC101928564 LOC101928565 LOC101928566 LOC101928567 LOC101928568 LOC101928569 LOC101928570 LOC101928571 LOC101928572 LOC101928573 LOC101928574 LOC101928575 LOC101928576 LOC101928577 LOC101928578 LOC101928579 LOC101928580 LOC101928581 LOC101928582 LOC101928583 LOC101928584 LOC101928585 LOC101928586 LOC101928587 LOC101928588 LOC101928589 LOC101928590 LOC101928591 LOC101928592 LOC101928593 LOC101928594 LOC101928595 LOC101928596 LOC101928597 LOC101928598 LOC101928599 LOC101928600 LOC101928601 LOC101928602 LOC101928603 LOC101928604 LOC101928605 LOC101928606 LOC101928607 LOC101928608 LOC101928609 LOC101928610 LOC101928611 LOC101928612 LOC101928613 LOC101928614 LOC101928615 LOC101928616 LOC101928617 LOC101928618 LOC101928619 LOC101928620 LOC101928621 LOC101928622 LOC101928623 LOC101928624 LOC101928625 LOC101928626 LOC101928627 LOC101928628 LOC101928629 LOC101928630 LOC101928631 LOC101928632 LOC101928633 LOC101928634 LOC101928635 LOC101928636 LOC101928637 LOC101928638 LOC101928639 LOC101928640 LOC101928641 LOC101928642 LOC101928643 LOC101928644 LOC101928645 LOC101928646 LOC101928647 LOC101928648 LOC101928649 LOC101928650 LOC101928651 LOC101928652 LOC101928653 LOC101928654 LOC101928655 LOC101928656 LOC101928657 LOC101928658 LOC101928659 LOC101928660 LOC101928661 LOC101928662 LOC101928663 LOC101928664 LOC101928665 LOC101928666 LOC101928667 LOC101928668 LOC101928669 LOC101928670 LOC101928671 LOC101928672 LOC101928673 LOC101928674 LOC101928675 LOC101928676 LOC101928677 LOC101928678 LOC101928679 LOC101928680 LOC101928681 LOC101928682 LOC101928683 LOC101928684 LOC101928685 LOC101928686 LOC101928687 LOC101928688 LOC101928689 LOC101928690 LOC101928691 LOC101928692 LOC101928693 LOC101928694 LOC101928695 LOC101928696 LOC101928697 LOC101928698 LOC101928699 LOC101928700 LOC101928701 LOC101928702 LOC101928703 LOC101928704 LOC101928705 LOC101928706 LOC101928707 LOC101928708 LOC101928709 LOC101928710 LOC101928711 LOC101928712 LOC101928713 LOC101928714 LOC101928715 LOC101928716 LOC101928717 LOC101928718 LOC101928719 LOC101928720 LOC101928721 LOC101928722 LOC101928723 LOC101928724 LOC101928725 LOC101928726 LOC101928727 LOC101928728 LOC101928729 LOC101928730 LOC101928731 LOC101928732 LOC101928733 LOC101928734 LOC101928735 LOC101928736 LOC101928737 LOC101928738 LOC101928739 LOC101928740 LOC101928741 LOC101928742 LOC101928743 LOC101928744 LOC101928745 LOC101928746 LOC101928747 LOC101928748 LOC101928749 LOC101928750 LOC101928751 LOC101928752 LOC101928753 LOC101928754 LOC101928755 LOC101928756 LOC101928757 LOC101928758 LOC101928759 LOC101928760 LOC101928761 LOC101928762 LOC101928763 LOC101928764 LOC101928765 LOC101928766 LOC101928767 LOC101928768 LOC101928769 LOC101928770 LOC101928771 LOC101928772 LOC101928773 LOC101928774 LOC101928775 LOC101928776 LOC101928777 LOC101928778 LOC101928779 LOC101928780 LOC101928781 LOC101928782 LOC101928783 LOC101928784 LOC101928785 LOC101928786 LOC101928787 LOC101928788 LOC101928789 LOC101928790 LOC101928791 LOC101928792 LOC101928793 LOC101928794 LOC101928795 LOC101928796 LOC101928797 LOC101928798 LOC101928799 LOC101928800 LOC101928801 LOC101928802 LOC101928803 LOC101928804 LOC101928805 LOC101928806 LOC101928807 LOC101928808 LOC101928809 LOC101928810 LOC101928811 LOC101928812 LOC101928813 LOC101928814 LOC101928815 LOC101928816 LOC101928817 LOC101928818					

MGC9042 STT3A	dolichyl-diphosphooligosaccharide--protein glycosyltransferase#iso	0	1	n.d.	2.295120475
MMGT1	membrane magnesium transporter 1	0	0	n.d.	n.d.
MRPL28	39S ribosomal protein L28, mitochondrial; isoform unknown	0	0	n.d.	n.d.
MRPS2	28S ribosomal protein S2, mitochondrial; isoform unknown	0	0	n.d.	n.d.
MRPS35	28S ribosomal protein S35, mitochondrial; isoform unknown	0	1	n.d.	5.714742623
MTHFD1	C-1-tetrahydrofolate synthase, cytoplasmic	1	3	1.614178912	2.230583447
MTMR1	myotubularin-related protein 1; isoform unknown	0	1	n.d.	1.751838614
MYH10 MYH11	; myosin-10 (isoform unknown) or myosin-11 (isoform unknown)	2	4	2.252538344	2.542827952
MYH10 MYH11 MYH14 MYH9	; myosin-10 (isoform unknown) or myosin-11 (isoform unknown) or m	1	2	4.584422663	6.050188307
NAA15 NAA16	N-alpha-acetyltransferase; 15, NatA auxiliary subunit (isoform unkno	1	0	0.550492826	n.d.
NAP1L4	nucleosome assembly protein 1-like 4	0	1	n.d.	7.014864151
NBAS	neuroblastoma-amplified sequence	1	0	0.851480198	n.d.
NBR1	next to BRCA1 gene 1 protein; isoform unknown	0	1	n.d.	1.597543023
NCKAP1	nck-associated protein 1; isoform unknown	0	0	n.d.	n.d.
NCLN	nicalin; isoform unknown	0	0	n.d.	n.d.
NDUFA13	NADH dehydrogenase [ubiquinone] 1 alpha subcomplex subunit 13	0	0	n.d.	n.d.
NDUFA8	NADH dehydrogenase [ubiquinone] 1 alpha subcomplex subunit 8;	0	0	n.d.	n.d.
NDUFB10	NADH dehydrogenase [ubiquinone] 1 beta subcomplex subunit 10	0	0	n.d.	n.d.
NDUFB3	NADH dehydrogenase [ubiquinone] 1 beta subcomplex subunit 3; i	0	1	n.d.	22.90312
NEK5	serine/threonine-protein kinase Nek5; isoform unknown	0	0	n.d.	n.d.
NEK9 Nek8	kinase family	2	0	13.65608594	n.d.
NELFE	negative elongation factor E; isoform unknown	0	1	n.d.	2.821868605
NHP2L1	NHP2-like protein 1; isoform unknown	0	1	n.d.	4.123013208
NOLC1	nucleolar and coiled-body phosphoprotein 1; isoform unknown	2	0	2.307198551	n.d.
NONO SFPQ	NOT mergeable descriptions	0	0	n.d.	n.d.
NRD1	nardilysin; isoform unknown	0	1	n.d.	1.260514388
NSMAF	protein FAN; isoform unknown	4	0	15.16419159	n.d.
NUP133	nuclear pore complex protein Nup133	0	0	n.d.	n.d.
ORC4	origin recognition complex subunit 4; isoform unknown	0	1	n.d.	2.315527692
OSIL SQSTM1	NOT mergeable descriptions	4	0	116.4578143	n.d.
PAAF1	proteasomal ATPase-associated factor 1; isoform unknown	0	0	n.d.	n.d.
PABP3 PABPC1 PABPC1P2 PABP	; testis-specific poly(A)-binding protein 3 or poly(A) binding protein,	1	0	2.70562777	n.d.
PABP3 PABPC1 PABPC3	; testis-specific poly(A)-binding protein 3 or polyadenylate-binding p	1	1	4.913710044	3.47125571
PAF1	RNA polymerase II-associated factor 1 homolog; isoform unknown	0	1	n.d.	4.20136988
PCCB	propionyl-CoA carboxylase beta chain, mitochondrial; isoform unknow	0	0	n.d.	n.d.
PCNP	PEST proteolytic signal-containing nuclear protein	0	1	n.d.	6.552694737
PDCL	phosducin-like protein	1	0	4.989746809	n.d.
PDIA3	protein disulfide-isomerase A3	3	3	4.710313095	3.603873016
PDZD8	PDZ domain-containing protein 8; isoform unknown	1	0	1.30049759	n.d.
PEF1	pefflin	1	0	13.47402273	n.d.
PEX14	peroxisomal membrane protein PEX14; isoform unknown	0	1	n.d.	6.428028947
PFDN2	prefoldin subunit 2	1	0	10.87058125	n.d.
PFDN4	prefoldin subunit 4	0	0	n.d.	n.d.
PFDN6	prefoldin subunit 6	0	1	n.d.	9.3541
PGK1 PGK2	phosphoglycerate kinase; 1 or 2	0	2	n.d.	3.306910177
PGRMC1	membrane-associated progesterone receptor component 1; isoform	0	0	n.d.	n.d.
POLA2	DNA polymerase alpha subunit B	0	0	n.d.	n.d.
POLR2G	DNA-directed RNA polymerase II subunit RPB7	0	0	n.d.	n.d.
POLR3A	DNA-directed RNA polymerase III subunit RPC1; isoform unknown	0	1	n.d.	0.517848261
PPP1CB	serine/threonine-protein phosphatase PP1-beta catalytic subunit;	0	0	n.d.	n.d.
PPP1CC	serine/threonine-protein phosphatase PP1-gamma catalytic subun	1	0	2.619826	n.d.
PPP4C	serine/threonine-protein phosphatase 4 catalytic subunit; isoform u	0	1	n.d.	16.76592973
PRDX5	peroxiredoxin-5, mitochondrial; isoform unknown	0	0	n.d.	n.d.
PRKAR1A	cAMP-dependent protein kinase type I-alpha regulatory subunit; isof	4	4	437.3779678	28.44861271
PRKCI	protein kinase C iota type	2	0	4.174807463	n.d.
PRRC2A	protein PRRC2A; isoform unknown	1	1	0.920065343	1.107397473
PRSS1	trypsin-1	0	1	n.d.	60.86980952
PRSS1 TMPRSS13	NOT mergeable descriptions	0	1	n.d.	98.63500549
PSMC1 PSMC1P4	; proteasome (prosome, macropain) 26S subunit, ATPase, 1 pseudog	0	0	n.d.	n.d.
PSME3	proteasome activator complex subunit 3; isoform unknown	0	0	n.d.	n.d.
PTBP1 PTBP3	polypyrimidine tract-binding protein; 1 (isoform unknown) or 3 (isof	1	0	21.62635799	n.d.
PTGES3 PTGES3P1 PTGES3P3	prostaglandin E synthase; 3 (cytosolic) pseudogene 1 or 3 (cytosolic)	2	3	36.06857366	68.83058818
PYCR1 PYCR2	pyrroline-5-carboxylate reductase; 1, mitochondrial (isoform unknow	1	1	24.76079722	31.29991667
PYCR2	pyrroline-5-carboxylate reductase 2; isoform unknown	0	0	n.d.	n.d.
PYCR1	pyrroline-5-carboxylate reductase 3; isoform unknown	0	0	n.d.	n.d.
QARS	glutamine-tRNA ligase; isoform unknown	0	0	n.d.	n.d.
QKI	protein quaking; isoform unknown	0	1	n.d.	5.517066
RAB10 RAB13 RAB15 RAB1A RAB	; ras-related protein Rab-10 or ras-related protein Rab-13 (isoform	0	0	n.d.	n.d.
RAB3GAP1	rab3 GTPase-activating protein catalytic subunit; isoform unknown	1	0	0.788183571	n.d.
RAB3GAP2	rab3 GTPase-activating protein non-catalytic subunit	1	0	1.127637576	n.d.
RABEP1	rab GTPase-binding effector protein 1; isoform unknown	1	0	0.776510976	n.d.
RABL6	rab-like protein 6; isoform unknown	2	0	3.134003571	n.d.
RASSF5	ras association domain-containing protein 5; isoform unknown	3	0	6.192336364	n.d.
RBM14 RBM14-RBM4	; RBM14-RBM4 protein (isoform unknown) or RNA-binding protein 1,	1	0	19.17486822	n.d.
RBM25	RNA-binding protein 25	1	0	0.56265396	n.d.
RBM39	RNA-binding protein 39; isoform unknown	2	0	3.320277397	n.d.
RBMX	RNA-binding motif protein, X chromosome; isoform unknown	4	0	41.66777184	n.d.
RBMX RBMXL1	; RNA binding motif protein, X-linked-like-1 or RNA-binding motif pr	2	0	41.3502973	n.d.
RBMX RBMXL1 RBMXL2 RBMXL3	; RNA binding motif protein, X-linked-like-1 or RNA-binding motif pr	3	0	24.51034984	n.d.
RBMX RBMXL2	; RNA-binding motif protein; X-linked-like-2 or X chromosome (isof	2	0	15.21381761	n.d.
RHOA RHOB RHOC	; transforming protein RhoA or rho-related GTP-binding protein Rho	0	0	n.d.	n.d.
RINT1	RAD50-interacting protein 1; isoform unknown	1	0	2.142171084	n.d.
ROCK2	rho-associated protein kinase 2; isoform unknown	0	1	n.d.	0.811921033
RPL11	60S ribosomal protein L11; isoform unknown	2	2	17.99674844	21.83790313
RPL15	60S ribosomal protein L15; isoform unknown	1	0	6.712088	n.d.
RPL23A RPL23AP42	; ribosomal protein L23a pseudogene 42 or 60S ribosomal protein L2	0	1	n.d.	9.140295952
RPL28	60S ribosomal protein L28; isoform unknown	2	3	28.15688947	22.04647105
RPL3 RPL3L	60S ribosomal protein; L3-like or L3 (isoform unknown)	0	0	n.d.	n.d.
RPL30	60S ribosomal protein L30	4	0	22.48505455	n.d.
RPL36A RPL36A-HNRNPH2 RPL3	; RPL36A-HNRNPH2 protein	1	1	11.02159356	9.713917645
RPL7 RPL7P23 RPL7P32 RPL7P9	; ribosomal protein L7 pseudogene 23 or ribosomal protein L7 pseud	2	0	4.972671274	n.d.
RPS14 RPS14P3	; 40S ribosomal protein S14 or ribosomal protein S14 pseudogene 3	0	0	n.d.	n.d.
RPS16 ZNF90	NOT mergeable descriptions	1	1	37.42602941	29.50458333
RPS26 RPS26P32 RPS26P58	; ribosomal protein S26 pseudogene 32 or ribosomal protein S26 pse	0	0	n.d.	n.d.
RUFY3	protein RUFY3; isoform unknown	1	0	2.565053636	n.d.

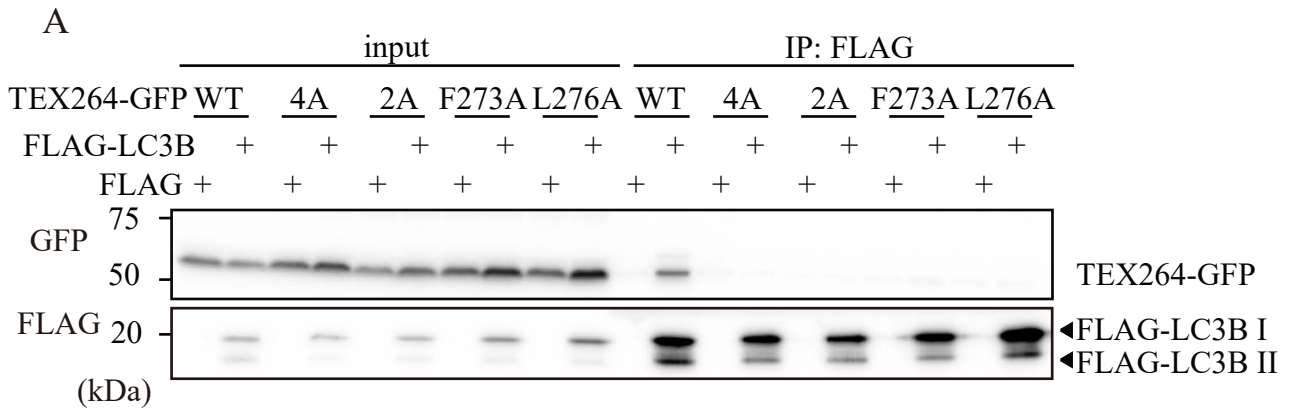
S100A11 S100A11P1 S100A11P2	; S100 calcium binding protein A11 pseudogene 1 or S100 calcium binding protein S100-A13; isoform unknown	0	1	n.d.	9.331876023
S100A13	protein S100-A13; isoform unknown	0	0	n.d.	n.d.
SAFB	scaffold attachment factor B1; isoform unknown	4	0	21.36624229	n.d.
SAFB SAFB2	scaffold attachment factor; B2 or B1 (isoform unknown)	4	0	114.8062099	n.d.
SAFB2	scaffold attachment factor B2	3	0	2.037828993	n.d.
SCD	acyl-CoA desaturase	1	1	8.444970455	13.46730909
SCFD1	sec1 family domain-containing protein 1; isoform unknown	0	1	n.d.	3.878811236
SCYL2	SCY1-like protein 2; isoform unknown	1	0	1.3044	n.d.
SDF2L1	stromal cell-derived factor 2-like protein 1	0	1	n.d.	18.04815833
SDHA	succinate dehydrogenase [ubiquinone] flavoprotein subunit; isoform unknown	0	1	n.d.	3.324572289
SEPT11 SEPT6	; septin-11 (isoform unknown) or septin-6 (isoform unknown)	0	0	n.d.	n.d.
SEPT14 SEPT7	; septin-14 or septin-7 (isoform unknown)	1	2	14.90814482	15.61600775
SEPT7 SEPT7P3	; septin 7 pseudogene 3 or septin-7 (isoform unknown)	0	1	n.d.	2.569302114
SLC25A31 SLC25A4 SLC25A5 SLC25A6	ADP/ATP translocase; 4 or 1 or 2 or 3	0	1	n.d.	12.43247589
SLK	STE20-like serine/threonine-protein kinase; isoform unknown	0	1	n.d.	0.843768636
SMARCC1	SWI/SNF complex subunit SMARCC1	3	3	2.814859785	2.876284516
SMARCC1 SMARCC2	SWI/SNF complex subunit; SMARCC1 or SMARCC2 (isoform unknown)	1	0	1.518427169	n.d.
SNAPIN	SNARE-associated protein Snapin	0	1	n.d.	28.8232
SNX2	sorting nexin-2; isoform unknown	0	2	n.d.	2.054083735
SPIN1 SPIN2A SPIN2B SPIN3 SPIN4	; spindlin-1 or spindlin-2A or spindlin-2B; isoform X4 or spindlin-3 or spindlin-4	0	1	n.d.	12.28619964
SPTAN1	spectrin alpha chain, non-erythrocytic 1; isoform unknown	1	1	2.748780538	0.335327122
SPTBN1	spectrin beta chain, non-erythrocytic 1; isoform unknown	0	0	n.d.	n.d.
SGSTM1	sequestosome-1; isoform unknown	4	0	455.1462288	n.d.
SRP19	signal recognition particle 19 kDa protein; isoform unknown	1	2	29.52879286	36.94219107
SRP9	signal recognition particle 9 kDa protein; isoform unknown	0	0	n.d.	n.d.
ST13 ST13P4 ST13P5	; suppression of tumorigenicity 13 (colon carcinoma) (Hsp70 or hsc70)	0	1	n.d.	70.68086504
STK26	serine/threonine-protein kinase MST4; isoform unknown	0	1	n.d.	113.8162
STK3	serine/threonine-protein kinase 3; isoform unknown	1	0	2.522574699	n.d.
SYNJ1	synaptotagmin-1; isoform unknown	0	1	n.d.	1.610726906
SYNRG	synergin gamma; isoform unknown	4	2	2.960346642	4.260179851
TAF4	transcription initiation factor TFIID subunit 4	3	2	2.20721985	3.944517978
TBC1D4	TBC1 domain family member 4; isoform unknown	0	1	n.d.	1.182694898
TBL1X TBL1XR1	F-box-like/WD repeat-containing protein; TBL1XR1 (isoform unknown)	0	0	n.d.	n.d.
TCEB2	transcription elongation factor B polypeptide 2; isoform X64 or alpha	1	0	8.03332381	n.d.
TCEB2 TCEB2P2	transcription elongation factor B; (SIII), polypeptide 2 (18kDa or poly	1	1	10.92848095	32.84729603
TCOF1	treacle protein; isoform unknown	2	3	0.80110534	1.364090453
TCP1 TCP1P1	; t-complex 1 pseudogene 1 or T-complex protein 1 subunit alpha (isoform unknown)	0	2	n.d.	14.30905526
TEX264	testis-expressed sequence 264 protein; isoform unknown	4	0	266.6575277	n.d.
TMOD3	tropomodulin-3; isoform unknown	0	3	n.d.	7.033038095
TNPO1 TNPO2	; transportin-1 (isoform unknown) or transportin-2 (isoform unknown)	0	0	n.d.	n.d.
TNRC6B	trinucleotide repeat-containing gene 6B protein; isoform unknown	0	0	n.d.	n.d.
TPI1 TPI1P1 TPI1P2	triosephosphate isomerase 1 pseudogene 1 or isomerase 1 pseudogene 1	0	1	n.d.	13.08796992
TRIP13	pachytene checkpoint protein 2 homolog; isoform X64 or alpha2 precursor	1	0	1.191947761	n.d.
TTLL12	tubulin-tyrosine ligase-like protein 12	1	0	1.703833766	n.d.
TUBA1B TUBA4A	tubulin; alpha-1B chain or alpha-4A chain (isoform unknown)	1	2	24.04589796	38.50383673
TUBB3	tubulin beta-3 chain; isoform unknown	0	0	n.d.	n.d.
UPF1	regulator of nonsense transcripts 1	2	1	1.452085507	2.076464493
USO1	general vesicular transport factor p115; isoform unknown	2	2	4.523919658	14.72320171
USP9X USP9Y	probable ubiquitin carboxyl-terminal hydrolase; FAF-X (isoform unknown)	0	0	n.d.	n.d.
VAT1	synaptic vesicle membrane protein VAT-1 homolog	0	0	n.d.	n.d.
VDAC3	voltage-dependent anion-selective channel protein 3; isoform unknown	0	0	n.d.	n.d.
VIM	vimentin; isoform unknown	2	4	11.56421576	9.392675543
VPS51	vacuolar protein sorting-associated protein 51 homolog	0	0	n.d.	n.d.
VPS52	vacuolar protein sorting-associated protein 52 homolog; isoform unknown	0	2	n.d.	3.580712136
WASF1	wiskott-Aldrich syndrome protein family member 1; isoform unknown	0	0	n.d.	n.d.
WASH6P	WAS protein family homolog 6 pseudogene	0	0	n.d.	n.d.
WBP11	WW domain-binding protein 11	1	0	1.912410976	n.d.
WDR45	WD repeat domain phosphoinositide-interacting protein 4; isoform unknown	1	0	3.147110417	n.d.
WDR82	WD repeat-containing protein 82	1	0	11.50162093	n.d.
YBX3	Y-box-binding protein 3; isoform unknown	0	0	n.d.	n.d.
YIPF3	protein YIPF3; isoform unknown	4	0	21.56679833	n.d.
YIPF4	protein YIPF4; isoform unknown	2	0	15.63485	n.d.
ZC3H4	zinc finger CCCH domain-containing protein 4; isoform unknown	0	1	n.d.	1.901734286
ZNF638	zinc finger protein 638; isoform unknown	2	0	0.532415347	n.d.
ZW10	centromere/kinetochore protein zw10 homolog; isoform unknown	0	2	n.d.	7.707046121

interacted with LC3B (Figure 4A). Human TEX264 contains a transmembrane domain and an evolutionarily conserved putative LIR motif (FEEL) in the N- and C-terminal (amino acids 273–276) regions, respectively (Figure 4B). The C terminus faces the cytosol because an N-terminal HA tag was resistant to proteinase K treatment whereas a C-terminal FLAG tag was sensitive (Figure 5). Substitution of F273 or L276 in TEX264 with alanine completely abolished the interaction with LC3B, suggesting that the FEEL sequence is a bona fide LIR (Figure 4A). These data suggest that TEX264 interacts with LC3B via the LIR motif in the cytosol-facing C-terminal region.

TEX264 is present in the ER and colocalizes with autophagosomes

To investigate the role of TEX264 in autophagy, I first monitored the intracellular localization of TEX264 tagged with green fluorescent protein (GFP) at the C-terminal end. TEX264-GFP showed a reticular pattern under nutrient-rich conditions and colocalized with the ER marker cytochrome *b₅* (Figure 6). Endogenous TEX264 also colocalized with the ER protein SEC61B (Figure 7). These data suggest that TEX264 is present throughout the ER.

By contrast, TEX264-GFP formed punctate structures under starvation conditions (Figures 8). Most of these structures colocalized with the autophagosomal



B

Homo sapiens TEX264

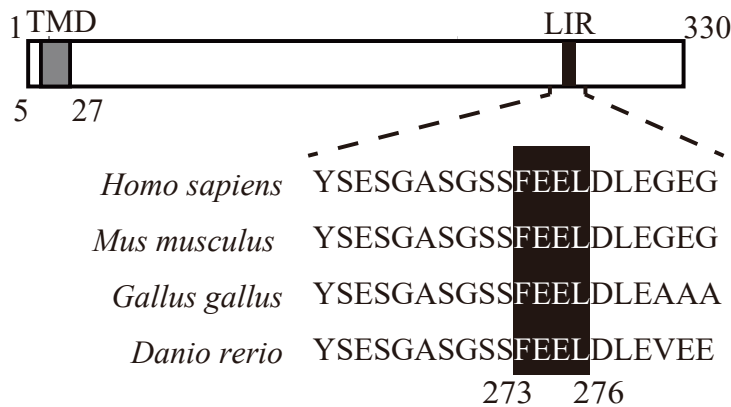


Figure 4. TEX264 interacts with LC3B in LIR-dependent manner

(A) HEK293T cells transiently expressing FLAG-LC3B and WT or mutated TEX264-GFP were subjected to immunoprecipitation with anti-FLAG antibody and detected with anti-GFP and anti-FLAG antibodies. The 4A and 2A mutants have AAAA and AEEA instead of FEEL in the LIR, respectively.

(B) Domain architecture of human TEX264 and alignment of the LIR motif in vertebrates. Gray and black boxes indicate a transmembrane domain (TMD) and LC3-interacting region (LIR), respectively.

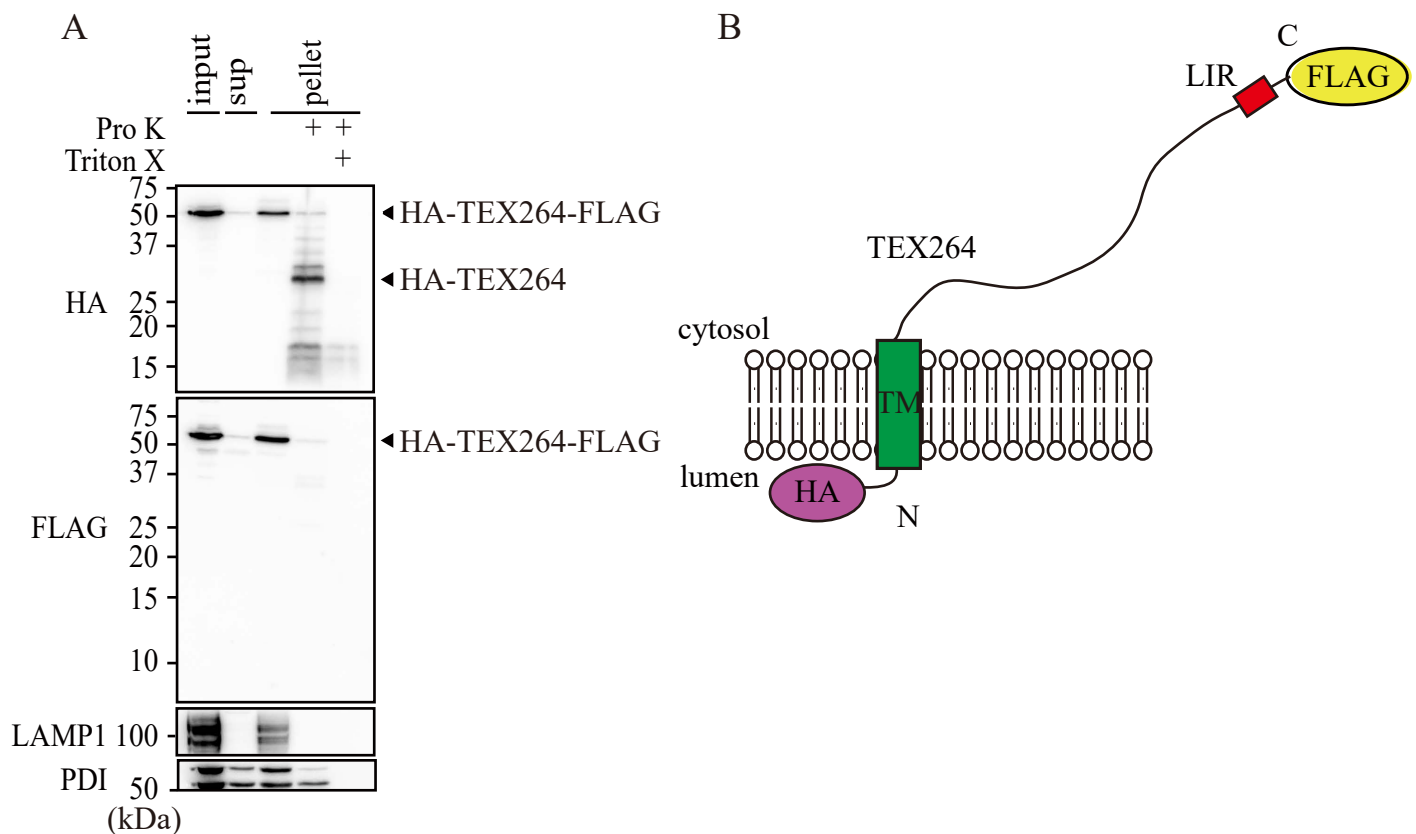


Figure 5. The C-terminus of TEX264 faces the cytosol

(A) Cell homogenates of HeLa cells expressing HA-TEX264-FLAG were fractionated into the $100,000 \times g$ supernatant (sup) and pellet (pellet) fractions. The pellet fraction was subjected to proteinase K protection assay. Proteinase K ($50 \mu\text{g}/\text{mL}$) and 1% of Triton X-100 were used. Antibodies against LAMP1 and PDI were used as controls to detect cytosol-facing and intraluminal epitopes.

(B) Schematic representation of the topology of TEX264.

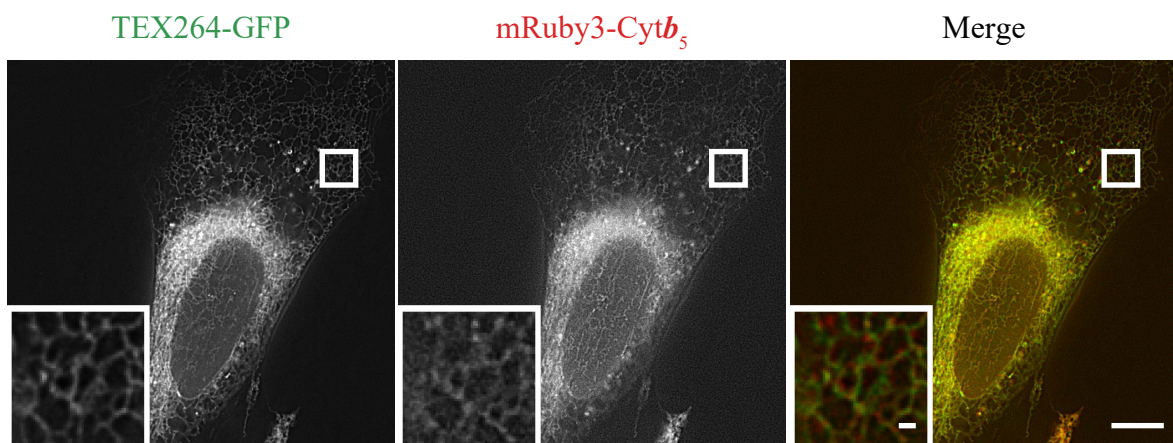


Figure 6. TEX264 is present in the ER.

MEFs stably expressing TEX264-GFP and mRuby3-cytochrom *b*₅ (Cyt*b*₅) were directly observed by fluorescence microscopy. Bars: 10 μ m and 1 μ m (insets).

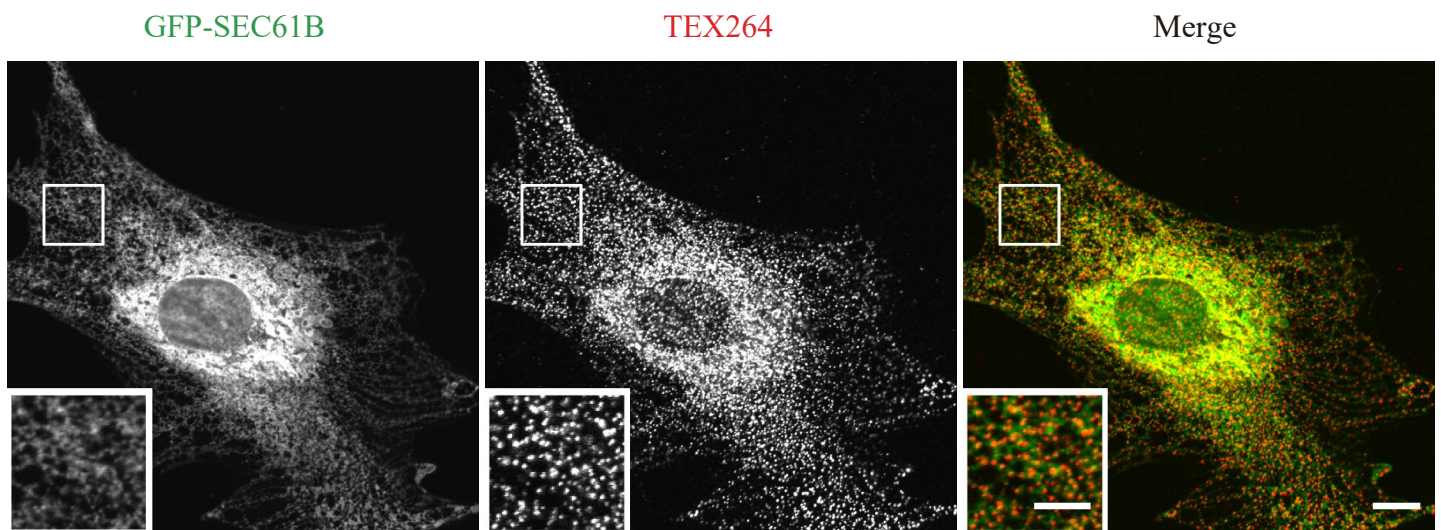


Figure 7. Endogenous TEX264 localizes in the ER

WT MEFs stably expressing GFP-SEC61B were subjected to immunostaining with anti-TEX264 antibody. Bars: 10 μm and 5 μm (insets).

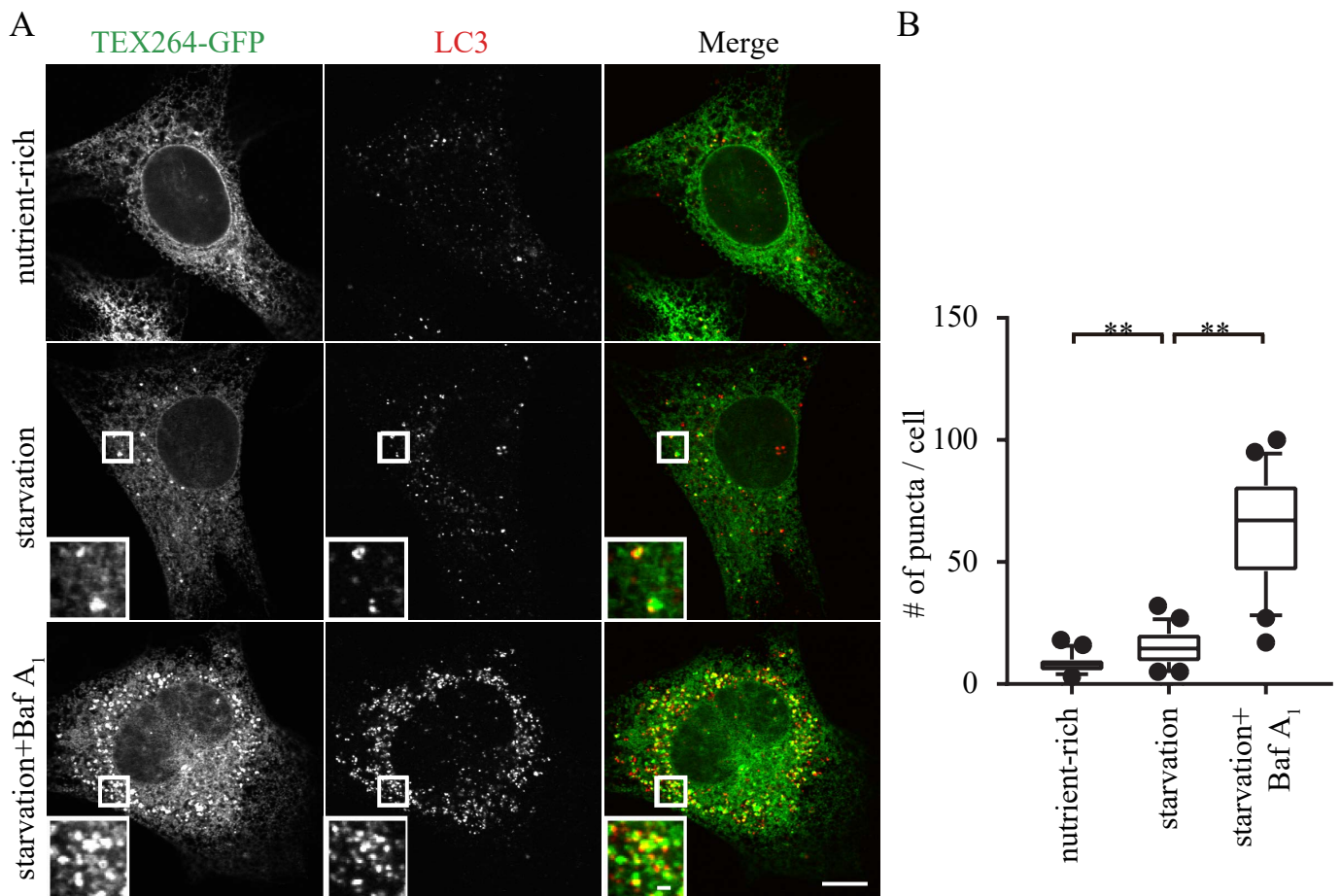


Figure 8. TEX264 colocalizes with autophagosomes

(A and B) MEFs stably expressing TEX264-GFP were cultured in starvation media with or without bafilomycin A₁ (Baf A₁) and immunostained with anti-LC3 antibody. Bars: 10 μm and 1 μm (insets) (A). Quantification of the number of TEX264 puncta per cell under nutrient-rich and starvation conditions with or without Baf A₁. Solid bars indicate the medians, boxes the interquartile range (25th to 75th percentile), and whiskers the 10th to 90th percentile. Differences were statistically analyzed by an unpaired two-tailed Student's t-test. ** P < 0.01. Data were collected from 20 cells for each cell type (B).

protein LC3 (Figures 8), as well as the isolation membrane proteins FIP200 and WIPI2 (Figure 9). These results suggest that TEX264 associates with autophagic membranes from an early phase of autophagosome formation. The formation of TEX264 puncta was dependent on LC3 interaction; the TEX264 LIR4A mutant, in which FEEL was replaced with AAAA, did not form punctate structures (Figure 10).

The number of these TEX264 structures increased following bafilomycin A₁ treatment, suggesting that TEX264 is delivered to lysosomes (Figure 8). In fact, some of the TEX264-positive puncta colocalized with LAMP1 under starvation conditions (Figure 9). These data suggest that TEX264 associates with autophagic membranes in a LIR-dependent manner and is delivered to lysosomes via autophagy.

TEX264 is degraded by autophagy

Since TEX264 is delivered to lysosomes, I tested whether endogenous TEX264 was degraded by autophagy in HeLa cells. Upon induction of autophagy by amino acid starvation, the amount of TEX264 was reduced in a time-dependent manner (Figure 11). This reduction was restored by the lysosome inhibitor bafilomycin A₁. Such reduction in TEX264 level was not observed in autophagy-deficient FIP200-knockout (KO) cells, even under starvation conditions (Figure 11). These data suggest that TEX264 is

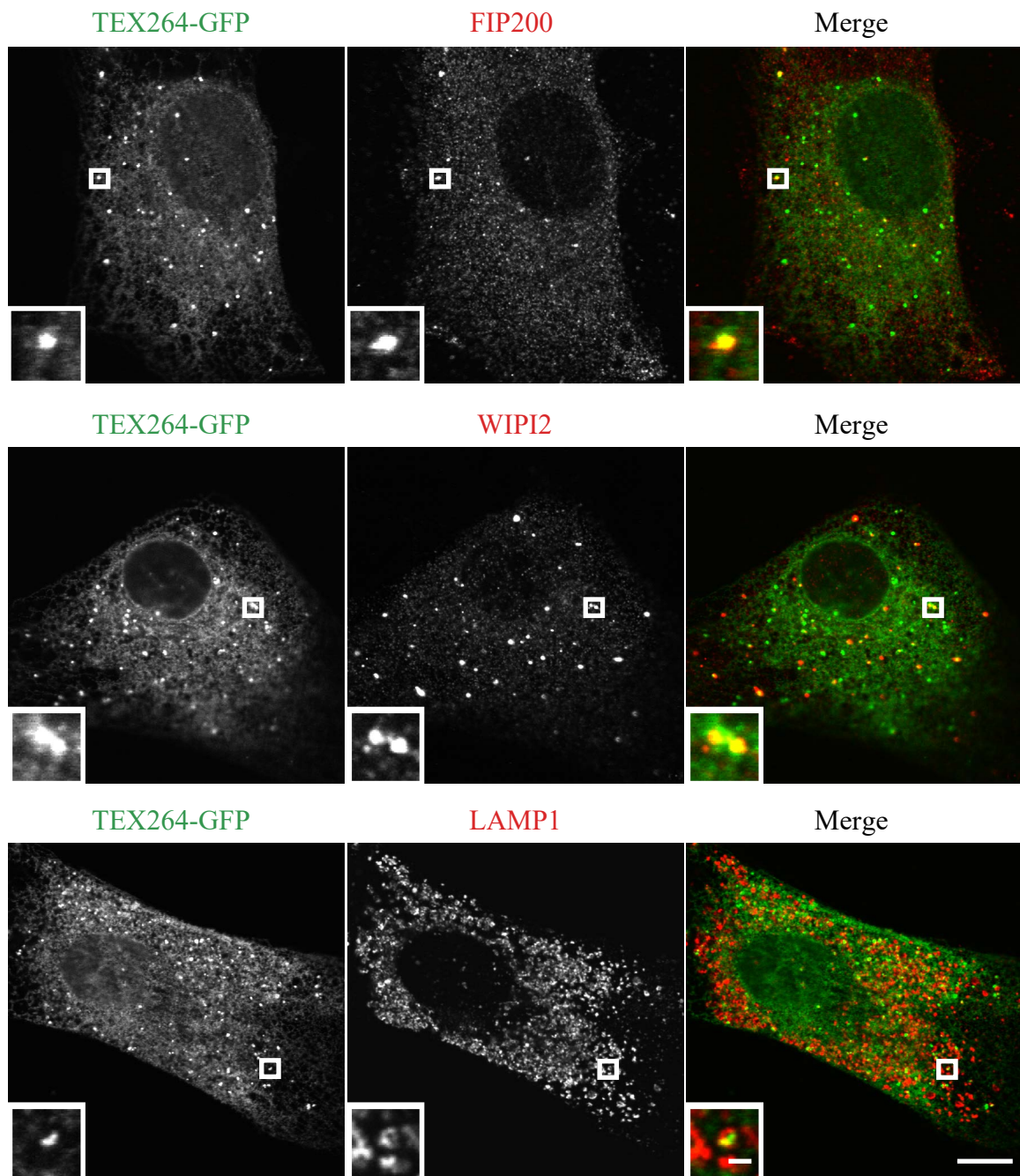


Figure 9. TEX264 associates with autophagic membranes from an early phase to late phase
 MEFs stably expressing TEX264-GFP were cultured under starvation media and immunostained with the indicated antibodies. Bars: 10 μm and 1 μm (insets).

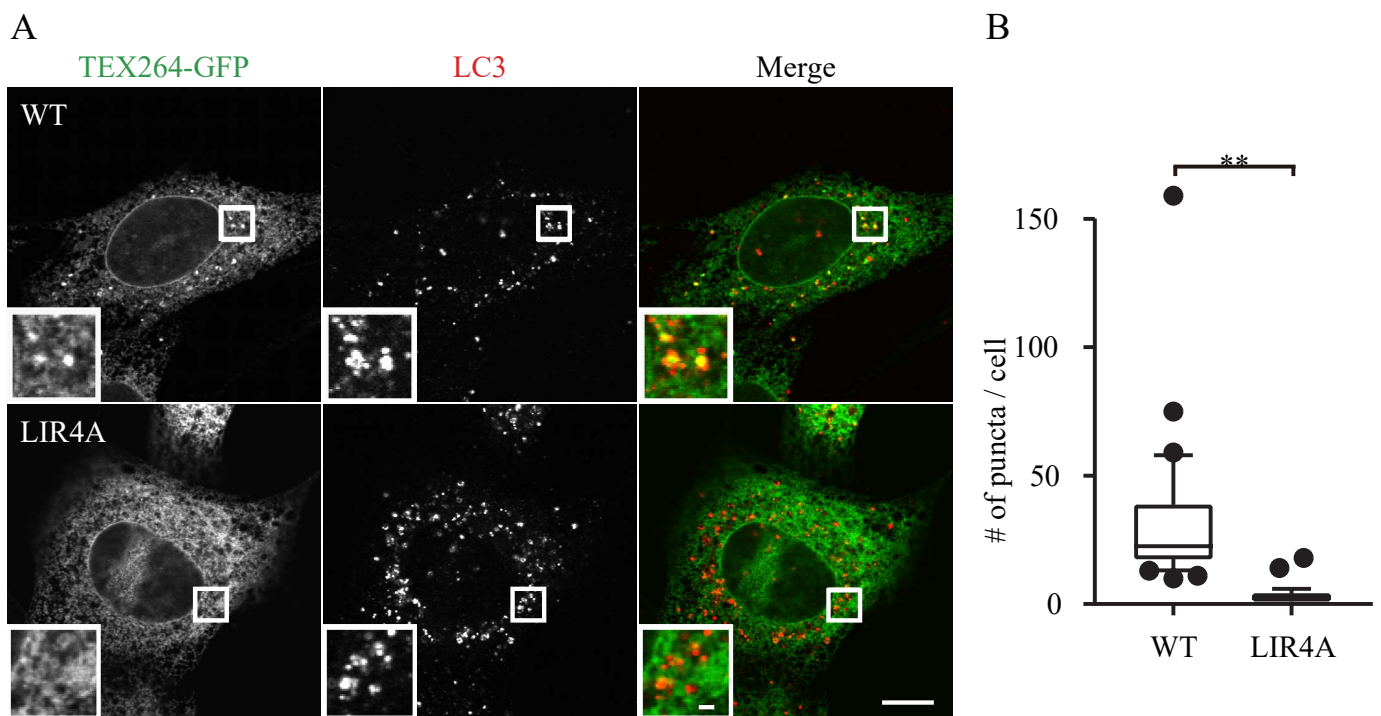


Figure 10. TEX264 is present in the ER and colocalizes with autophagosomes

(A and B) MEFs stably expressing TEX264-GFP or its LIR4A mutant were cultured in starvation media and immunostained with anti-LC3 antibody. Bars: 10 μm and 1 μm (insets) (A). Quantification of the number of TEX264 puncta per cell. Solid bars indicate the medians, boxes the interquartile range (25th to 75th percentile), and whiskers the 10th to 90th percentile. Differences were statistically analyzed by unpaired two-tailed Student's t-test. ** $P < 0.01$. Data were collected from 30 cells for each cell type (B).

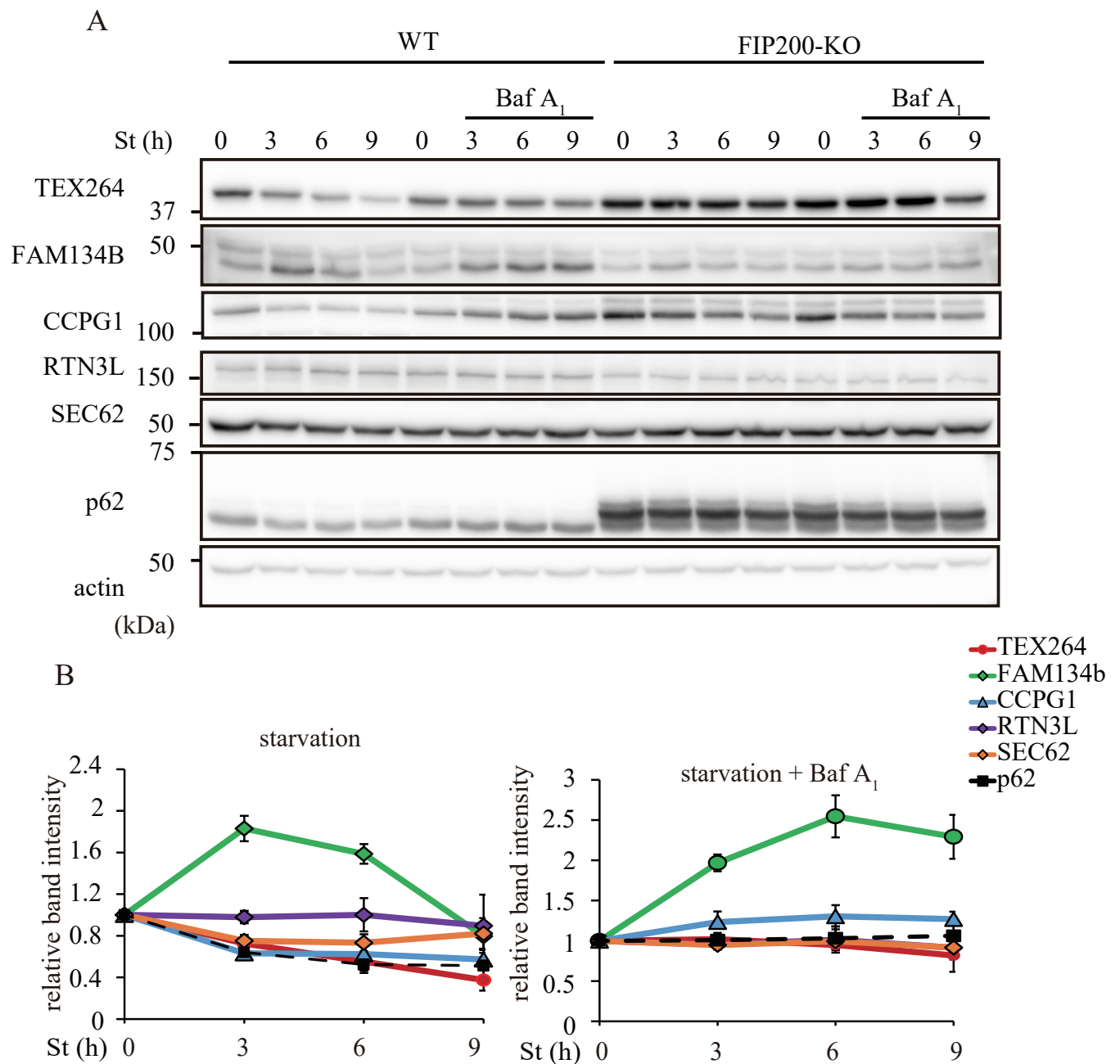


Figure 11. TEX264 is degraded by autophagy

(A and B) WT and FIP200-KO HeLa cells were cultured in starvation medium lacking amino acids and serum with or without bafilomycin A₁ for 3, 6, and 9 h. Cell lysates were analyzed by immunoblotting using the indicated antibodies (A). Relative changes during starvation of the band intensities (normalized with those of HSP90) (B). Data represent the mean \pm standard error of the mean (SEM) of three independent experiments.

degraded by the autophagy-lysosome pathway.

Next, I compared the expression levels of TEX264 in various tissues between WT and autophagy-deficient mice. Because autophagy is essential for survival in mice, I used the brain from neuronal cell-specific FIP200-KO mice [44] (Figure 12A) and the other tissues from systemic Atg5-KO mice with neuron-specific rescue [43] (Figure 12B). TEX264 accumulated heavily in all the autophagy-deficient tissues tested (Figures 12A and 12B). These data suggest that TEX264 is degraded by autophagy in both cultured cells and mouse tissues.

TEX264 is a novel ER-phagy receptor

Given that TEX264 is an ER transmembrane protein and delivered to lysosomes, I hypothesized that TEX264 functions as a receptor for ER-phagy. I developed a doxycycline-inducible ER-phagy reporter that has an N-terminal ER signal sequence followed by tandem monomeric red fluorescent protein (RFP) and GFP sequences and the ER retention sequence KDEL (Figure 13). The full length of this reporter was detected as an approximately 50-kD band under nutrient-rich conditions (Figure 14A). When ER-phagy was activated by starvation, the RFP fragment appeared as a result of degradation of the reporter inside the ER because the linker between RFP and GFP was

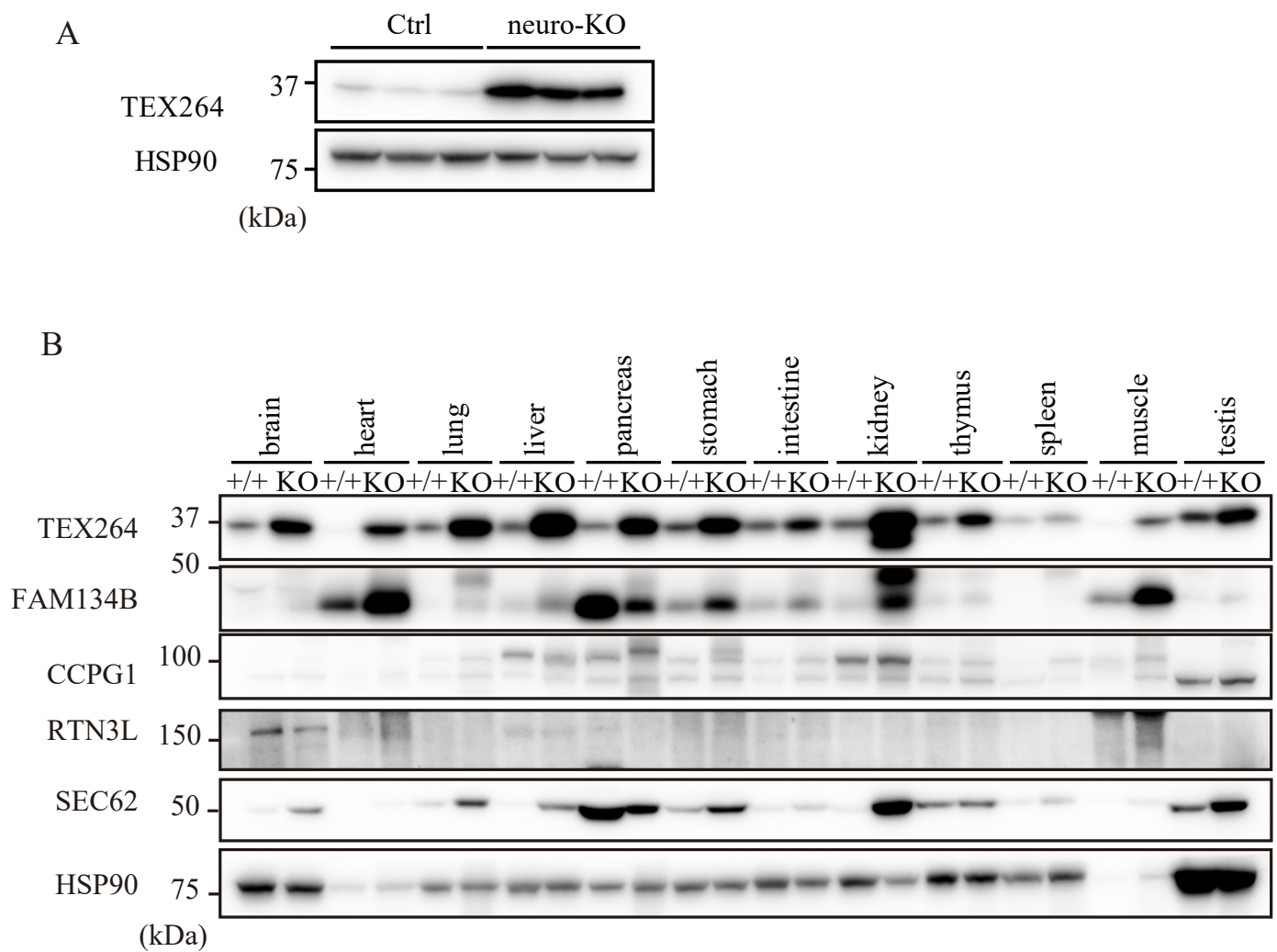


Figure 12. TEX264 is degraded by autophagy

(A and B) Immunoblotting of endogenous TEX264 (and other ER-phagy receptors) in postnuclear supernatants of brains from three independent *Fip200^{fl/fl};nestin-CRE* (Ctrl) and *Fip200^{fl/fl};nestin-CRE* (neuro-KO) mice (A) and the indicated organs from *Atg5^{+/+};NSE-Atg5* (+/+) and *Atg5^{-/-};NSE-Atg5* (KO) mice (B).

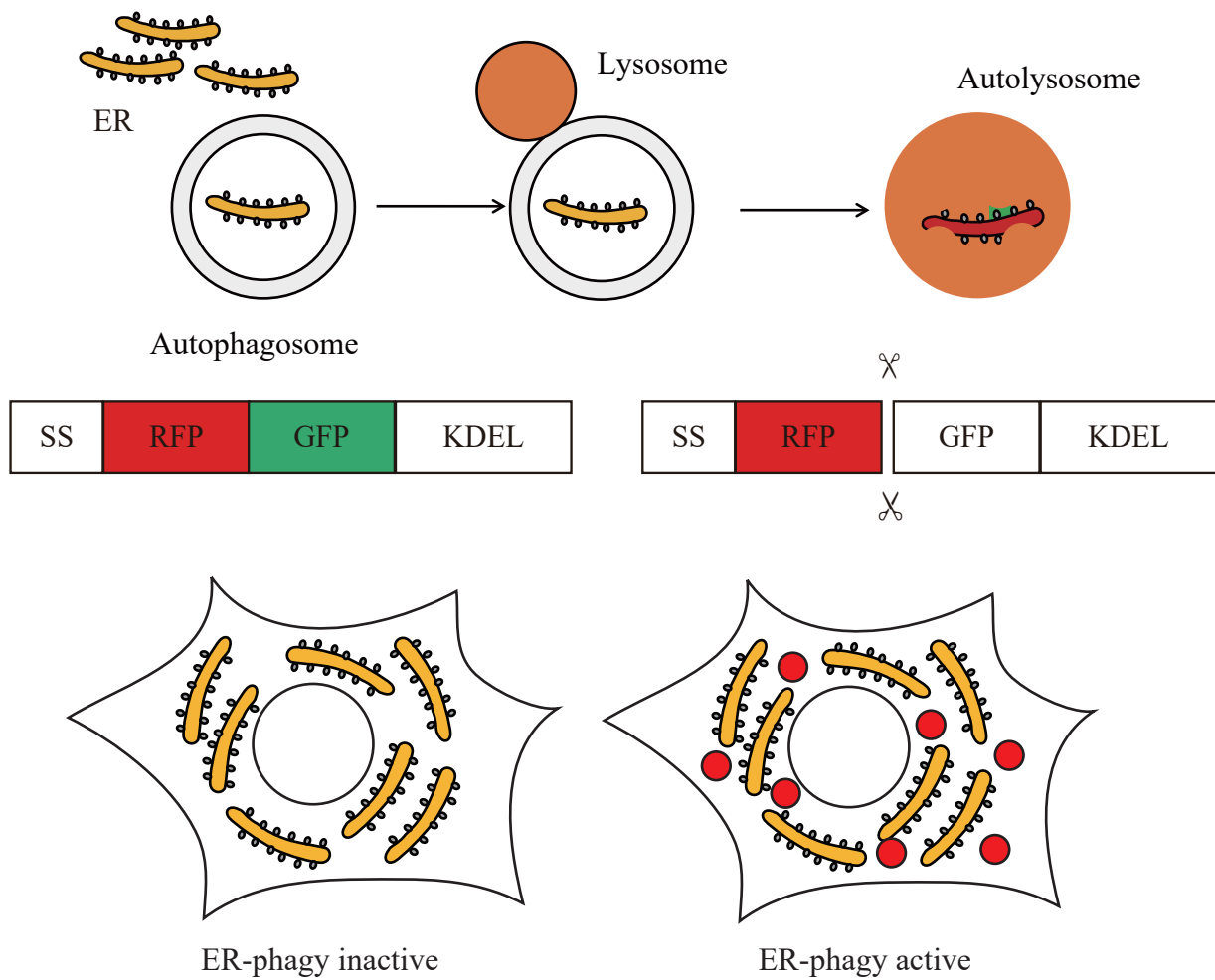


Figure 13. Novel reporter to monitor ER-phagy activity

Schematic representation of the ER-phagy reporter ssRFP-GFP-KDEL. ssRFP-GFP-KDEL cleaved by lysosomal enzymes to yield the RFP fragment. The GFP signal quenched in lysosomes. SS, the signal sequence.

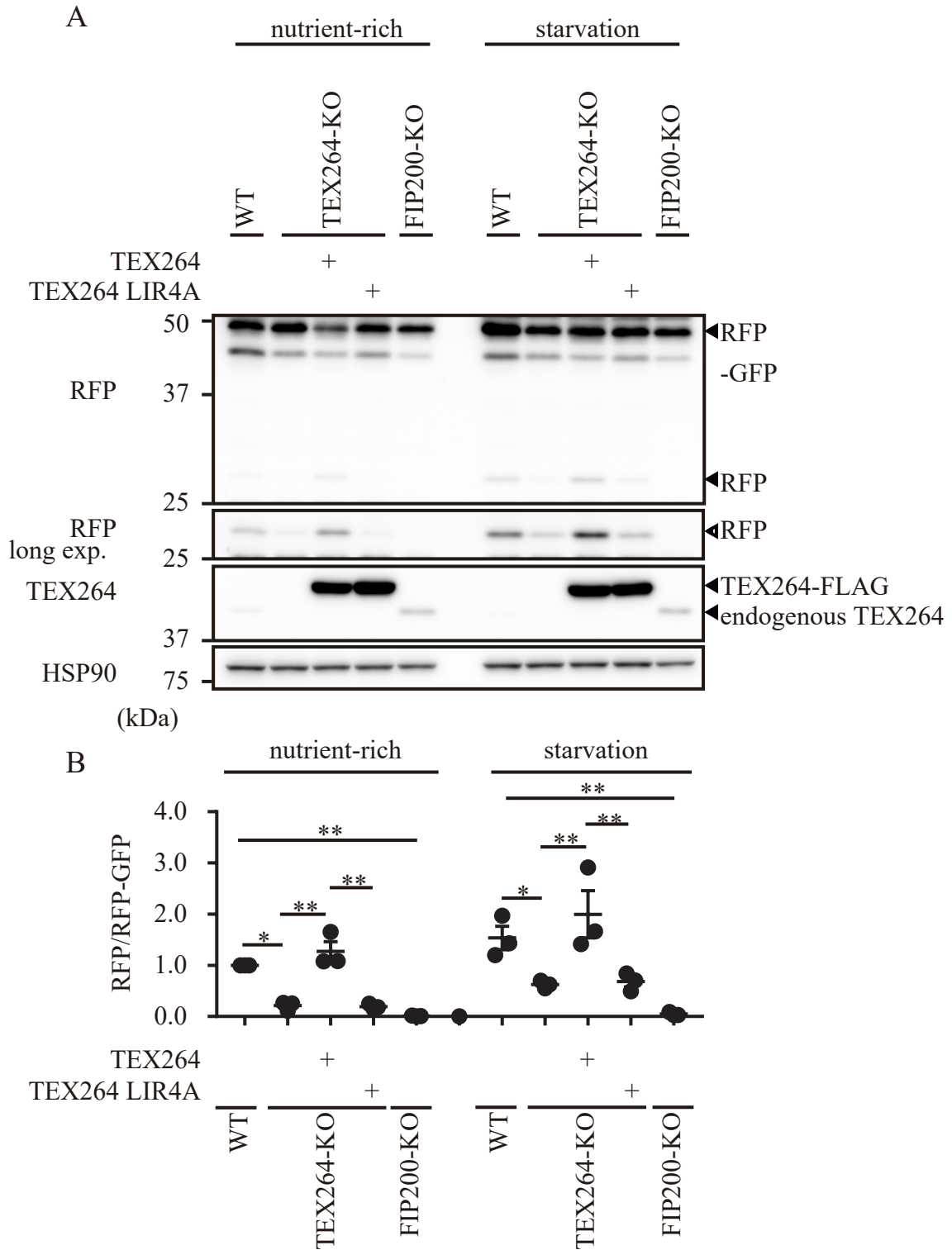


Figure 14. TEX264 is a novel ER-phagy receptor

(A and B) WT, TEX264-KO (with or without TEX264-FLAG or TEX264 LIR4A-FLAG), and FIP200-KO HeLa cells stably expressing the ER-phagy probe were cultured in the presence of doxycycline for 24 h to induce the reporter. After doxycycline was removed, cells were cultured in starvation medium lacking amino acids and serum for 9 h (A). The band intensities of RFP and RFP-GFP were quantified and the ratio of RFP:RFP-GFP (normalized to WT) is shown. Data represent the mean \pm SEM of three independent experiments. Differences were statistically analyzed by one-way ANOVA and Sidak's multiple comparison test. * $P < 0.05$; ** $P < 0.01$ (B).

cleaved, thus producing RFP, which is relatively stable in lysosomes (Figure 14A) [48].

As a negative control, I confirmed that cleavage did not occur in FIP200-KO cells (Figure 14A). These results validated this ER-phagy reporter.

Next, I determined the role of TEX264 in ER-phagy. I generated TEX264-KO HeLa cells using the CRISPR-Cas9 method, and the cells showed normal growth. In TEX264-KO cells, the production of the RFP fragment was significantly impaired under both nutrient-rich and starvation conditions (Figures 14A and 14B). Cleavage of the reporter was restored by re-expression of exogenous TEX264 but not by the LIR4A mutant (Figures 14A and 14B). These data suggest that TEX264 and its LIR motif are important for ER-phagy.

ER-phagy activity was also monitored by fluorescence microscopy using the same reporter. This reporter should appear yellow (green and red) in the ER matrix. When it is transported to lysosomes by autophagy, it becomes red because GFP but not RFP is quickly quenched in the acidic environment [48] (Figure 15). Hence, the total RFP intensity of these red puncta should indicate the amount of the ER-phagy reporter delivered to lysosomes. WT cells showed yellow reticular signals (the ER) with few red punctate structures (lysosomes) (Figures 16A and 16B), while red puncta were not observed in autophagy-deficient FIP200-KO cells (Figures 16A and 16B). The intensity

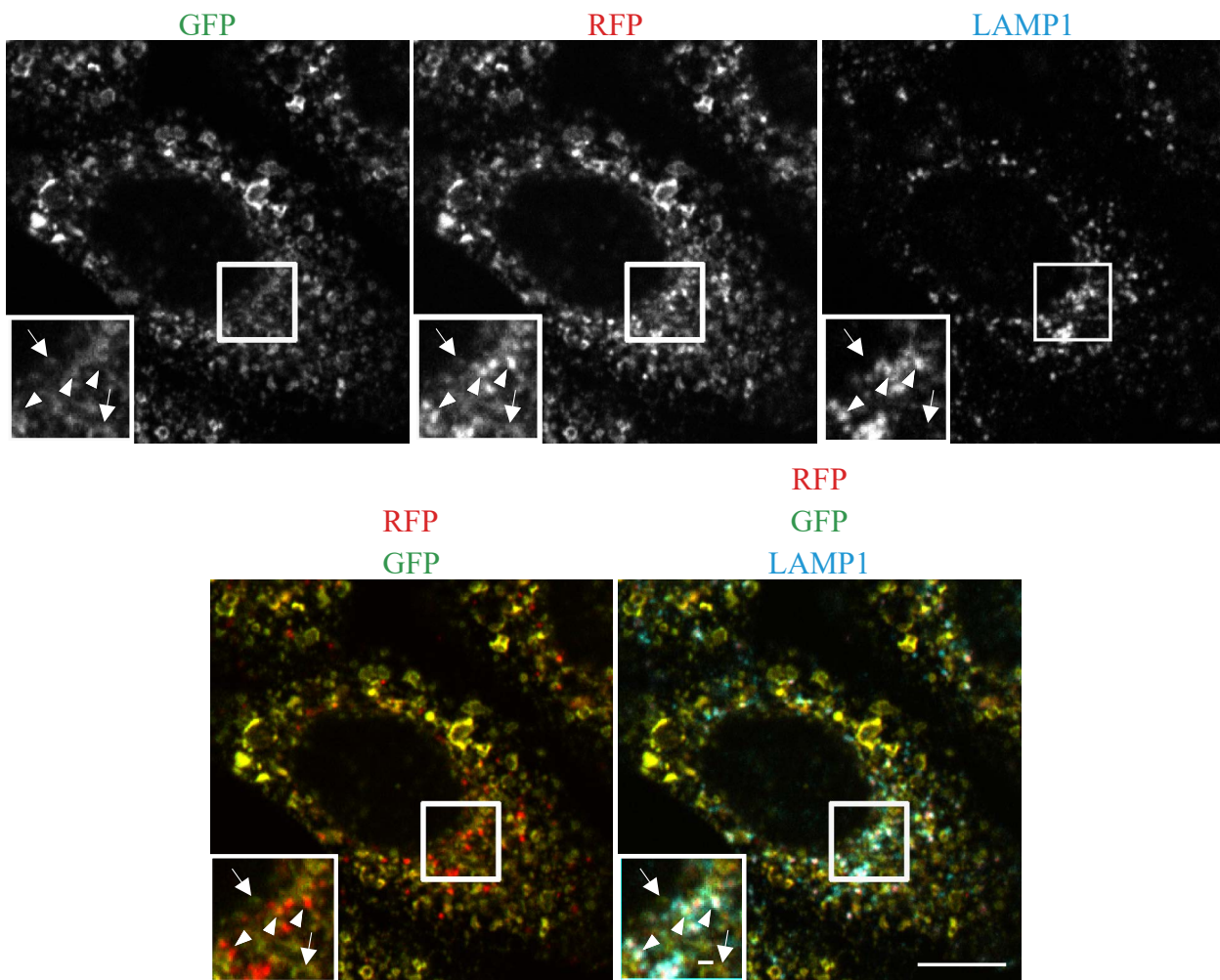


Figure 15. Delivery of the ER-phagy reporter to lysosomes

WT HeLa cells stably expressing the doxycycline-inducible ER-phagy probe were cultured in the presence of doxycycline for 24 h. After doxycycline was removed, cells were cultured in starvation medium lacking amino acids and serum for 9 h. Cells were fixed and subjected to immunostaining with anti-LAMP1 antibody. Arrows indicate the GFP⁺RFP⁺LAMP1⁻ structures (isolation membranes and autophagosomes) and arrowheads indicate GFP-RFP⁺LAMP1⁺ structures (autolysosomes). Bars: 10 μ m and 1 μ m (insets).

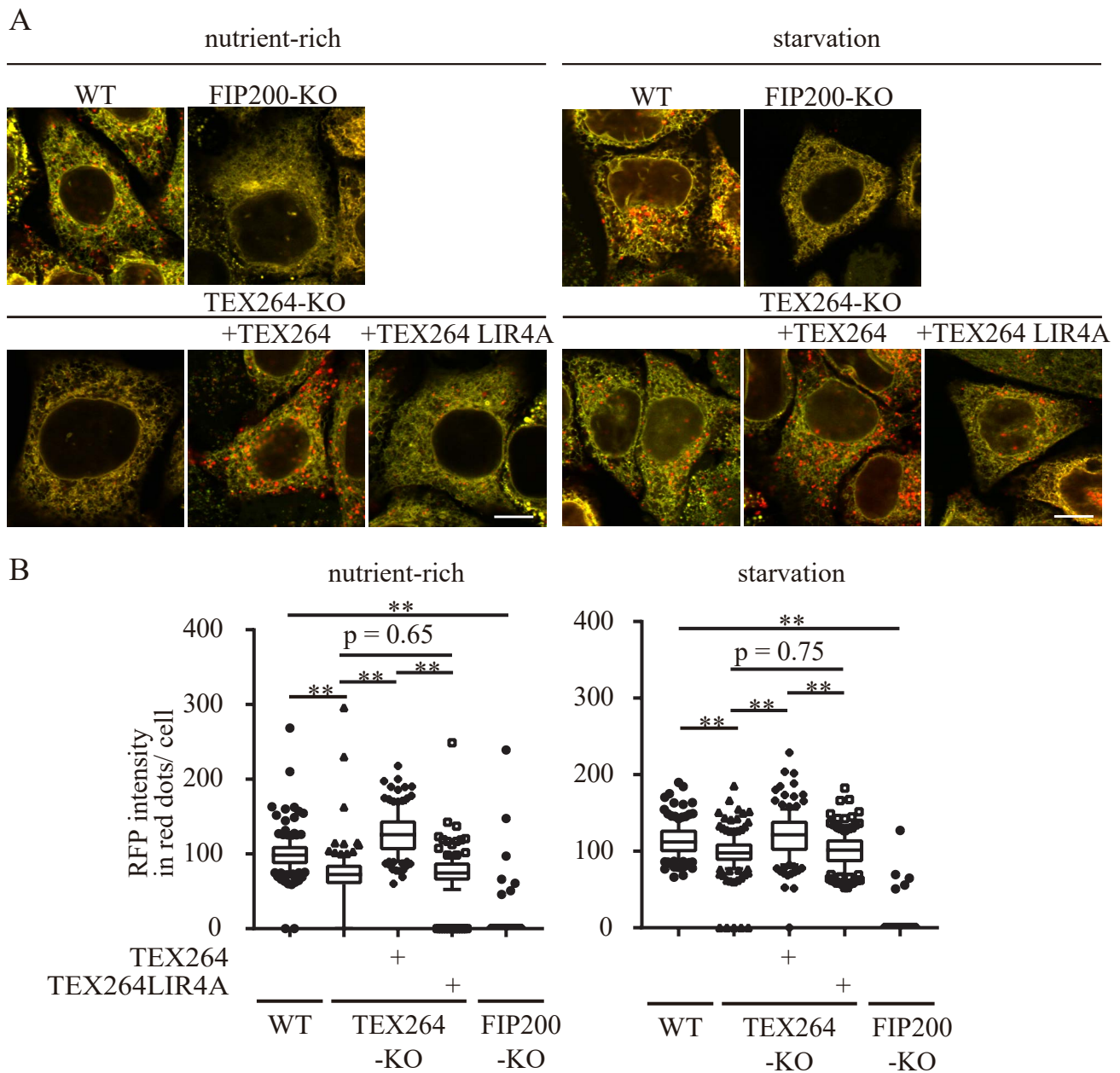


Figure 16. The depletion of TEX264 impairs ER-phagy

(A and B) WT, TEX264-KO (with or without TEX264-FLAG or TEX264 LIR4A-FLAG), and FIP200-KO HeLa cells stably expressing the ER-phagy probe were cultured in the presence of doxycycline for 24 h to induce the reporter. After doxycycline was removed, cells were fixed and observed by fluorescence microscopy. Bars: 10 μ m (A). The total signal intensity of RFP in red puncta was quantified. Data were collected from > 120 cells for each cell type. Solid bars indicate medians, boxes the interquartile range (25th to 75th percentile), and whiskers the 10th to 90th percentile. Differences were statistically analyzed by one-way ANOVA and Sidak's multiple comparison test. ** P < 0.01 (B).

of the RFP signals in red puncta was lower in TEX264-KO cells than in WT cells under both nutrient-rich and starvation conditions. The reduction in the RFP intensity was restored by re-expression of exogenous TEX264 but not by the TEX264 LIR4A mutant (Figures 16A and 16B). Thus, TEX264 is a novel ER-phagy receptor.

TEX264 is a major ER-phagy receptor

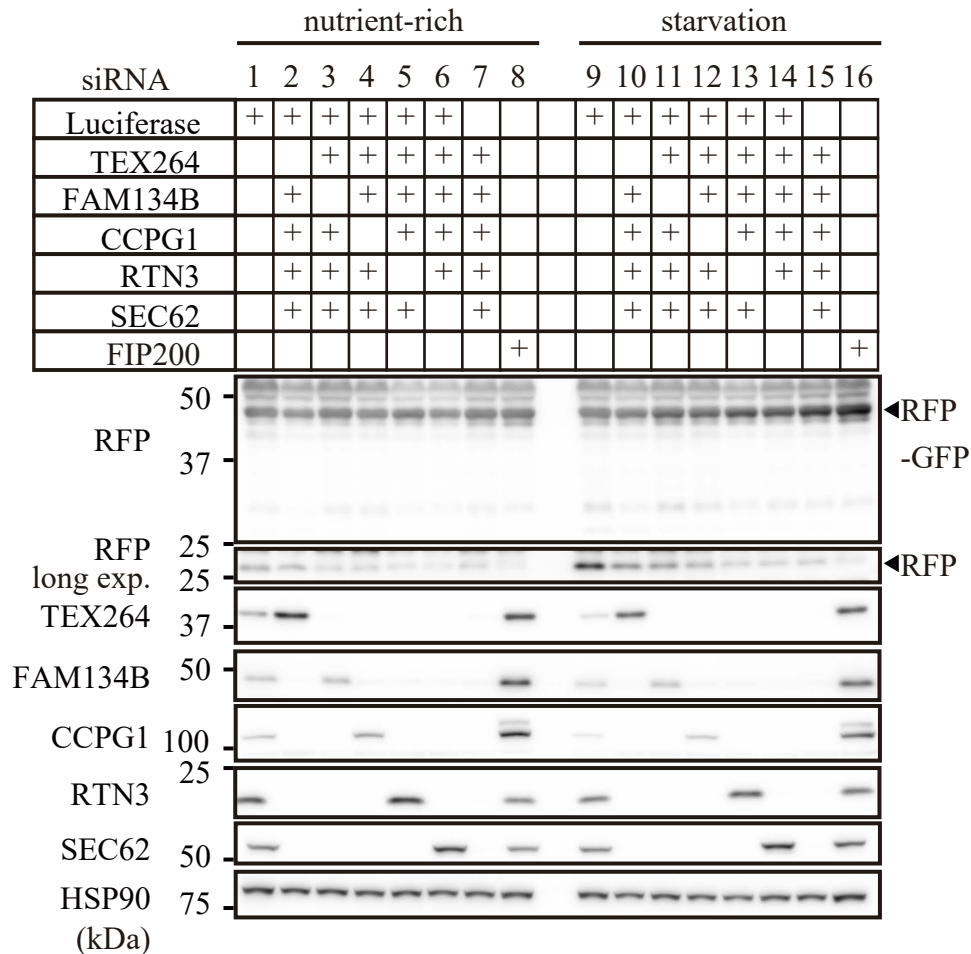
To date, four ER-phagy receptors, namely, FAM134B, CCPG1, RTN3, and SEC62, have been reported in mammals [11,24-27]. To determine the relative contributions of these known ER-phagy receptors and TEX264, the endogenous level of each receptor was monitored during autophagy. The levels of TEX264 and CCPG1 reduced during starvation similarly to that of p62 (Figure 11) [26]. The level of FAM134B was unchanged, probably because both degradation and synthesis were enhanced during starvation; bafilomycin A₁ treatment caused accumulation of FAM134B (Figure 11). By contrast, the levels of RTN3 and SEC62 were stable irrespective of bafilomycin A₁ treatment. These data suggest that large amounts of TEX264, FAM134B, and CCPG1 are subjected to autophagic degradation, and so I hypothesized that these three proteins are major receptors for general ER-phagy. SEC62 may be more important during recovery from ER stress [27], and RTN3 may be specific for the degradation of tubular

ER [25].

The relative importance of these receptors was further determined by small interfering RNA (siRNA)-mediated knockdown of four of the five receptors. Depletion of FAM134B, CCPG1, RTN3, and SEC62 (except TEX264) caused a partial reduction in the cleavage of the ER-phagy reporter under basal and starvation conditions, but a significant level (>50%) of ER-phagy activity remained (Figures 17A and 17B, lanes 2 and 10). Cells expressing one of the other ER-phagy receptors (all lacking TEX264) showed much lower ER-phagy activity (Figures 17A and 17B, lanes 3-6, and 11-14). Knockdown of all ER-phagy receptors suppressed the reporter cleavage to a level comparable with that in FIP200-depleted cells (Figures 17A and 17B, lanes 7, 8, 15, and 16). Furthermore, single knockdown of each ER-phagy receptor showed that depletion of TEX264 most efficiently suppressed ER-phagy activity under nutrient-rich and starvation conditions (Figure 18A and 18B). Single knockdown of FAM134B and CCPG1 also suppressed ER-phagy but less efficiently (Figure 18A and 18B). These data suggest that, although there is some redundancy, TEX264 is a major ER-phagy receptor in HeLa cells.

To compare the binding efficiency of each ER-phagy receptor with LC3/GABARAP family proteins, I determined the pull-down efficiency of all binding

A



B

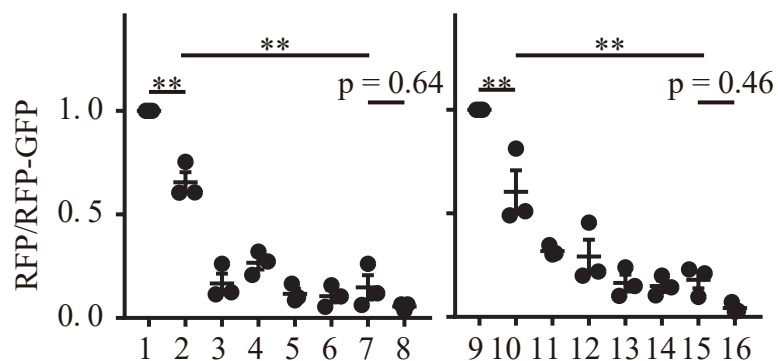


Figure 17. Comparison of ER-phagy receptors in ER-phagic activity

(A and B) HeLa cells stably expressing the ER-phagy reporter were transfected with the indicated siRNAs. After 2 days, cells were cultured in the presence of doxycycline for 24 h. After doxycycline was removed, cells were cultured in starvation medium lacking amino acids and serum for 9 h. Cell lysates were analyzed by immunoblotting using the indicated antibodies (A). The band intensities of RFP and RFP-GFP were quantified and the ratio of RFP:RFP-GFP (normalized to WT) is shown. Data represent the mean \pm SEM of three independent experiments. Differences were statistically analyzed by one-way ANOVA and Sidak's multiple comparison test. ** $P < 0.01$ (B).

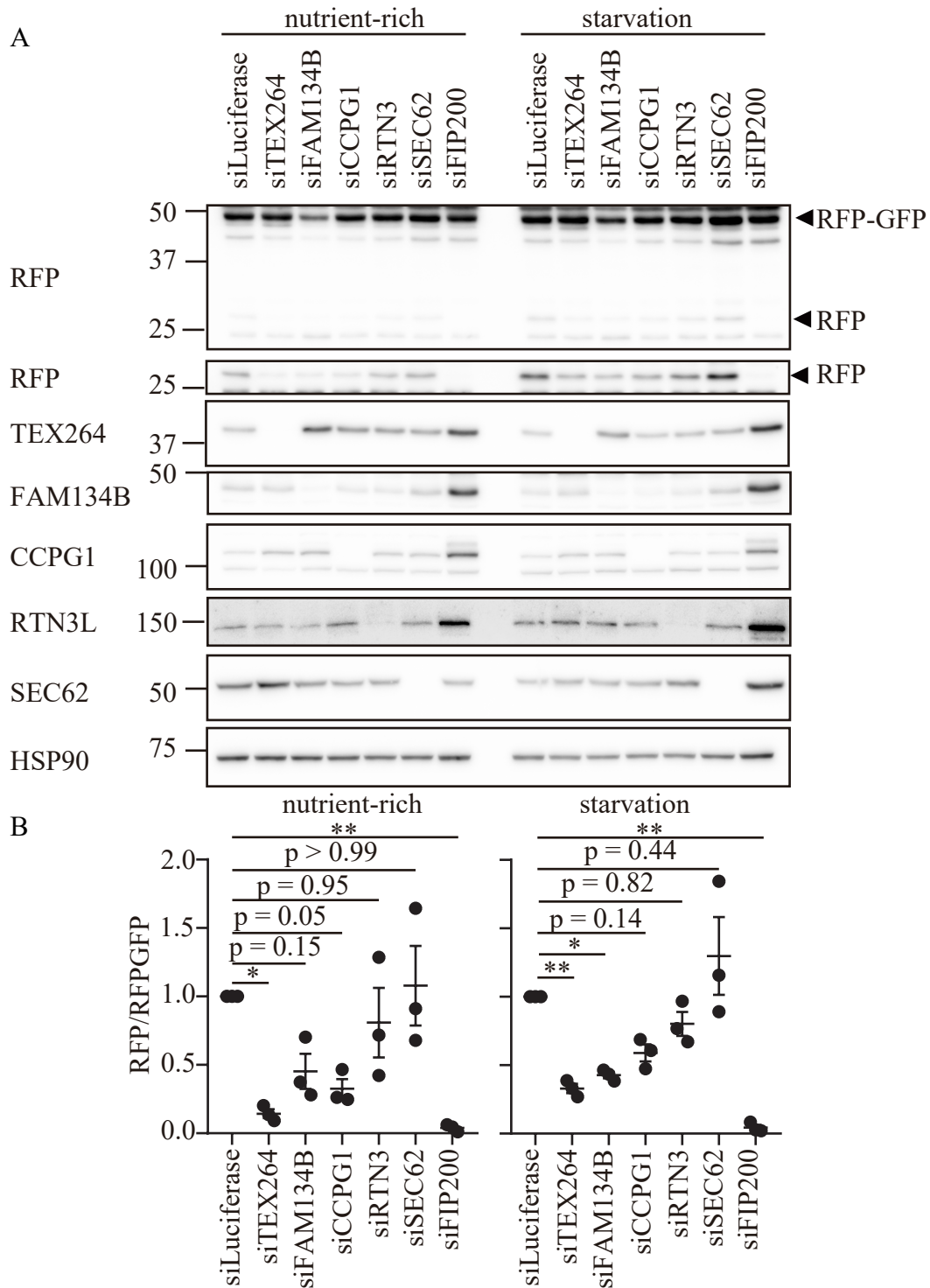


Figure 18. TEX264 is a major ER-phagy receptor

(A and B) HeLa cells stably expressing the ER-phagy reporter were transfected with the indicated siRNAs. After 2 days, cells were cultured in the presence of doxycycline for 24 h. After doxycycline was removed, cells were cultured in starvation medium lacking amino acids and serum for 9 h. Cell lysates were analyzed by immunoblotting using the indicated antibodies (A). Quantification of the band intensities was performed as in Figure 4C. Data represent the mean \pm SEM of three independent experiments. Differences were statistically analyzed by one-way ANOVA and Sidak's multiple comparison test. ** $P < 0.01$ (B).

pairs. The best-known selective substrate p62 strongly interacted with all LC3/GABARAP family proteins, and the band intensities of the immunoprecipitates were higher than those of the inputs (Figure 19). TEX264 interacted strongly with LC3A and GABARAPL1. FAM134B and CCPG1 interacted preferentially with GABARAP family proteins, as previously reported [26]; however, their binding efficiencies were weaker than those of TEX264-LC3A and TEX264-GABARAPL1 interactions (Figure 19). These data suggested that TEX264 interacts most efficiently with LC3/GABARAP family proteins among the ER-phagy receptors.

To further determine the function of these ER-phagy receptors, I generated TEX264, FAM134B, and CCPG1 triple-KO HeLa cells. In triple-KO cells, the amount of LC3-II increased under starvation conditions and further increased with bafilomycin A₁ treatment similar to WT cells. The maturation of cathepsinD was not affected in triple-KO cells. These data suggested that bulk autophagy and lysosome functions were not impaired in triple-KO cells (Figure 20). As shown in Figures 14 and 16, single KO of TEX264 caused a significant reduction in ER-phagy activity monitored by cleavage of the ER-phagy reporter (Figures 21A and 21B). The slight amount of remaining ER-phagy activity in TEX264-KO cells was almost completely suppressed in triple-KO cells (Figures 21A and 21B). Fluorescence microscopy also showed a significant

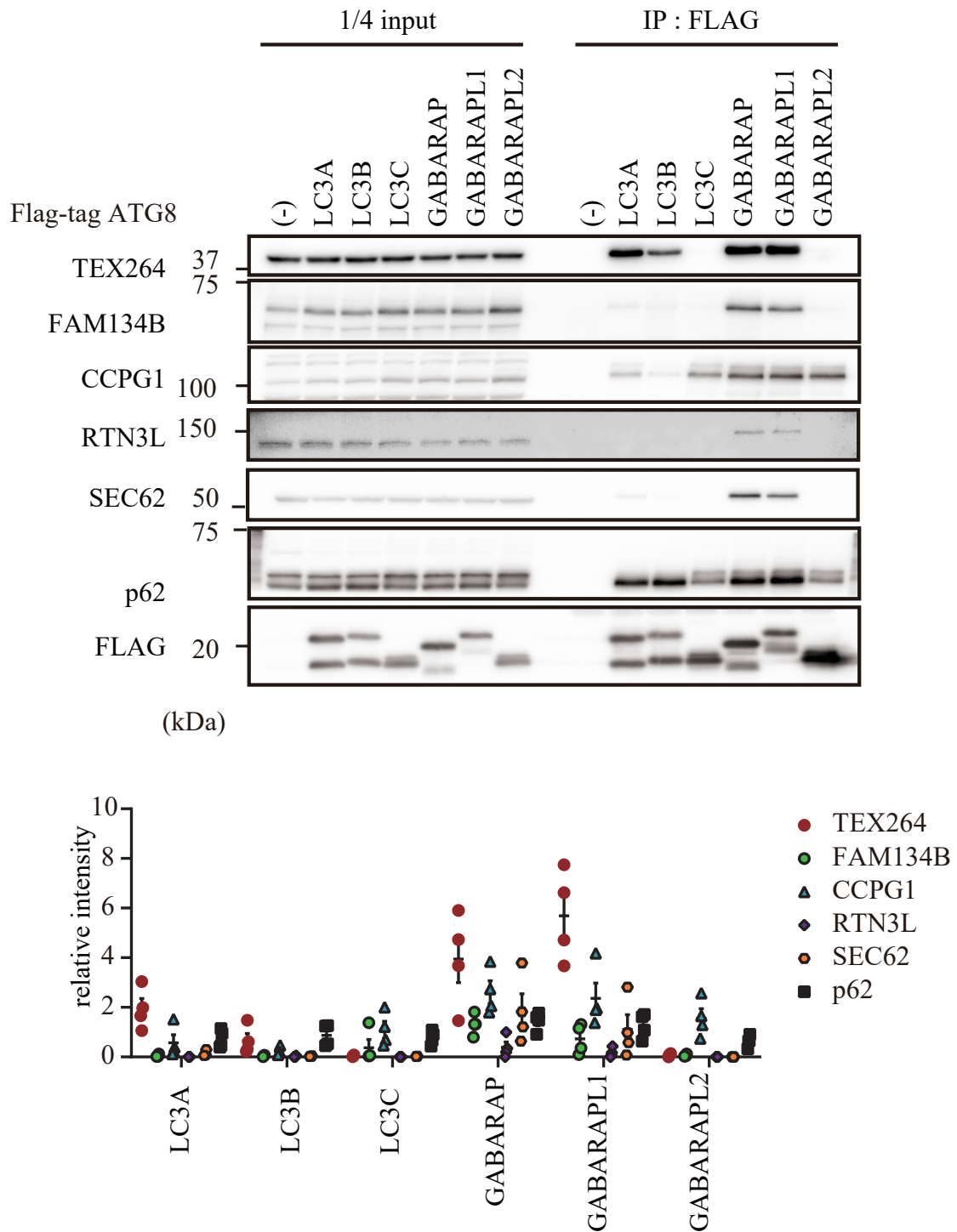


Figure 19. Comparison of ER-phagy receptors in LC3/GABARAP binding
 HEK293T cells transiently expressing each FLAG-tagged LC3 or GABARAP family protein were subjected to immunoprecipitation (IP). Lysates (1/4 IP input) and immunoprecipitates were analyzed by immunoblotting using the indicated antibodies.

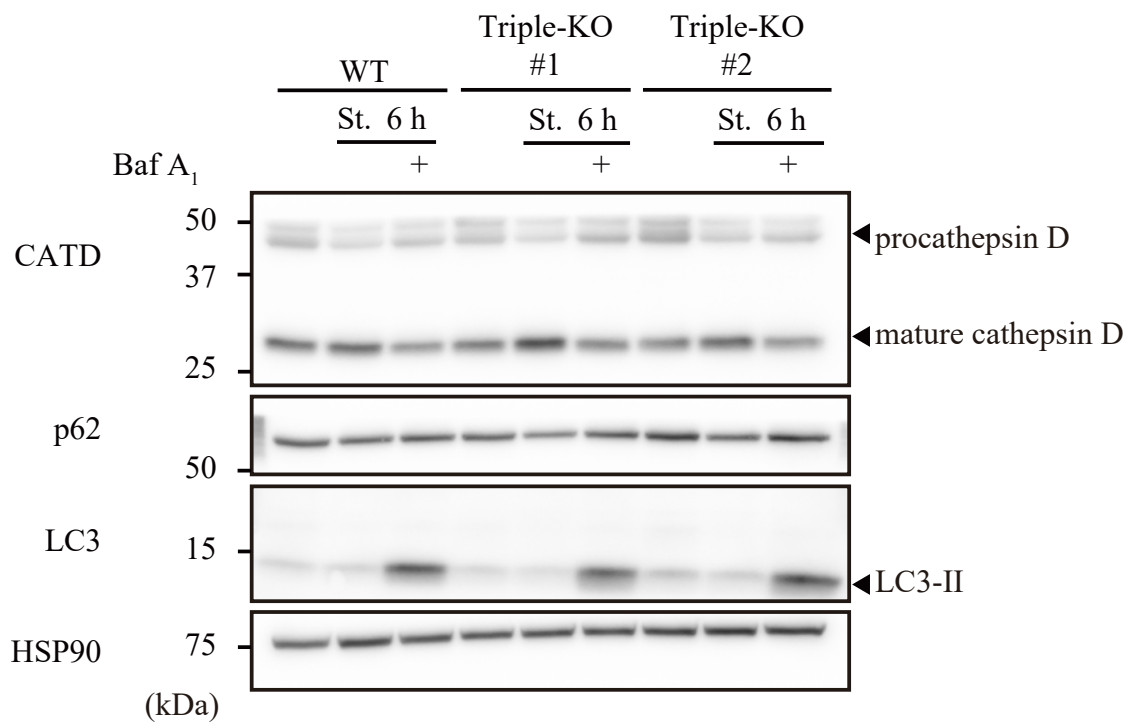


Figure 20. ER-phagy receptors are not required for bulk autophagy

Autophagy flux and cathepsin D maturation in TEX264, FAM134B, and CCPG1 triple-KO Cells (two independent clones). Cells were cultured with or without 100 nM bafilomycin A₁ under nutrient-rich or starvation conditions for 6 h. Cell lysates were analyzed by immunoblotting using the indicated antibodies. Bafilomycin A₁-dependent accumulation of LC3-II represents autophagic flux.

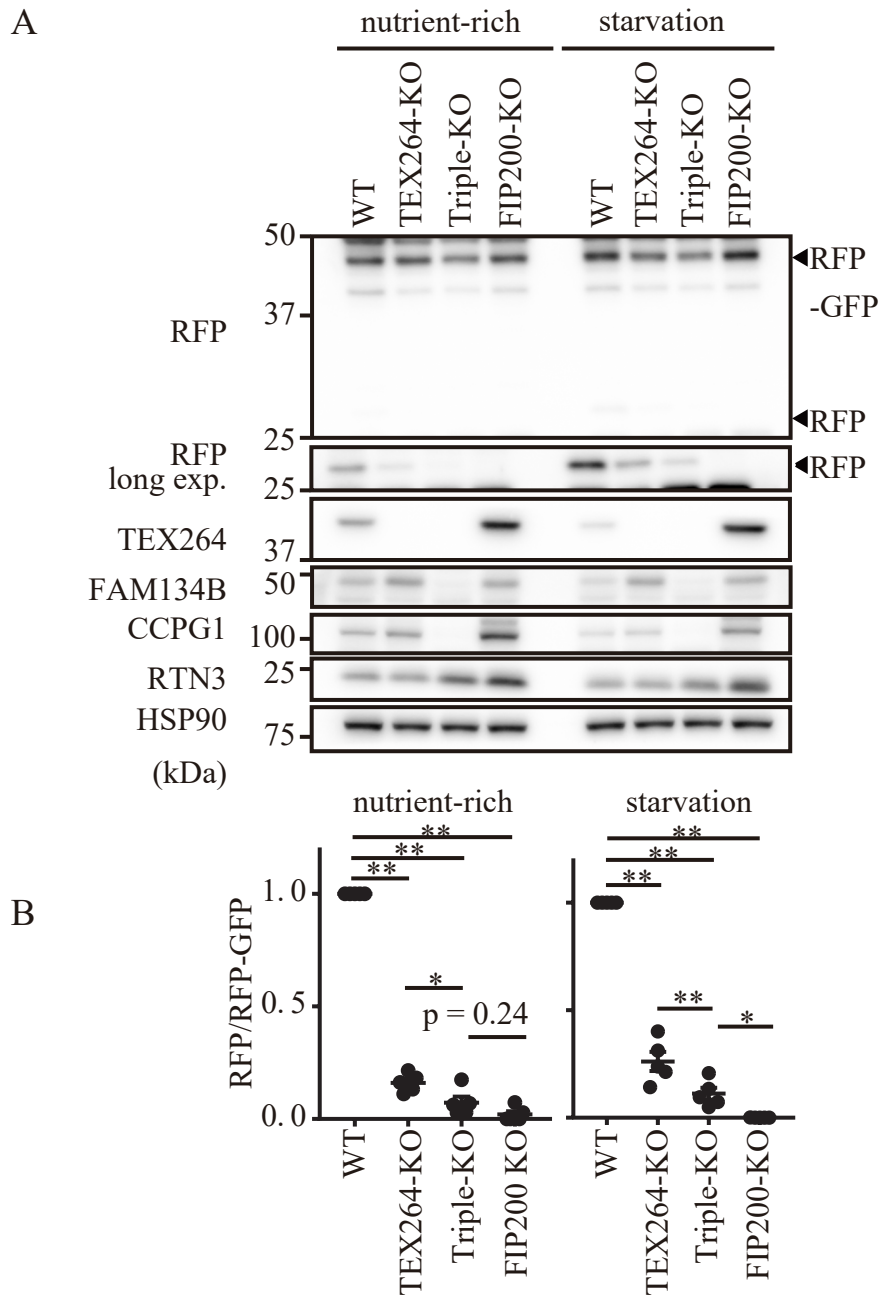


Figure 21. TEX264, CCPG1 and FAM134B work cooperatively as ER-phagy receptors

(A and B) ER-phagy activity of WT, TEX264-KO, TEX264, FAM134B, and CCPG1 triple-KO, and FIP200-KO HeLa cells stably expressing the ER-phagy reporter were cultured in the presence of doxycycline for 24 h to induce the reporter. After doxycycline was removed, cells were cultured in starvation medium lacking amino acids and serum for 9 h (A). Data represent the mean \pm SEM of five independent experiments. Differences were statistically analyzed by one-way ANOVA and Sidak's multiple comparison test. *, $P < 0.05$; **, $P < 0.01$ (B).

reduction in total RFP intensity of red puncta in TEX264-KO cells under basal conditions (Figures 22A and 22B). RFP intensity tended to reduce in TEX264-KO cells under starvation conditions, although this was not significant, probably because the dynamic range of this imaging assay was no larger than that of the immunoblotting assay (Figures 22A and 22B). Under both conditions, the RFP intensity was further reduced in triple-KO cells (Figures 22A and 22B). Additional knockdown of SEC62 or RTN3 in triple-KO cells did not further suppress reporter cleavage under these experimental conditions (Figures 23A and 23B). ER-phagy in triple-KO cells was rescued by exogenous expression of TEX264, although more efficiently than that by FAM134B or CCPG1 (Figures 24A and 24B). Moreover, although autophagic degradation of TEX264 was observed in almost all tissues, that of the other receptors was observed in only some tissues (Figure 12B). Taken together, these data suggest that TEX264 contributes most among the ER-phagy receptors.

We next determined the effect of ER-phagy receptor deletion on ER morphology and ER stress responses. Immunofluorescence microscopy showed that peripheral ERs appeared to be slightly expanded in TEX264-KO and Triple-KO cells as previously observed in FAM134B-KO and CCPG1-KO cells [24,26] (Figure 25). However, it might reflect a change in ER distribution rather than an increase in ER volume because

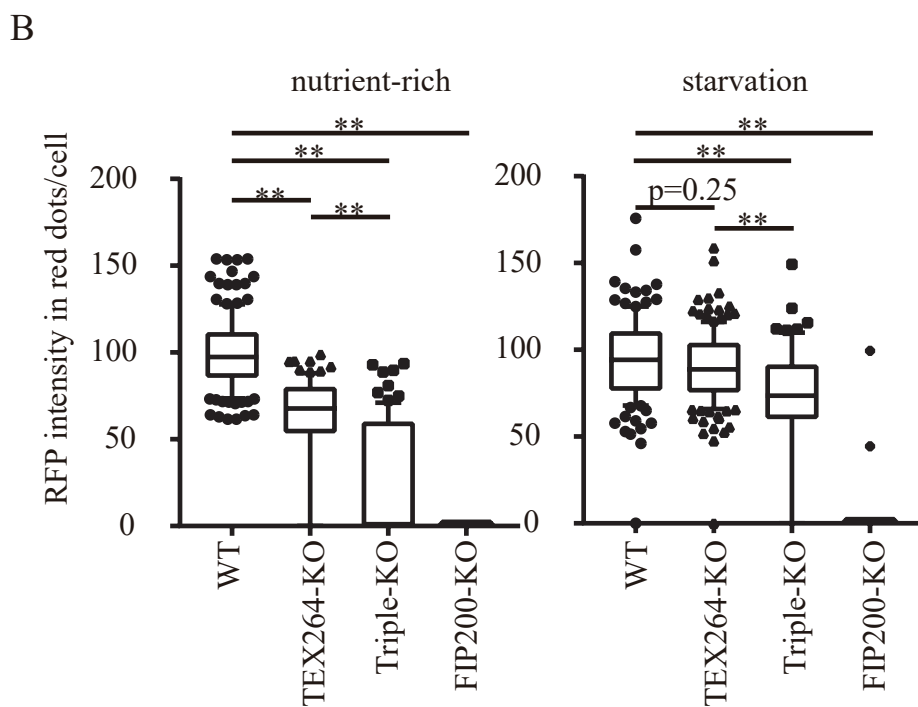
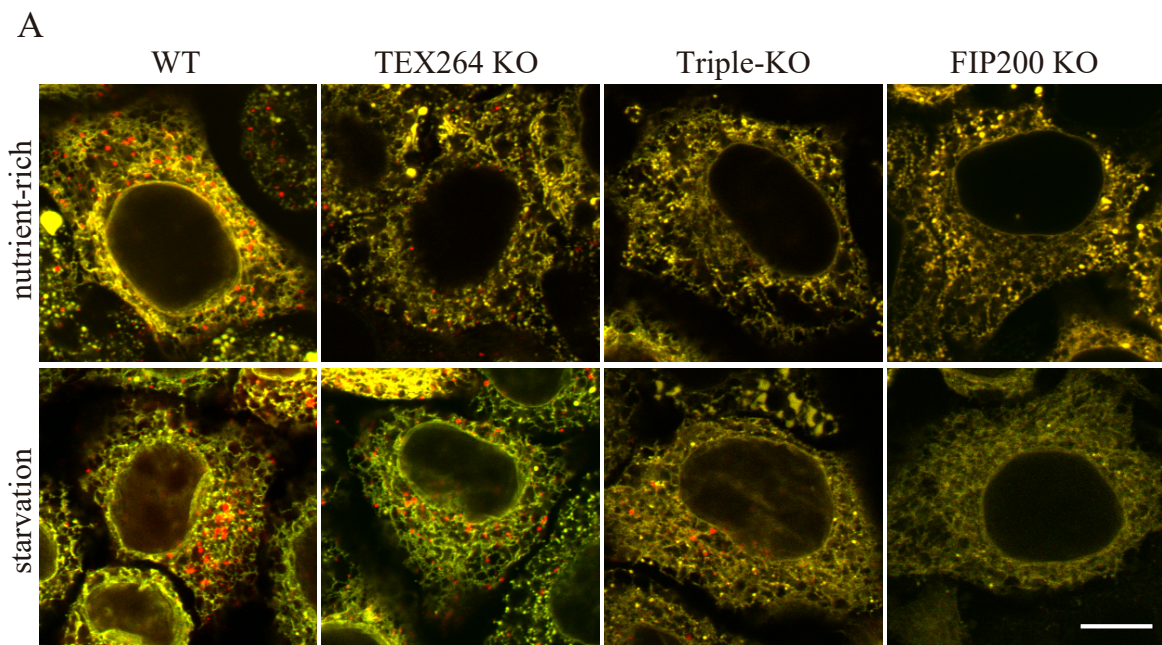


Figure 22. TEX264, CCPG1 and FAM134B work cooperatively as ER-phagy receptors

(A and B) Cells used in Figure 20 were fixed and analyzed by fluorescence microscopy. Bars:

10 μ m (A). The total RFP intensity of red puncta was quantified and normalized with the average of RFP intensity of non-starved WT cells as 100. Data were collected from > 86 cells for each clone. Solid bars indicate medians, boxes the interquartile range (25th to 75th percentile), and whiskers the 10th to 90th percentile. Differences were statistically analyzed by one-way ANOVA and Sidak's multiple comparison test. **, $P < 0.01$ (B).

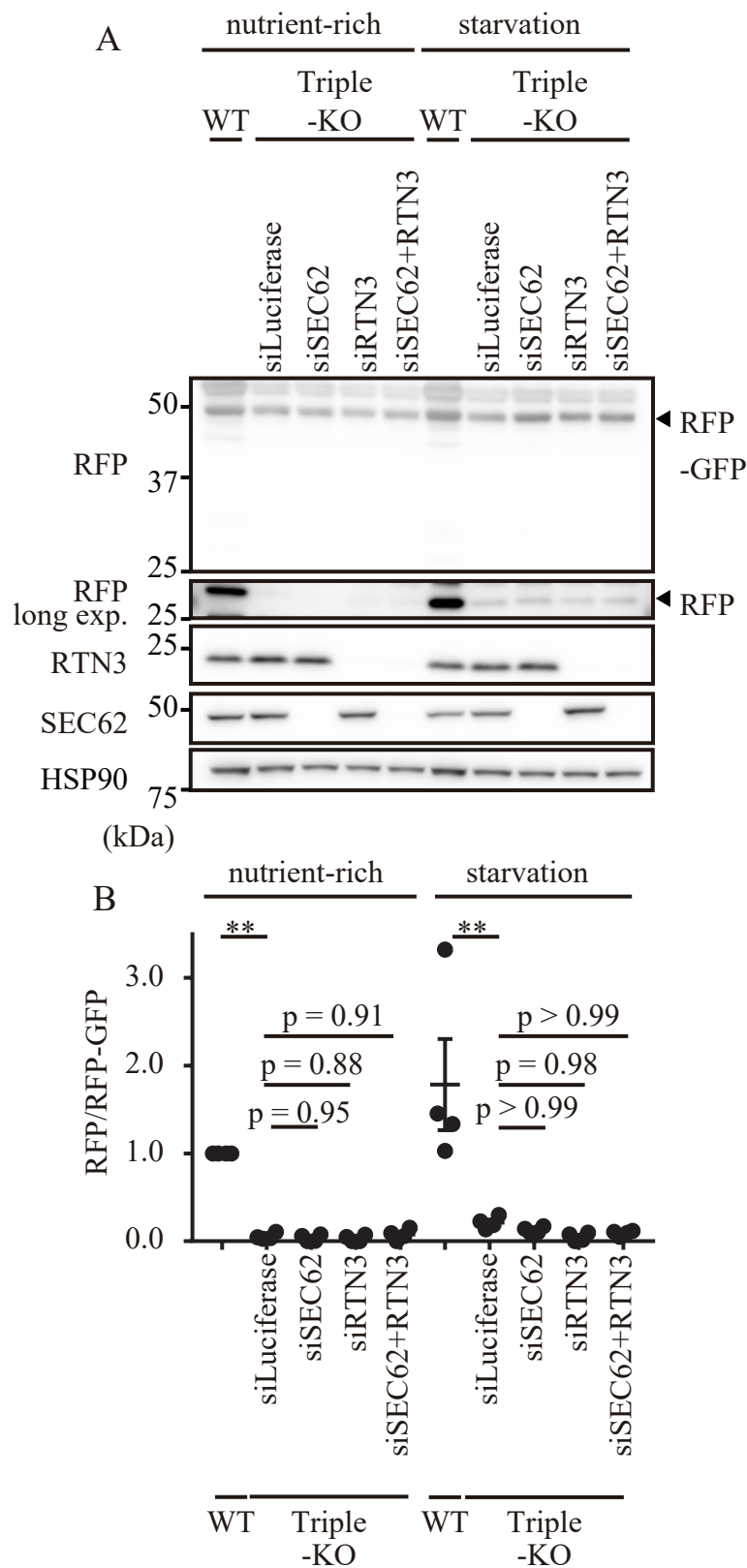


Figure 23. TEX264, FAM134B, and CCPG1 are important for general ER-phagy

(A and B) WT and TEX264, FAM134B, and CCPG1 triple-KO HeLa cells expressing the ER-phagy reporter were transfected with the indicated siRNA and analyzed as in Figure 4C (A). Data represent the mean \pm SEM of four independent experiments. Differences were statistically analyzed by one-way ANOVA and Sidak's multiple comparison test.

** P < 0.01 (B).

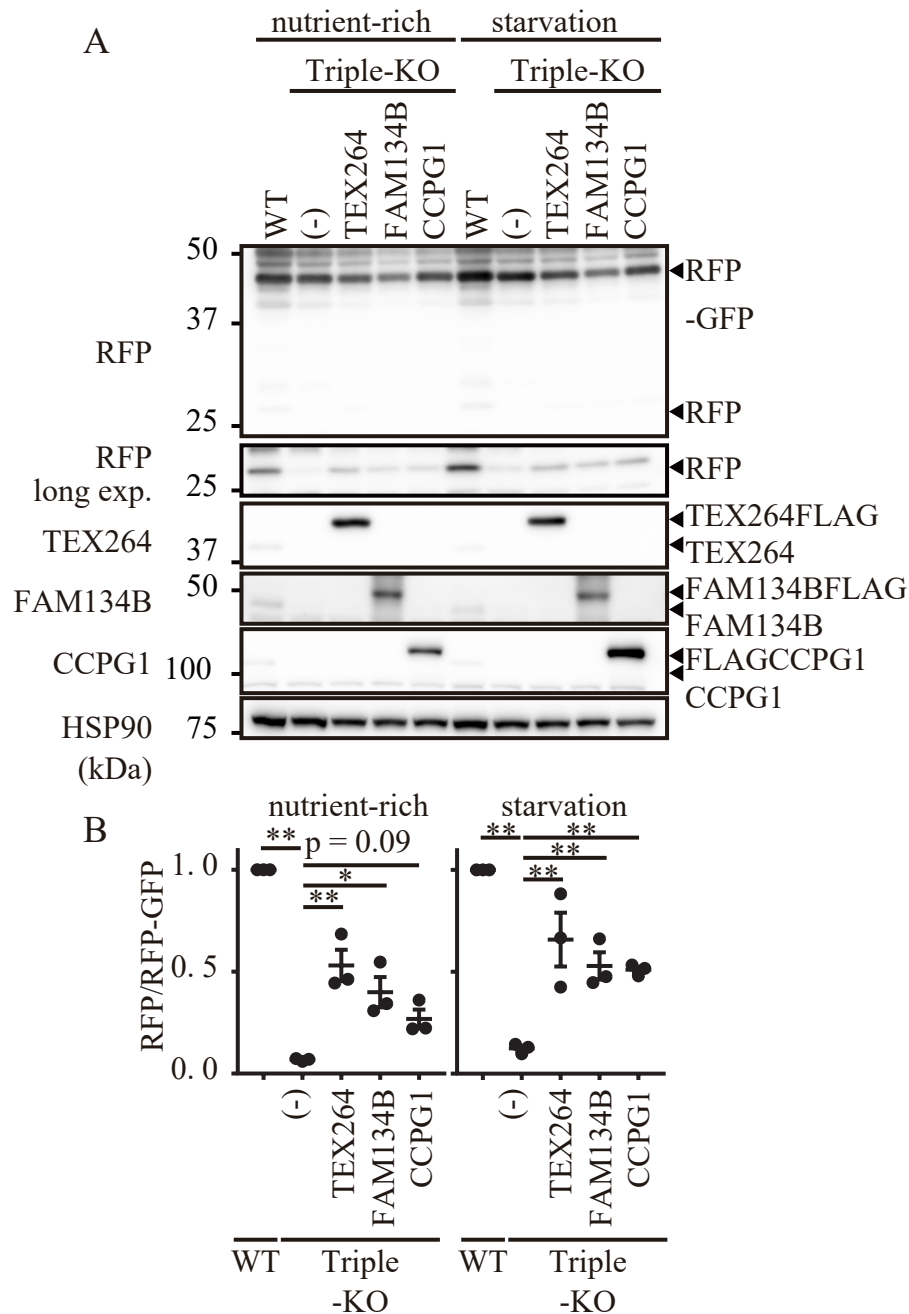


Figure 24. TEX264, CCPG1 and FAM134B work cooperatively as ER-phagy receptors

(A and B) ER-phagy in WT and triple-KO HeLa cells rescued with TEX264-FLAG, FAM134B-FLAG and FLAG-CCPG1 was monitored as in Figure 20 (A). Data represent the mean \pm SEM of three independent experiments. Differences were statistically analyzed by one-way ANOVA and Sidak's multiple comparison test. * $P < 0.05$; ** $P < 0.01$ (B).

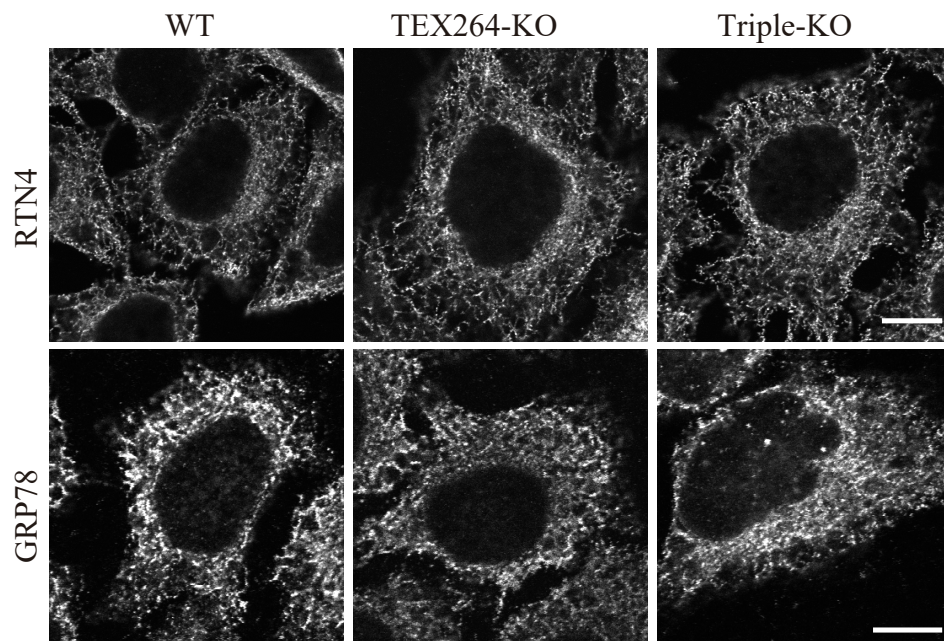


Figure 25. Peripheral ERs appeared to be slightly expanded in TEX264-KO and Triple-KO cells

WT, TEX264-KO and Triple-KO cells were immunostained with anti-RTN4 and anti-GRP78 antibodies. Bars: 10 μ m.

no significant change in the amount of ER resident proteins such as RTN4 was detected in TEX264-KO and Triple-KO cells by immunoblotting (Figure 26). Also, overexpression of TEX264 did not cause a significant change in ER morphology and protein levels (Figure 27 and 28). Electron microscopy did not show any abnormal signs such as dilatation of the ER lumen (Figure 29). The apoptotic sign PARP cleavage was observed differently between ER-stress inducers and there was no consistent changes, suggesting that these cells are not significantly sensitive to ER stresses (Figure 30).

The long intrinsically disordered region in TEX264 is required for autophagosome binding and ER-phagy

Rough ER membranes associate with both outer and inner autophagic membranes [49-51]. However, the two membranes are not directly attached because ribosomes exist between them (Figure 31). Considering the size of ribosomes at approximately 20 nm, ER-phagy receptors that link these two membranes should be longer than 20 nm (Figure 31). Because TEX264 is a relatively small molecule, I assumed that part of TEX264 should not be tightly folded. PSIPRED analysis revealed that TEX264 contains a long intrinsically disordered region (IDR) near the LIR (Figure 32). IDR does not fold into a compact structure and is rather dynamic and flexible [52]. The length of disordered

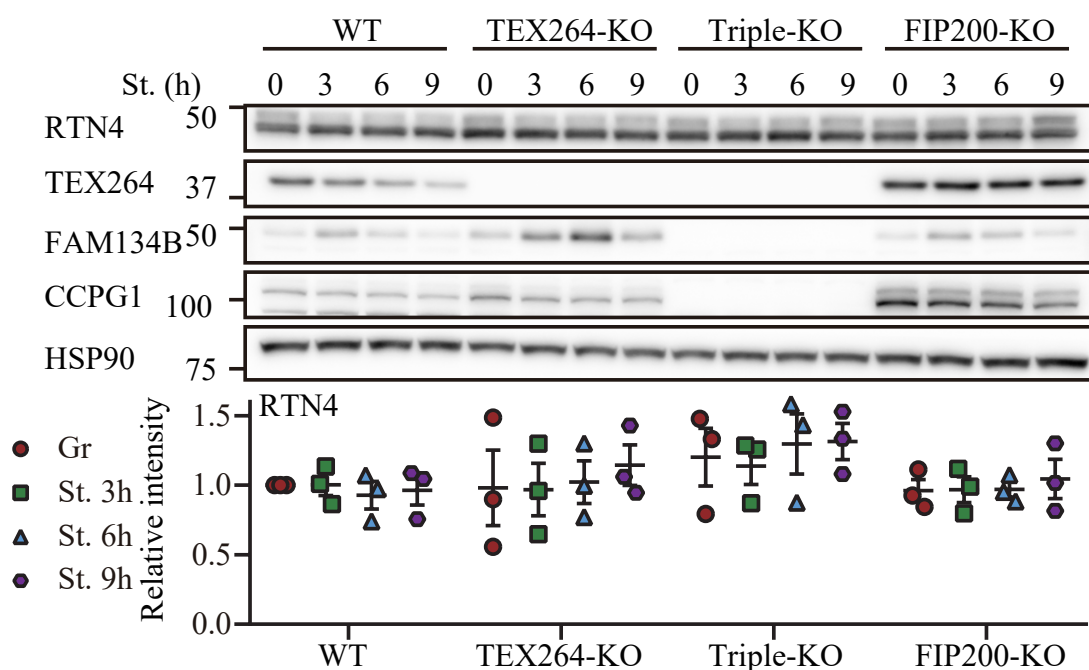


Figure 26. No significant change in the amount of ER resident proteins was detected in TEX264-KO and Triple-KO cells

WT, TEX264-KO, Triple-KO and FIP200-KO HeLa cells were cultured in starvation media lacking amino acids and serum for 3, 6, and 9 h. Cell lysates were analyzed by immunoblotting using the indicated antibodies. Relative changes during starvation of the band intensities (normalized with those of HSP90) (below). Data represent the mean \pm standard error of the mean (SEM) of three independent experiments.

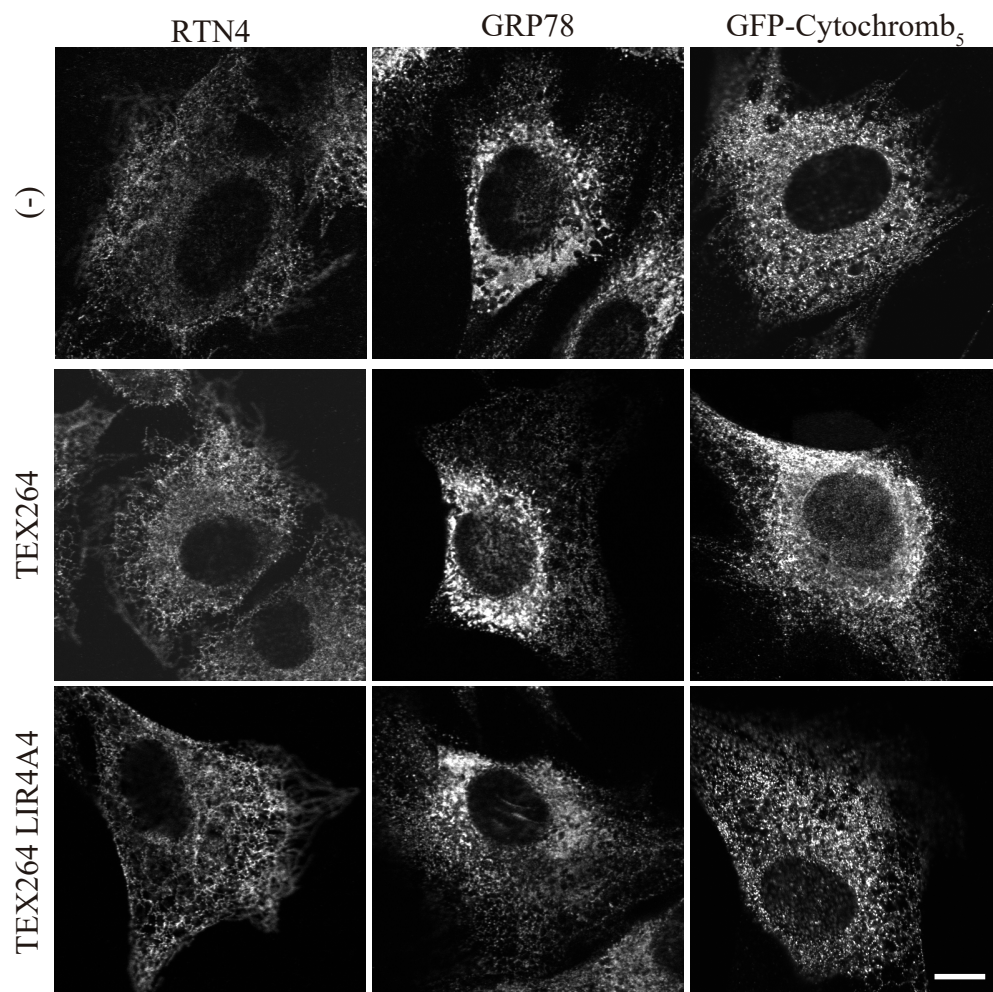


Figure 27. Overexpression of TEX264 leads no significant ER morphological change

WT MEFs expressing GFP-cytochrome b5 and TEX264-FLAG or TEX264 LIR4A-FLAG were immunostained with anti-RTN4 and anti-GRP78 antibodies. Bars: 10 μ m

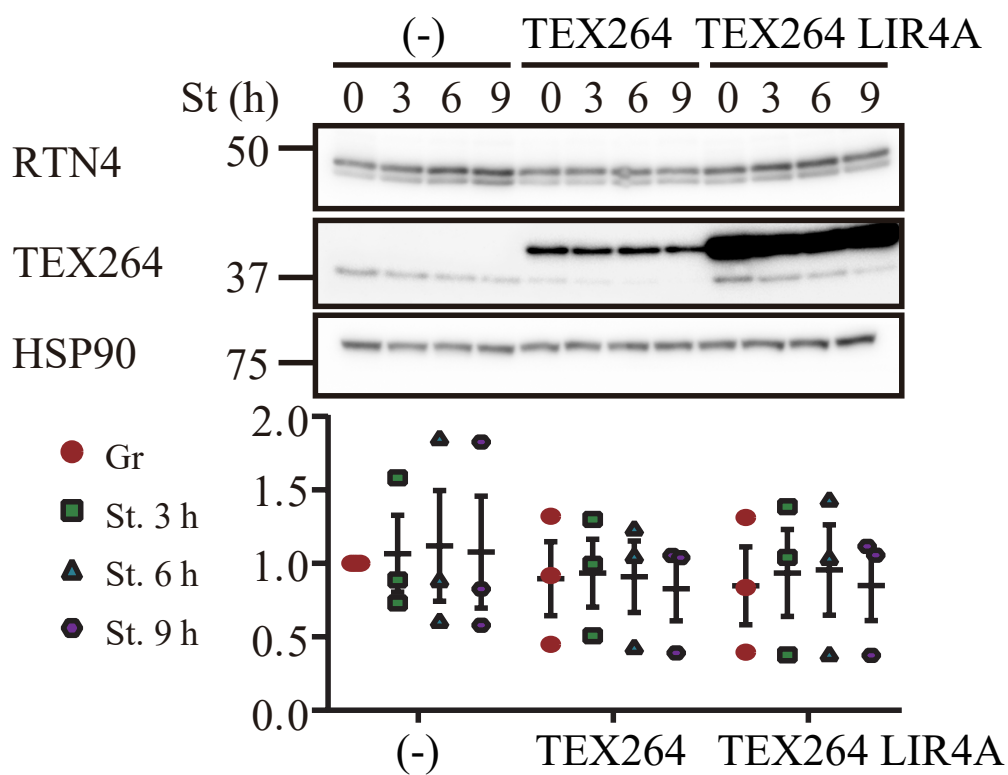


Figure 28. Overexpression of TEX264 leads no significant change of ER resident protein

WT HeLa cells overexpressing TEX264-FLAG or TEX264 LIR4A-FLAG were cultured in starvation media lacking amino acids and serum for 3, 6, and 9 h. Cell lysates were analyzed by immunoblotting using the indicated antibodies.

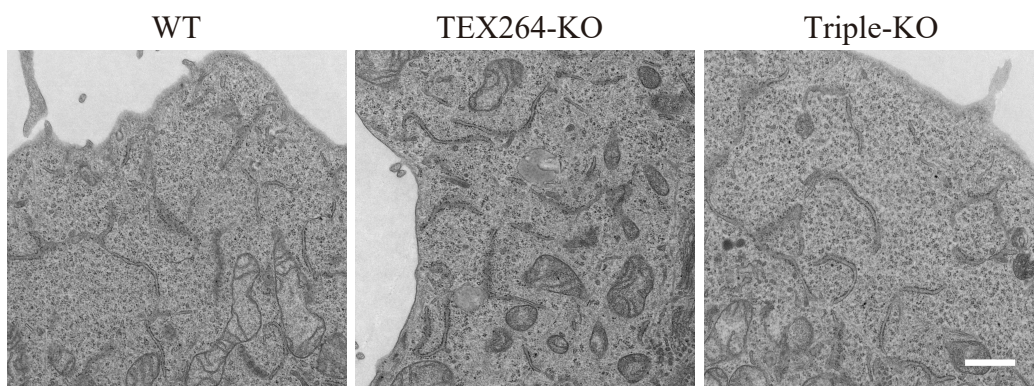


Figure 29. ER morphology in TEX264-KO and Triple-KO cells

Transmission electron microscopy of WT, TEX264-KO and Triple-KO cells.

Bars: 800 nm.

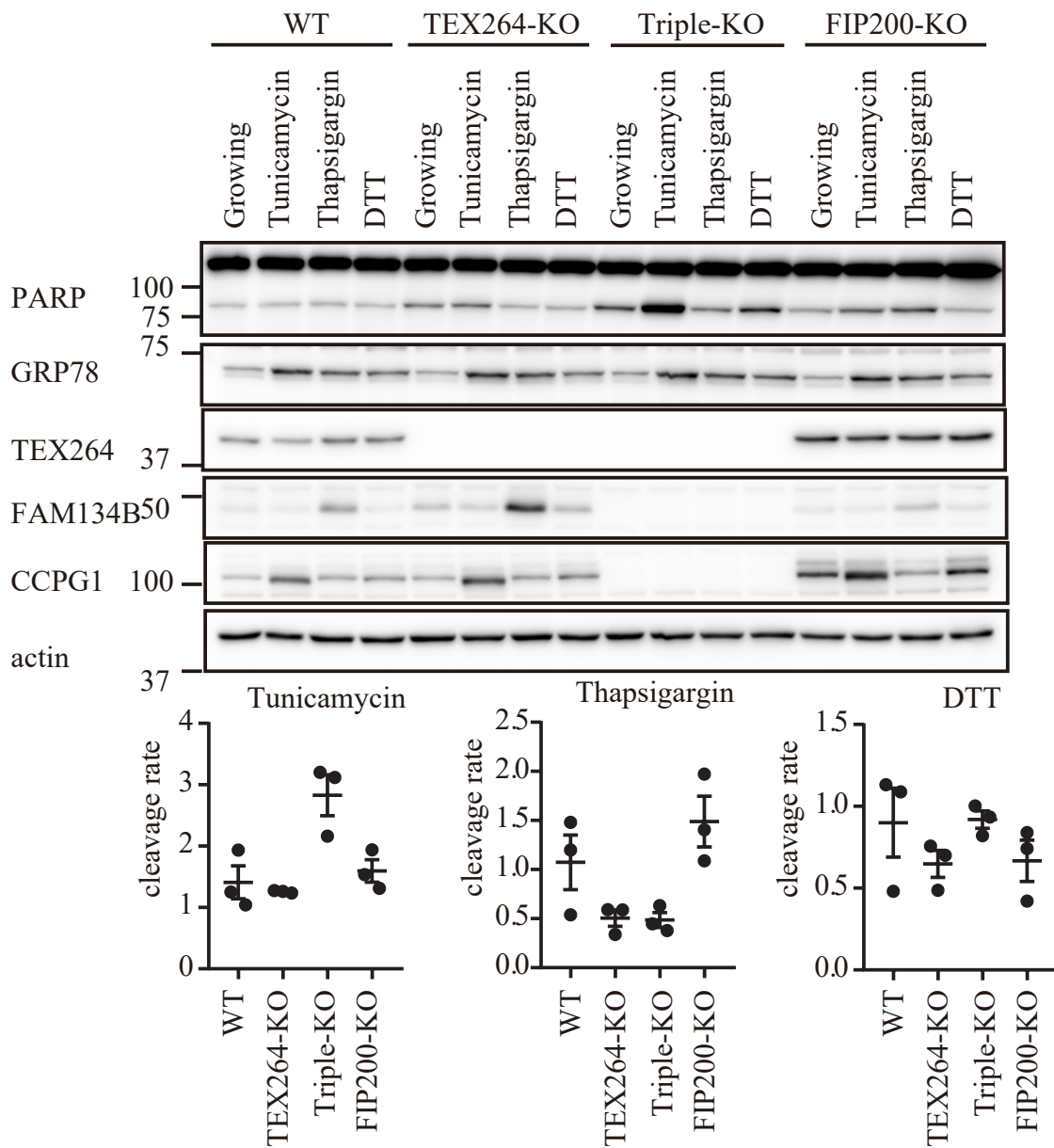


Figure 30. Triple-KO cells are not significantly sensitive to ER stresses

WT, TEX264-KO and Triple-KO cells were cultured with tunicamycin (5 μ g/ml), thapsigargin (5 μ M), or dithiothreitol (DTT) (1 mM) for 12 h. Cell lysates were analyzed with immunoblotting using indicated antibodies..

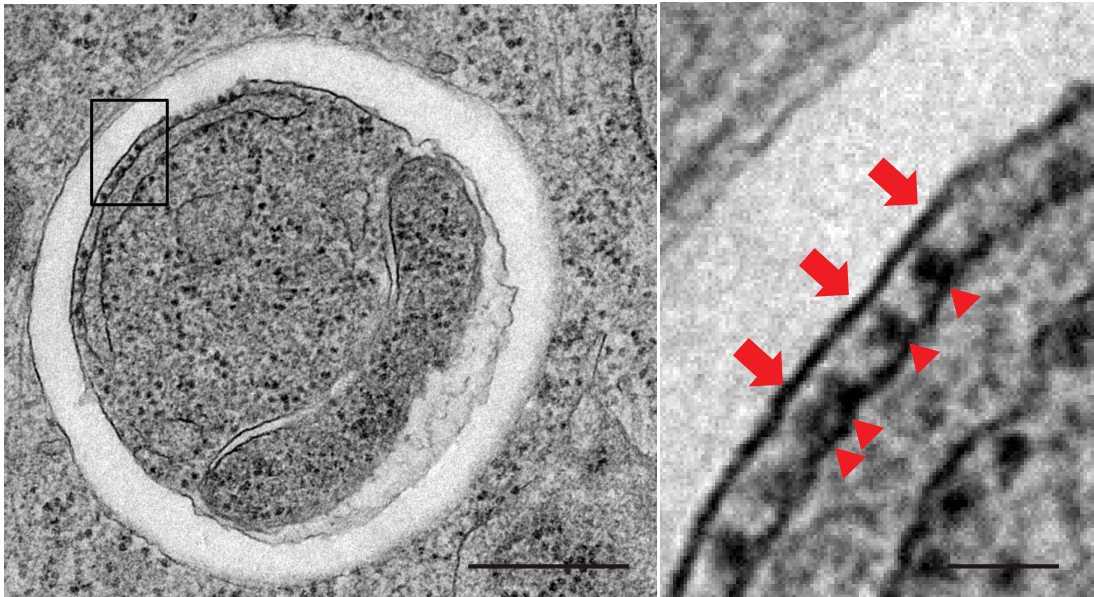


Figure 31. Ribosomes exist between ER and autophagosome membrane

Transmission electron microscopy of WT MEFs under starvation conditions (2 h). The autophagosomal inner membrane (arrow) and endoplasmic reticulum membrane (arrowhead) are indicated. Bars: 400 nm and 50 nm (inset).

domains can be estimated by multiplying the length of a single amino acid (0.38 nm) by the total number of amino acids in the domain [53]. Accordingly, the length of the IDR in TEX264 may exceed 40 nm, which would be longer than the size of a ribosome.

First, I determined whether the IDR is required for TEX264 to connect with autophagic membranes. To this end, I generated TEX264 mutants with different deletions in the IDR (Figure 32A). TR2, which lacked approximately half of the IDR, still colocalized with LC3 (Figures 32B and 32C). In contrast, TR1, which lacked almost the entire IDR but retained the LIR, failed to colocalize with LC3 (Figures 32). When I inserted an IDR sequence from human ATG13 (amino acids 191–248) corresponding to the previously characterized IDR region in yeast Atg13 [54], LC3 colocalization was rescued (Figures 32B and 32C). Thus, the length of the IDR rather than a specific amino acid sequence is critical for the association between TEX264 and the autophagic membranes.

Finally, I tested whether the IDR is required for the ER-phagy receptor function of TEX264. Expression of the short truncated mutant (TR2) but not the full-deletion mutant (TR1) restored ER-phagy in TEX264-KO cells (Figures 33A and 33B). Furthermore, expression of the TEX264 mutant replaced with the IDR from ATG13 was also functional (Figures 33A and 33B). These data suggest that the long IDR in TEX264

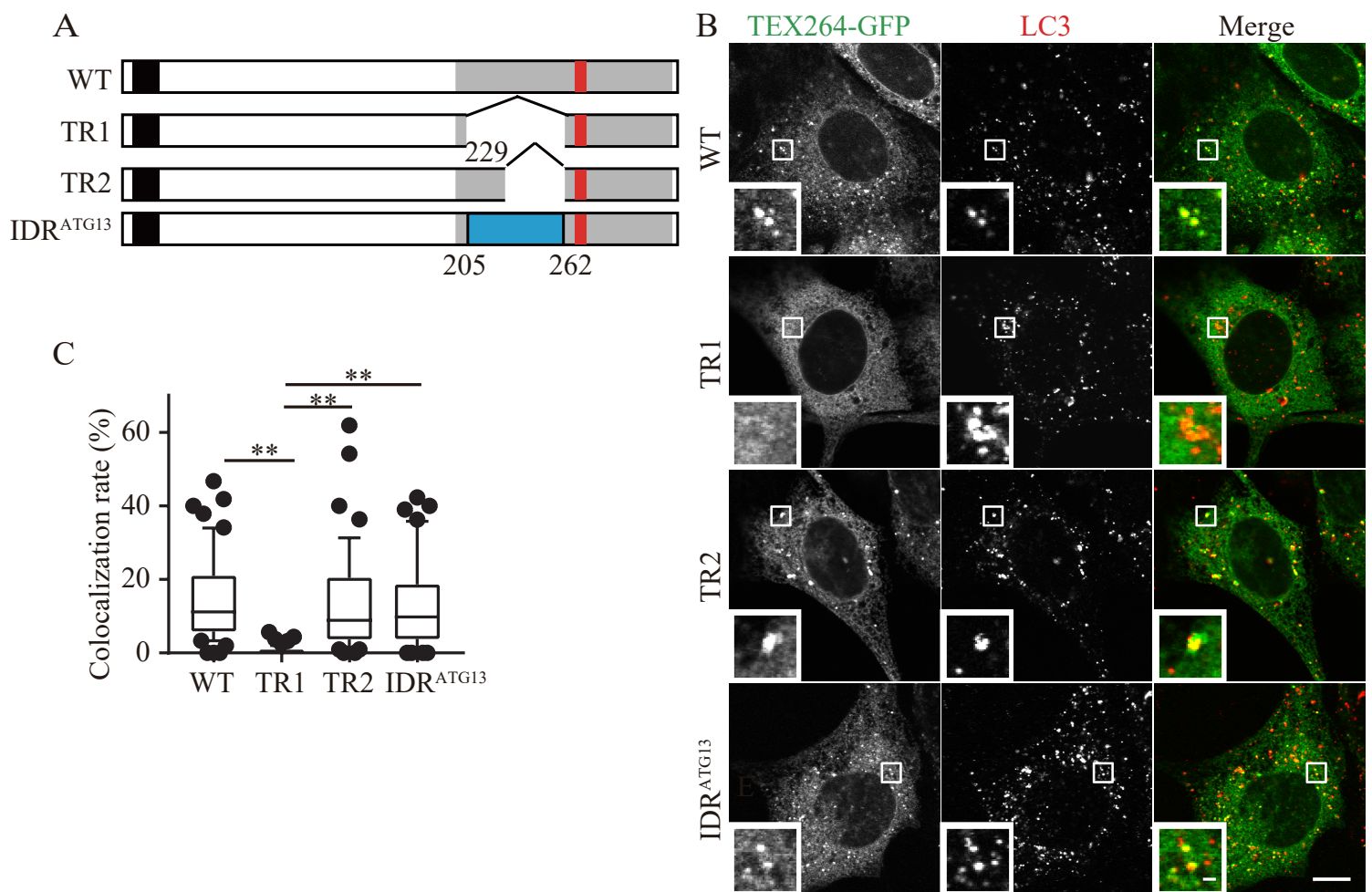


Figure 32. The long intrinsically disordered region in TEX264 is required for autophagosome binding and ER-phagy

(A) Schematic representation of TEX264 IDR mutants that have truncated IDRs or an IDR from human ATG13 (blue). Gray and red boxes indicate the IDR and LIR, respectively.

(B and C) MEFs stably expressing TEX264-GFP or its mutant were cultured in starvation medium for 2 h, and immunostained with anti-LC3 antibody. Bars: 10 μm and 1 μm (insets) (B). Colocalization between TEX264-GFP puncta and endogenous LC3 was determined in > 45 cells. Solid bars indicate median, boxes the interquartile range (25th to 75th percentile), and whiskers the 10th to 90th percentile. Differences were statistically analyzed by one-way ANOVA and Sidak's multiple comparison test. **, $P < 0.01$ (C).

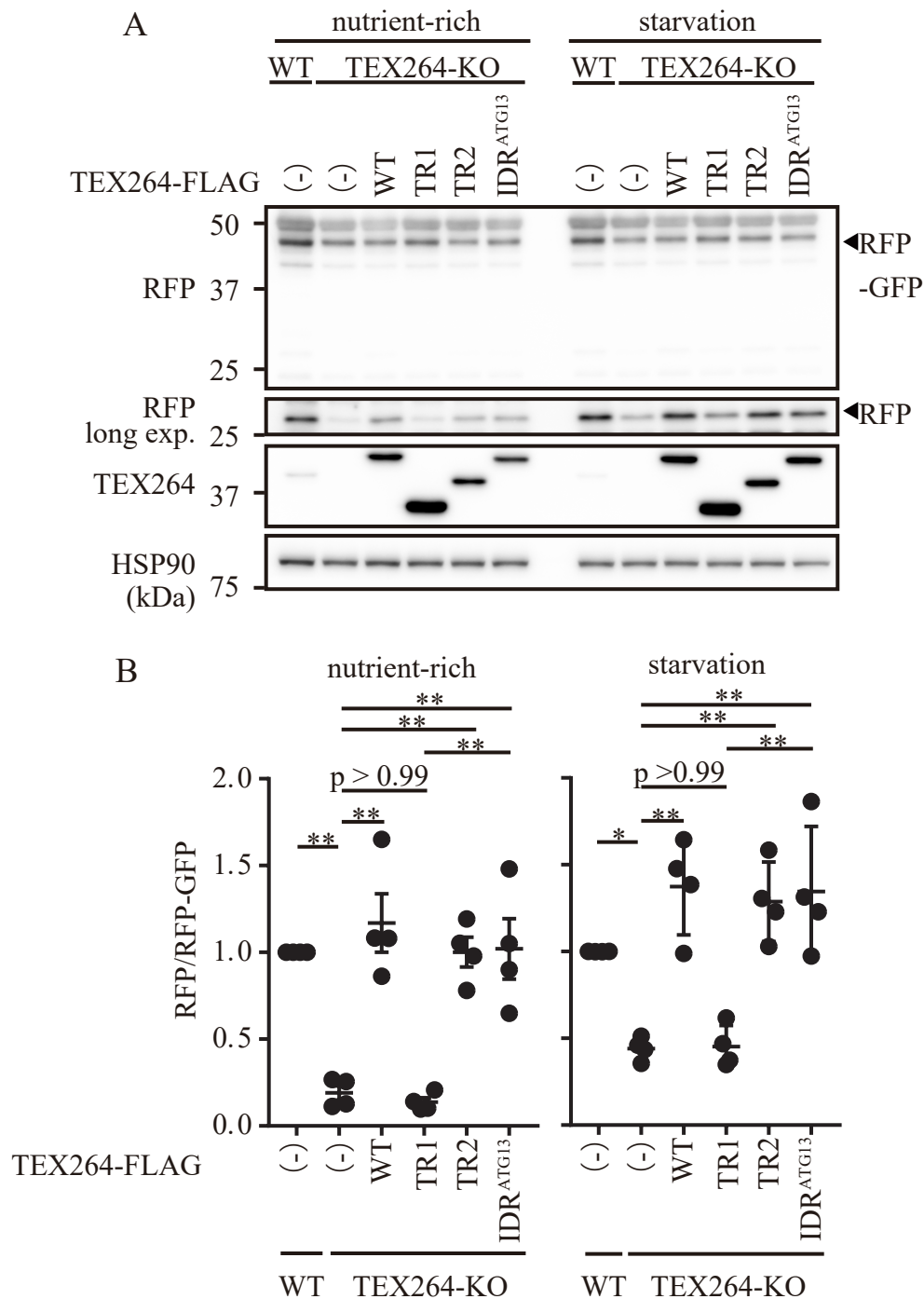


Figure 33. The long intrinsically disordered region in TEX264 is required for ER-phagy receptor function

(A and B) ER-phagy was monitored in WT and TEX264-KO HeLa cells expressing the indicated TEX264 mutants tagged with FLAG at C-terminus as in Figure 14 (A). Data represent the mean \pm SEM of four independent experiments. Differences were statistically analyzed by one-way ANOVA and Sidak's multiple comparison test. *, $P < 0.05$; **, $P < 0.01$ (B).

functions as a bridge between the ER and autophagosomal membranes to act as an ER-phagy receptor (Figure 34).

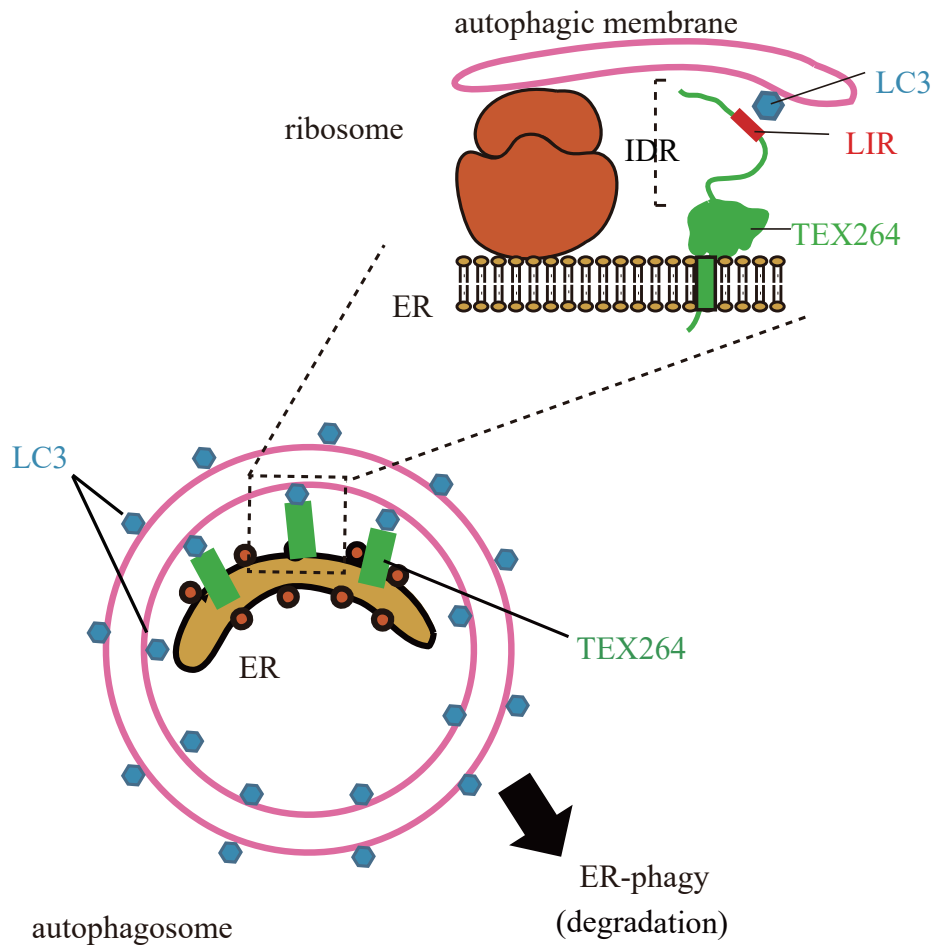


Figure 34. A disordered region in TEX264 bridges the gap between the ER and autophagosomes.
 A model of TEX264 bridging between the ER and autophagic membranes. IDR, intrinsically disordered region.

Discussion

In this study, I identified TEX264 as a novel ER-phagy receptor. Although four ER-phagy receptors have already been reported in mammals, this study has provided the following novel insights into this topic.

First, I analyzed the relative importance of the five ER-phagy receptors including TEX264. TEX264 is ubiquitously expressed in all tissues that I have tested, whereas the other four receptors are expressed in only some tissues (Figures 12A and 12B). The binding affinity of TEX264 to LC3/GABARAP family proteins is stronger than that of the other four receptors; thus, TEX264 is the most efficient of the known receptors (Figures 19). Furthermore, our results using multiple knockdown and knockout cells suggest that deletion of TEX264 causes the largest inhibition of ER-phagy at least in HeLa cells (Figures 17A and 24A). Based on these data, I hypothesized that, although there is redundancy, TEX264 contributes the most among the ER-phagy receptors.

As discussed in a recent review [11], ER-phagy receptors can be classified into two groups: single or double transmembrane receptors (TEX264, CCPG1, and SEC62) and reticulon-type receptors (FAM134B and RTN3) (Figure 35). The former may simply act as linkers between the ER and autophagosomal membranes, whereas the

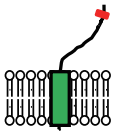
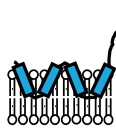
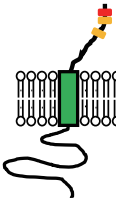
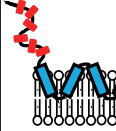
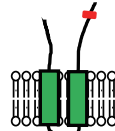
Receptors	TEX264	FAM134B	CCPG1	RTN3	SEC62
					
TM/ RHD	1 TM	RHD	1 TM	RHD	2 TMs
IDR	Yes	Yes	Yes	Yes	Yes
LIR	Yes	Yes	Yes	Yes	Yes
LC3 family binding	LC3A GABARAP	GABARAP family	GABARAP family		GABARAP L2
Tissue specificity	Ubiquitous	Ubiquitous	liver pancreas kidney	muscle brain	Ubiquitous
Trigger	Basal Starvation	Starvation	ER stress	Starvation	Recovery from ER stress

Figure 35. Mammalian ER-phagy receptors

Characterization of ER-phagy receptors. Green, transmembrane domain; blue, reticulon homology domain; red, LIR; yellow, FIP200-interacting region (FIR)

latter have additional functions that remodel or fragment the ER membranes, allowing them to be engulfed by autophagosomes [24]. Thus, these receptors may function somewhat sequentially, which would explain why deletion of TEX264 alone has such a profound inhibitory effect on ER-phagy (Figures 14–34).

Second, TEX264 has a long IDR domain, which is required for its ER-phagy receptor function (Figures 31-34). As I found using the PSIPRED protein sequence analysis workbench, IDRs are contained in the other ER-phagy receptors (Figure 36), and so this may be a common feature of ER-phagy receptors. In general, the IDR has multiple functions, including in protein–protein interactions, membrane curvature, signaling, and intracellular liquid-liquid phase separation [24,55-58]. In the case of ER-phagy, I hypothesize that IDRs are required to bridge the long distance between ER and autophagosome membranes because ribosomes exist on ER membranes that attach to autophagic membranes (Figure 31) [40,50,59]. It was also reported that Ist2 requires an IDR to exert its tethering function at the ER-plasma membrane junction in yeast [60]. However, given that ribosomes are generally excluded from the ER-plasma membrane contact sites [61], IDRs in membrane contacting proteins, including TEX264, may have additional roles.

Third, I generated a novel ER-phagy reporter, with which I could quantitatively

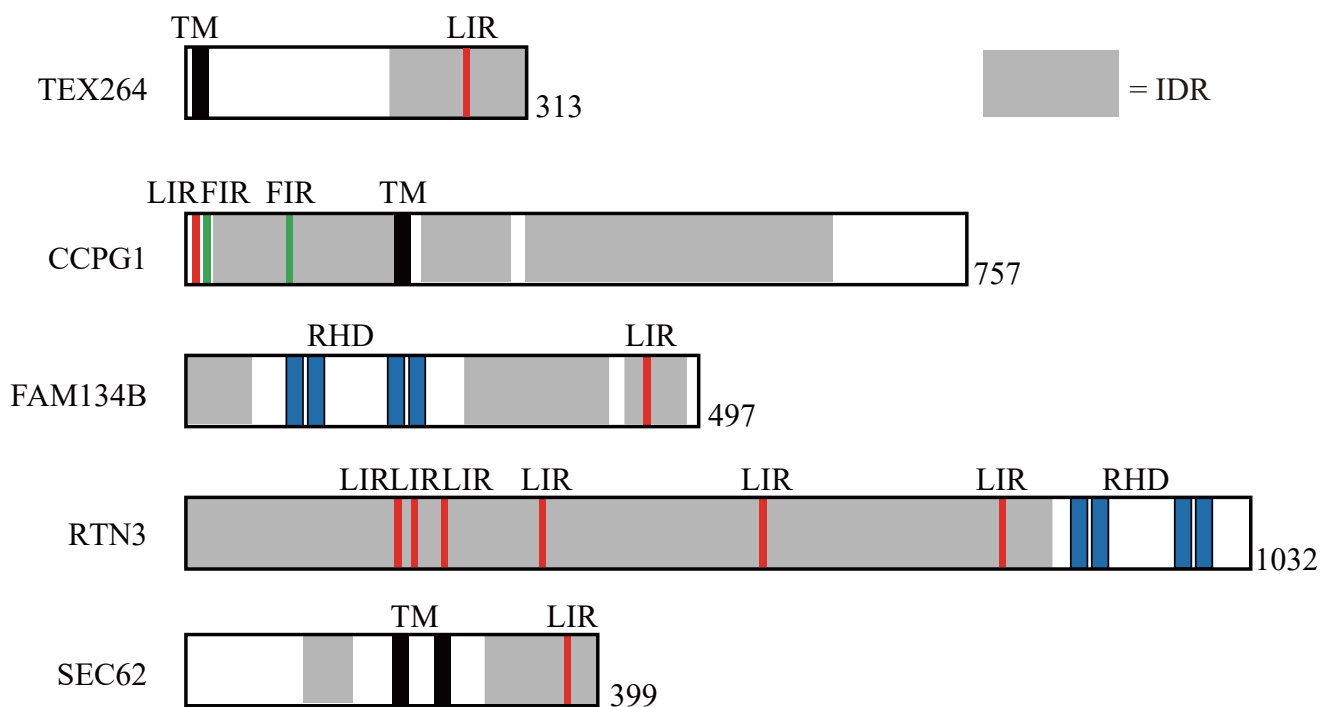


Figure 36. Characterization of ER-phagy receptors

Domain architecture of ER-phagy receptors. Black, transmembrane domain; blue, reticulon homology domain; red, LIR; green, FIP200-interacting region (FIR); gray, intrinsically disordered region.

measure ER-phagic flux. Traditional electron microscopy has shown that ER fragments are sequestered by autophagosomes, but quantification is difficult. ER-phagy could be also monitored by evaluating the ER protein turnover rate and ER distribution [24-26]. Instead, I established a more quantitative method to measure ER-phagy activity, namely, doxycycline-induced ER-targeted tandem RFP-GFP. As this is an inducible system, I can eliminate the effect of the synthesis of this reporter during measurement. Such tandem fluorescent-based reporters have been widely used to monitor bulk and selective autophagy [62-67]. Very recently, Liang et al. also generated a similar ER-phagy reporter using a dual fluorescence-labeled ER transmembrane protein [68]. Using our new reporter, I could quantify ER-phagy activity not only during starvation but also under basal conditions, and found that TEX264 was required for both. Thus, TEX264 may have homeostatic roles in the ER under normal conditions in a wide range of tissues. In particular, TEX264 is highly expressed in the testis, where smooth ER is abundant for the production of steroid hormones; a high demand for ER homeostasis may exist.

So far, our reporter can evaluate only bulk degradation of ER but not selective degradation of ER subdomains because KDEL-based probes can diffusely spread in the ER. Whether ER-phagy receptors can recognize some specific ER subdomains would be

the next important question. Generation of each subdomain reporter would help us to understand the overall picture of ER-phagy. Also, an investigation into the different functions of ER-phagy receptors in vivo would facilitate our understanding of their physiological and pathological roles.

References

- 1 Mizushima, N. & Komatsu, M. Autophagy: renovation of cells and tissues. *Cell* **147**, 728-741, doi:10.1016/j.cell.2011.10.026 (2011).
- 2 Lamb, C. A., Yoshimori, T. & Tooze, S. A. The autophagosome: origins unknown, biogenesis complex. *Nat Rev Mol Cell Biol* **14**, 759-774, doi:10.1038/nrm3696 (2013).
- 3 Soreng, K., Neufeld, T. P. & Simonsen, A. Membrane Trafficking in Autophagy. *Int Rev Cell Mol Biol* **336**, 1-92, doi:10.1016/bs.ircmb.2017.07.001 (2018).
- 4 Morita, K., Hama, Y., Izume, T., Tamura, N., Ueno, T., Yamashita, Y., Sakamaki, Y., Mimura, K., Morishita, H., Shihoya, W., Nureki, O., Mano, H. & Mizushima, N. Genome-wide CRISPR screen identifies TMEM41B as a gene required for autophagosome formation. *J Cell Biol* **217**, 3817-3828, doi:10.1083/jcb.201804132 (2018).
- 5 Mizushima, N. A brief history of autophagy from cell biology to physiology and disease. *Nat Cell Biol* **20**, 521-527, doi:10.1038/s41556-018-0092-5 (2018).
- 6 Dikic, I. & Elazar, Z. Mechanism and medical implications of mammalian autophagy. *Nat Rev Mol Cell Biol* **19**, 349-364, doi:10.1038/s41580-018-0003-4 (2018).
- 7 Gatica, D., Lahiri, V. & Klionsky, D. J. Cargo recognition and degradation by selective autophagy. *Nat Cell Biol* **20**, 233-242, doi:10.1038/s41556-018-0037-z (2018).

- 8 Anding, A. L. & Baehrecke, E. H. Cleaning House: Selective Autophagy of Organelles. *Dev Cell* **41**, 10-22, doi:10.1016/j.devcel.2017.02.016 (2017).
- 9 Fregno, I. & Molinari, M. Endoplasmic reticulum turnover: ER-phagy and other flavors in selective and non-selective ER clearance. *F1000Res* **7**, 454, doi:10.12688/f1000research.13968.1 (2018).
- 10 Gomes, L. C. & Dikic, I. Autophagy in antimicrobial immunity. *Mol Cell* **54**, 224-233, doi:10.1016/j.molcel.2014.03.009 (2014).
- 11 Grumati, P., Dikic, I. & Stolz, A. ER-phagy at a glance. *J Cell Sci* **131**, doi:10.1242/jcs.217364 (2018).
- 12 Lamark, T., Svenning, S. & Johansen, T. Regulation of selective autophagy: the p62/SQSTM1 paradigm. *Essays Biochem* **61**, 609-624, doi:10.1042/ebc20170035 (2017).
- 13 Yamamoto, A. & Simonsen, A. The elimination of accumulated and aggregated proteins: a role for aggrephagy in neurodegeneration. *Neurobiol Dis* **43**, 17-28, doi:10.1016/j.nbd.2010.08.015 (2011).
- 14 Deng, Z., Purtell, K., Lachance, V., Wold, M. S., Chen, S. & Yue, Z. Autophagy Receptors and Neurodegenerative Diseases. *Trends Cell Biol* **27**, 491-504, doi:10.1016/j.tcb.2017.01.001 (2017).

- 15 Pickrell, A. M. & Youle, R. J. The roles of PINK1, parkin, and mitochondrial fidelity in Parkinson's disease. *Neuron* **85**, 257-273, doi:10.1016/j.neuron.2014.12.007 (2015).
- 16 Khaminets, A., Behl, C. & Dikic, I. Ubiquitin-Dependent And Independent Signals In Selective Autophagy. *Trends Cell Biol* **26**, 6-16, doi:10.1016/j.tcb.2015.08.010 (2016).
- 17 Noda, N. N., Ohsumi, Y. & Inagaki, F. Atg8-family interacting motif crucial for selective autophagy. *FEBS Lett* **584**, 1379-1385, doi:10.1016/j.febslet.2010.01.018 (2010).
- 18 Slobodkin, M. R. & Elazar, Z. The Atg8 family: multifunctional ubiquitin-like key regulators of autophagy. *Essays Biochem* **55**, 51-64, doi:10.1042/bse0550051 (2013).
- 19 Birgisdottir, A. B., Lamark, T. & Johansen, T. The LIR motif - crucial for selective autophagy. *J Cell Sci* **126**, 3237-3247, doi:10.1242/jcs.126128 (2013).
- 20 Rogov, V. V., Stolz, A., Ravichandran, A. C., Rios-Szwed, D. O., Suzuki, H., Kniss, A., Lohr, F., Wakatsuki, S., Dotsch, V., Dikic, I., Dobson, R. C. & McEwan, D. G. Structural and functional analysis of the GABARAP interaction motif (GIM). *EMBO Rep* **18**, 1382-1396, doi:10.15252/embr.201643587 (2017).

- 21 Stolz, A., Ernst, A. & Dikic, I. Cargo recognition and trafficking in selective autophagy. *Nat Cell Biol* **16**, 495-501, doi:10.1038/ncb2979 (2014).
- 22 Noda, N. N., Kumeta, H., Nakatogawa, H., Satoo, K., Adachi, W., Ishii, J., Fujioka, Y., Ohsumi, Y. & Inagaki, F. Structural basis of target recognition by Atg8/LC3 during selective autophagy. *Genes Cells* **13**, 1211-1218, doi:10.1111/j.1365-2443.2008.01238.x (2008).
- 23 Mochida, K., Oikawa, Y., Kimura, Y., Kirisako, H., Hirano, H., Ohsumi, Y. & Nakatogawa, H. Receptor-mediated selective autophagy degrades the endoplasmic reticulum and the nucleus. *Nature* **522**, 359-362, doi:10.1038/nature14506 (2015).
- 24 Khaminets, A., Heinrich, T., Mari, M., Grumati, P., Huebner, A. K., Akutsu, M., Liebmann, L., Stolz, A., Nietzsche, S., Koch, N., Mauthe, M., Katona, I., Qualmann, B., Weis, J., Reggiori, F., Kurth, I., Hubner, C. A. & Dikic, I. Regulation of endoplasmic reticulum turnover by selective autophagy. *Nature* **522**, 354-358, doi:10.1038/nature14498 (2015).
- 25 Grumati, P., Morozzi, G., Holper, S., Mari, M., Harwardt, M. I., Yan, R., Muller, S., Reggiori, F., Heilemann, M. & Dikic, I. Full length RTN3 regulates turnover of tubular endoplasmic reticulum via selective autophagy. *Elife* **6**, doi:10.7554/eLife.25555 (2017).

- 26 Smith, M. D., Harley, M. E., Kemp, A. J., Wills, J., Lee, M., Arends, M., von Kriegsheim, A., Behrends, C. & Wilkinson, S. CCPG1 Is a Non-canonical Autophagy Cargo Receptor Essential for ER-Phagy and Pancreatic ER Proteostasis. *Dev Cell* **44**, 217-232.e211, doi:10.1016/j.devcel.2017.11.024 (2018).
- 27 Fumagalli, F., Noack, J., Bergmann, T. J., Cebollero, E., Pisoni, G. B., Fasana, E., Fregno, I., Galli, C., Loi, M., Solda, T., D'Antuono, R., Raimondi, A., Jung, M., Melnyk, A., Schorr, S., Schreiber, A., Simonelli, L., Varani, L., Wilson-Zbinden, C., Zerbe, O., Hofmann, K., Peter, M., Quadroni, M., Zimmermann, R. & Molinari, M. Translocon component Sec62 acts in endoplasmic reticulum turnover during stress recovery. *Nat Cell Biol* **18**, 1173-1184, doi:10.1038/ncb3423 (2016).
- 28 Loi, M., Fregno, I., Guerra, C. & Molinari, M. Eat it right: ER-phagy and recovER-phagy. *Biochem Soc Trans* **46**, 699-706, doi:10.1042/bst20170354 (2018).
- 29 Smith, M. & Wilkinson, S. ER homeostasis and autophagy. *Essays Biochem* **61**, 625-635, doi:10.1042/ebc20170092 (2017).
- 30 Kurth, I., Pamminger, T., Hennings, J. C., Soehendra, D., Huebner, A. K., Rothier, A., Baets, J., Senderek, J., Topaloglu, H., Farrell, S. A., Nurnberg, G., Nurnberg, P., De Jonghe, P., Gal, A., Kaether, C., Timmerman, V. & Hubner, C. A. Mutations in FAM134B, encoding a newly identified Golgi protein, cause severe

- sensory and autonomic neuropathy. *Nat Genet* **41**, 1179-1181, doi:10.1038/ng.464 (2009).
- 31 Gan, B., Peng, X., Nagy, T., Alcaraz, A., Gu, H. & Guan, J. L. Role of FIP200 in cardiac and liver development and its regulation of TNFalpha and TSC-mTOR signaling pathways. *J Cell Biol* **175**, 121-133, doi:10.1083/jcb.200604129 (2006).
- 32 Tsuboyama, K., Koyama-Honda, I., Sakamaki, Y., Koike, M., Morishita, H. & Mizushima, N. The ATG conjugation systems are important for degradation of the inner autophagosomal membrane. *Science* **354**, 1036-1041, doi:10.1126/science.aaf6136 (2016).
- 33 Nishimura, T., Tamura, N., Kono, N., Shimanaka, Y., Arai, H., Yamamoto, H. & Mizushima, N. Autophagosome formation is initiated at phosphatidylinositol synthase-enriched ER subdomains. *Embo j* **36**, 1719-1735, doi:10.15252/emboj.201695189 (2017).
- 34 Itakura, E. & Mizushima, N. Characterization of autophagosome formation site by a hierarchical analysis of mammalian Atg proteins. *Autophagy* **6**, 764-776 (2010).
- 35 Hara, T., Takamura, A., Kishi, C., Iemura, S., Natsume, T., Guan, J. L. & Mizushima, N. FIP200, a ULK-interacting protein, is required for autophagosome formation in mammalian cells. *J Cell Biol* **181**, 497-510, doi:10.1083/jcb.200712064

(2008).

36 Saitoh, T., Nakano, H., Yamamoto, N. & Yamaoka, S. Lymphotoxin-beta receptor mediates NEMO-independent NF-kappaB activation. *FEBS Lett* **532**, 45-51

(2002).

37 Morita, K., Hama, Y., Izume, T., Tamura, N., Ueno, T., Yamashita, Y., Sakamaki, Y., Mimura, K., Morishita, H., Shihoya, W., Nureki, O., Mano, H. & Mizushima, N. Genome-wide CRISPR screen identifies TMEM41B as a gene required for autophagosome formation. *J Cell Biol*, doi:10.1083/jcb.201804132 (2018).

38 Kitamura, T., Koshino, Y., Shibata, F., Oki, T., Nakajima, H., Nosaka, T. & Kumagai, H. Retrovirus-mediated gene transfer and expression cloning: powerful tools in functional genomics. *Exp Hematol* **31**, 1007-1014 (2003).

39 Kabeya, Y., Mizushima, N., Ueno, T., Yamamoto, A., Kirisako, T., Noda, T., Kominami, E., Ohsumi, Y. & Yoshimori, T. LC3, a mammalian homologue of yeast Apg8p, is localized in autophagosome membranes after processing. *Embo j* **19**, 5720-5728, doi:10.1093/emboj/19.21.5720 (2000).

40 Kishi-Itakura, C., Koyama-Honda, I., Itakura, E. & Mizushima, N. Ultrastructural analysis of autophagosome organization using mammalian autophagy-deficient cells. *J Cell Sci* **127**, 4089-4102, doi:10.1242/jcs.156034 (2014).

- 41 Schindelin, J., Arganda-Carreras, I., Frise, E., Kaynig, V., Longair, M., Pietzsch, T., Preibisch, S., Rueden, C., Saalfeld, S., Schmid, B., Tinevez, J. Y., White, D. J., Hartenstein, V., Eliceiri, K., Tomancak, P. & Cardona, A. Fiji: an open-source platform for biological-image analysis. *Nat Methods* **9**, 676-682, doi:10.1038/nmeth.2019 (2012).
- 42 Natsume, T., Yamauchi, Y., Nakayama, H., Shinkawa, T., Yanagida, M., Takahashi, N. & Isobe, T. A direct nanoflow liquid chromatography-tandem mass spectrometry system for interaction proteomics. *Anal Chem* **74**, 4725-4733 (2002).
- 43 Yoshii, S. R., Kuma, A., Akashi, T., Hara, T., Yamamoto, A., Kurikawa, Y., Itakura, E., Tsukamoto, S., Shitara, H., Eishi, Y. & Mizushima, N. Systemic Analysis of Atg5-Null Mice Rescued from Neonatal Lethality by Transgenic ATG5 Expression in Neurons. *Dev Cell* **39**, 116-130, doi:10.1016/j.devcel.2016.09.001 (2016).
- 44 Liang, C. C., Wang, C., Peng, X., Gan, B. & Guan, J. L. Neural-specific deletion of FIP200 leads to cerebellar degeneration caused by increased neuronal death and axon degeneration. *J Biol Chem* **285**, 3499-3509, doi:10.1074/jbc.M109.072389 (2010).
- 45 Gotoh, M., Ichikawa, H., Arai, E., Chiku, S., Sakamoto, H., Fujimoto, H., Hiramoto, M., Nammo, T., Yasuda, K., Yoshida, T. & Kanai, Y. Comprehensive

- exploration of novel chimeric transcripts in clear cell renal cell carcinomas using whole transcriptome analysis. *Genes Chromosomes Cancer* **53**, 1018-1032, doi:10.1002/gcc.22211 (2014).
- 46 Jan, S. Z., Vormer, T. L., Jongejan, A., Roling, M. D., Silber, S. J., de Rooij, D. G., Hamer, G., Repping, S. & van Pelt, A. M. M. Unraveling transcriptome dynamics in human spermatogenesis. *Development* **144**, 3659-3673, doi:10.1242/dev.152413 (2017).
- 47 Liu, X. X. & Liu, F. J. Novel bioinformatic identification of differentially expressed tissue-specific and cancer-related proteins from the Human Protein Atlas for biomarker discovery. *Genet Mol Res* **14**, 4557-4565, doi:10.4238/2015.May.4.14 (2015).
- 48 Katayama, H., Yamamoto, A., Mizushima, N., Yoshimori, T. & Miyawaki, A. GFP-like proteins stably accumulate in lysosomes. *Cell Struct Funct* **33**, 1-12 (2008).
- 49 Biazik, J., Yla-Anttila, P., Vihinen, H., Jokitalo, E. & Eskelinen, E. L. Ultrastructural relationship of the phagophore with surrounding organelles. *Autophagy* **11**, 439-451, doi:10.1080/15548627.2015.1017178 (2015).
- 50 Eskelinen, E. L., Reggiori, F., Baba, M., Kovacs, A. L. & Seglen, P. O. Seeing is believing: the impact of electron microscopy on autophagy research. *Autophagy* **7**, 935-

956 (2011).

- 51 Hayashi-Nishino, M., Fujita, N., Noda, T., Yamaguchi, A., Yoshimori, T. & Yamamoto, A. A subdomain of the endoplasmic reticulum forms a cradle for autophagosome formation. *Nat Cell Biol* **11**, 1433-1437, doi:10.1038/ncb1991 (2009).
- 52 Uversky, V. N. Functional roles of transiently and intrinsically disordered regions within proteins. *Febs j* **282**, 1182-1189, doi:10.1111/febs.13202 (2015).
- 53 Zhou, H.-X. Polymer Models of Protein Stability, Folding, and Interactions. *Biochemistry* **43**, 2141-2154, doi:10.1021/bi036269n (2004).
- 54 Yamamoto, H., Fujioka, Y., Suzuki, S. W., Noshiro, D., Suzuki, H., Kondo-Kakuta, C., Kimura, Y., Hirano, H., Ando, T., Noda, N. N. & Ohsumi, Y. The Intrinsically Disordered Protein Atg13 Mediates Supramolecular Assembly of Autophagy Initiation Complexes. *Dev Cell* **38**, 86-99, doi:10.1016/j.devcel.2016.06.015 (2016).
- 55 Dunker, A. K., Silman, I., Uversky, V. N. & Sussman, J. L. Function and structure of inherently disordered proteins. *Curr Opin Struct Biol* **18**, 756-764, doi:10.1016/j.sbi.2008.10.002 (2008).
- 56 Kjaergaard, M. & Kragelund, B. B. Functions of intrinsic disorder in transmembrane proteins. *Cell Mol Life Sci* **74**, 3205-3224, doi:10.1007/s00018-017-

2562-5 (2017).

57 Oldfield, C. J. & Dunker, A. K. Intrinsically disordered proteins and intrinsically disordered protein regions. *Annu Rev Biochem* **83**, 553-584, doi:10.1146/annurev-biochem-072711-164947 (2014).

58 Shin, Y. & Brangwynne, C. P. Liquid phase condensation in cell physiology and disease. *Science* **357**, doi:10.1126/science.aaf4382 (2017).

59 Kovacs, A. L., Palfia, Z., Rez, G., Vellai, T. & Kovacs, J. Sequestration revisited: integrating traditional electron microscopy, de novo assembly and new results. *Autophagy* **3**, 655-662 (2007).

60 Kralt, A., Carretta, M., Mari, M., Reggiori, F., Steen, A., Poolman, B. & Veenhoff, L. M. Intrinsically disordered linker and plasma membrane-binding motif sort Ist2 and Ssy1 to junctions. *Traffic* **16**, 135-147, doi:10.1111/tra.12243 (2015).

61 Phillips, M. J. & Voeltz, G. K. Structure and function of ER membrane contact sites with other organelles. *Nat Rev Mol Cell Biol* **17**, 69-82, doi:10.1038/nrm.2015.8 (2016).

62 Allen, G. F., Toth, R., James, J. & Ganley, I. G. Loss of iron triggers PINK1/Parkin-independent mitophagy. *EMBO Rep* **14**, 1127-1135, doi:10.1038/embor.2013.168 (2013).

- 63 Kaizuka, T., Morishita, H., Hama, Y., Tsukamoto, S., Matsui, T., Toyota, Y., Kodama, A., Ishihara, T., Mizushima, T. & Mizushima, N. An Autophagic Flux Probe that Releases an Internal Control. *Mol Cell* **64**, 835-849, doi:10.1016/j.molcel.2016.09.037 (2016).
- 64 Katayama, H., Kogure, T., Mizushima, N., Yoshimori, T. & Miyawaki, A. A sensitive and quantitative technique for detecting autophagic events based on lysosomal delivery. *Chem Biol* **18**, 1042-1052, doi:10.1016/j.chembiol.2011.05.013 (2011).
- 65 Kimura, S., Noda, T. & Yoshimori, T. Dissection of the autophagosome maturation process by a novel reporter protein, tandem fluorescent-tagged LC3. *Autophagy* **3**, 452-460 (2007).
- 66 Takayama, K., Matsuura, A. & Itakura, E. Dissection of ubiquitinated protein degradation by basal autophagy. *FEBS Lett* **591**, 1199-1211, doi:10.1002/1873-3468.12641 (2017).
- 67 Yoshii, S. R. & Mizushima, N. Monitoring and Measuring Autophagy. *Int J Mol Sci* **18**, doi:10.3390/ijms18091865 (2017).
- 68 Liang, J. R., Lingeman, E., Ahmed, S. & Corn, J. E. Atlastins remodel the endoplasmic reticulum for selective autophagy. *J Cell Biol*,

doi:10.1083/jcb.201804185 (2018).

Acknowledgments

First and foremost, I deeply appreciate Professor Noboru Mizushima for the constructive discussion and encouragement throughout my doctoral life. He taught me the way to enjoy, imagine and think for science. I also thank Professor Takahide Nagase for all the help during my doctoral life.

I have been fortunate to have excellent collaborators. I would like to thank Drs. Tohru Natsume and Tomohisa Hatta for performing the immunoprecipitation and MS screening.

Next, I would thank Drs. Akiko Kuma, Takahide Matsui, Ikuko Honda and Hayashi Yamamoto for giving me technical help and important suggestions about my project.

I appreciate Ms. Yuriko Sakamaki for providing electron microscopy pictures, Dr. Saori Yoshii for mice sampling, Dr. Toshio Kitamura for pMXs-IP, Dr. Shoji Yamaoka for pMRXIP, Dr. Teruhito Yasui for pCG-VSV-G and pCG-gag-pol, Dr. Robert A. Weinberg for pCMV-VSV-G, Dr. Didier Trono for psPAX2, and Dr. Toshiya Endo for anti-RFP antibodies.

Finally, I would like to thank my all labmates for all the encouragement and joy they brought into my life. I also appreciate my family and fiance for all their help and support.